

JUNE 2018

Ph.D. in Civil Engineering

KHAMEES NAYYEF ABDULHALEM

**UNIVERSITY OF GAZIANTEP
GRADUATE SCHOOL OF
NATURAL & APPLIED SCIENCES**

**MECHANICAL BEHAVIOR OF SELF-COMPACTING FIBER
REINFORCED CONCRETE AT ELEVATED TEMPERATURES**

**Ph.D. THESIS
IN
CIVIL ENGINEERING**

**BY
KHAMEES NAYYEF ABDULHALEM
JUNE 2018**

**Mechanical Behavior of Self-Compacting Fiber Reinforced Concrete
at Elevated Temperatures**

Ph.D. Thesis

in

Civil Engineering

University of Gaziantep

Supervisor

Prof. Dr. Abdulkadir ÇEVİK

Co. Supervisor

Assist. Prof. Dr. Mehmet Eren GÜLŞAN

by

Khamees Nayyef ABDULHALEEM

June 2018



©2018 [Khamees Nayyef ABDULHALEEM]

REPUBLIC OF TURKEY
UNIVERSITY OF GAZIANTEP
GRADUATE SCHOOL OF NATURAL & APPLIED SCIENCES
CIVIL ENGINEERING DEPARTMENT

Name of the thesis: Mechanical Behavior of Self-Compacting Fiber Reinforced Concrete at Elevated Temperatures

Name of the student: Khamees Nayyef ABDULHALEEM

Exam date: June 20, 2018

Approval of the Graduate School of Natural and Applied Sciences.

Prof. Dr. A. Necmeddin YAZICI
Director

I certify that this thesis satisfies all the requirements as a thesis for the degree of Doctor of Philosophy.

Prof. Dr. Hanifi ÇANAKCI
Head of Department

This is to certify that we have read this thesis and that in our opinion it is fully adequate, in scope and quality, as a thesis for the degree of Doctor of Philosophy.

Assist. Prof. Dr. Mehmet Eren GÜLŞAN
Co. Supervisor

Prof. Dr. Abdulkadir ÇEVİK
Supervisor

Examining Committee Members:

Signature

Prof. Dr. Abdulkadir ÇEVİK

.....

Assoc. Prof. Dr. Nihat ATMACA

.....

Assist. Prof. Dr. M. Tolga GÖĞÜŞ

.....

Assist. Prof. Dr. Ahmet Emin KURTOĞLU

.....

Assist. Prof. Dr. Anıl NİŞ

.....

I hereby declare that all information in this document has been obtained and presented in accordance with academic rules and ethical conduct. I also declare that, as required by these rules and conduct, I have fully cited and referenced all material and results that are not original to this work.

Khamees Nayyef ABDULHALEM

ABSTRACT

MECHANICAL BEHAVIOR OF SELF-COMPACTING FIBER REINFORCED CONCRETE AT ELEVATED TEMPERATURES

ABDULHALEEM, Khamees Nayyef

Ph.D. in Civil Engineering

Supervisor: Prof. Dr. Abdulkadir ÇEVİK

Co. Supervisor: Assist. Prof. Dr. Mehmet Eren GÜLŞAN

June 2018

106 pages

It is worth mentioning that the dense microstructure of the self-compacting concrete (SCC) makes it more brittle and thus less resistant to high temperatures. Therefore, it tends to fail due to spalling and development of cracks are rapid at elevated temperatures. In the present study, the influence of steel fibers on the mechanical properties of SCC after exposure to elevated temperatures are investigated. The effect of steel fiber (SF) on the mechanical properties including compressive and tensile strengths of SCC has been studied. Also, the characteristics of stress-strain curves for fiber reinforced SCC (FR-SCC) were discussed in detail. Experimental results have shown that the addition of SF leads to significant improvement in mechanical properties of SCC, particularly after elevated temperatures. The findings revealed that the polypropylene (PP) fibers were able to prevent the risk of spalling in SCC during heating processes.

None of the respective previous studies have investigated the mechanical behavior of fiber-reinforced concrete corbels subjected to elevated temperatures. For this reason, the other aim of the present thesis is a novel experimental attempt to understand the behavior of FR-SCC corbels after exposure to temperatures. This study accounts for the ability of SFs to improve ductility and enhance mechanical behavior of RC-corbels after exposure to elevated temperatures. The results were presented in terms of load-deflection curves, crack patterns and failure modes. Experimental results showed that the SFs have a positive effect on load-carrying capacity and ductility of RC-corbels before and after exposure to elevated temperatures.

Keywords: Mechanical Behavior; Self-Compacting Concrete; Elevated Temperatures; Steel and Polypropylene Fibers; Corbels.

ÖZET

LİF TAKVİYELİ KENDİLİĞİNDEN YERLEŞEN BETONUN YÜKSEK SICAKLIKLARDAKİ MEKANİK DAVRANIŞI

ABDULHALEEM, Khamees Nayyef
Doktora Tezi, İnşaat Mühendisliği
Tez Danışmanı: Prof. Dr. Abdulkadir ÇEVİK
Yardımcı Tez Danışmanı: Dr. Öğr. Üyesi Mehmet Eren GÜLŞAN
Haziran 2018
106 sayfa

Kendiliğinden yerleşen betonun yoğun mikro yapısı bu beton türünü daha kırılğan ve dolayısıyla yüksek sıcaklıklara karşı daha az dayanımlı yapmaktadır. Bundan dolayı kendiliğinden yerleşen beton patlamadan dolayı göçmeye meyillidir ve bu betondaki çatlak gelişimi yüksek sıcaklıklarda hızlıdır. Bu çalışmada, çelik liflerin kendiliğinden yerleşen betonun yüksek sıcaklıklara maruz bırakıldıktan sonraki mekanik özelliklerine etkisi araştırılmıştır. Çelik liflerin kendiliğinden yerleşen betonun basınç ve çekme mukavemeti gibi mekanik özellikleri üzerindeki etkisi çalışılmıştır. Ayrıca, çelik lif takviyeli kendiliğinden yerleşen betonun gerilim-birim şekil değiştirme grafiklerinin karakteristikleri detaylı bir şekilde tartışılmıştır. Deneysel sonuçlar, çelik lif katkısının kendiliğinden yerleşen betonun mekanik özelliklerini, özellikle yüksek sıcaklıklardan sonra, önemli bir şekilde iyileştirdiğini göstermiştir. Deneysel bulgular polipropilen liflerin kendiliğinden yerleşen betonda ısıtma süresince patlama riskini engellediğini ortaya çıkarmıştır.

Daha önceki hiçbir çalışma yüksek sıcaklığa maruz kalmış çelik lif katkılı kısa konsolların mekanik davranışını araştırmamıştır. Bu nedenden ötürü, bu tezin bir diğer amacı da çelik lif takviyeli kendiliğinden yerleşen betondan üretilmiş kısa konsolların yüksek sıcaklıklardan sonraki davranışını anlamak için yenilikçi bir deneysel çalışmadır. Bu çalışma, çelik liflerin yüksek sıcaklıklardan sonra betonarme kısa konsolların sünekliğini ve mekanik özelliklerini iyileştirme kabiliyetine açıklık getirmektedir. İlgili sonuçlar yük-deplasman grafikleri, çatlak oluşumları ve göçme türleri açısından sunulmuştur. Deneysel sonuçlar, çelik liflerin betonarme kısa konsolların yük taşıma kapasitesini ve sünekliğini yüksek sıcaklıklara maruz kalmadan önce ve sonra olumlu yönde etkilediğini göstermiştir.

Anahtar Kelimeler: Mekanik Davranış; Kendiliğinden Yerleşen Beton; Yüksek Sıcaklıklar; Çelik ve Polipropilen lifler, Kısa Konsollar.



*To my father, who passed away
before I get my Ph.D. degree.*

ACKNOWLEDGEMENTS

I would like to express my deepest gratitude to my supervisor, **Prof. Abdulkadir ÇEVİK**, for his unlimited guidance, patience, and support during this research. Without his supervision and advice, this thesis would not have been possible. I would like also to thank my Co-supervisor **Assist. Prof. Dr. Mehmet Eren GÜLŞAN** for his continuous help and also facilitate the experimental works. I am really glad and proud that I have had an opportunity to work closely with them.

Besides my advisor, I would like to extend my sincere gratitude to committee members. I would like to thank also the jury members for their participation and criticism.

My sincere thanks also go to the Instructors of the civil engineering department and all my friends whose helped me in all stages of my study.

Sincere thanks to **IRAQI Ministry of Higher Education and Scientific Research** and **Kirkuk University** to their provision this scholarship to complete my study. Thanks to **Gaziantep University** to provide me the opportunity to obtain a doctorate degree.

I am very grateful for the spirit of my father and for my mother's prayer, caring and supporting me over the years. Without them I will not be anywhere closer to the position I am in now, my brothers and sisters, whose encouragement, love and support served as the foundation for all of my past achievements and future endeavors in life.

Finally, I would like to thank my wife, for her endless support and sacrifice, and my wonderful kids, for their endless energy, without their continuous support the successful completion of this work would not have been possible.

TABLE OF CONTENTS

	Page
ABSTRACT	v
ÖZET	vi
ACKNOWLEDGEMENTS	viii
TABLE OF CONTENTS	ix
LIST OF TABLES	xiii
LIST OF FIGURES	xiv
LIST OF SYMBOLS AND ABBREVIATIONS	xviii
CHAPTER 1	1
INTRODUCTION	1
1.1 General	1
1.2 Temperature effect on concrete behavior	1
1.3 The fibers effects on characteristics of heated concrete	2
1.4 Behavior of fiber-reinforced SCC after exposure to elevated temperatures	2
1.5 Aim of the study	3
1.6 Layout of the thesis	3
CHAPTER 2	5
LITERATURE REVIEW	5
2.1 Mechanical properties of FRC after exposure to elevated temperatures	5
2.1.1 Compressive strength	5
2.1.2 Splitting tensile strength	8
2.1.3 Modulus of elasticity	9
2.1.4 Peak strain	10
2.1.5 Characteristic the stress-strain curves	11
2.2 Size effect on the mechanical properties of concrete	12
2.3 Mechanical behavior of FRC corbels	13
2.3.1 Load-deflection behavior	13
2.3.2 Cracks pattern and failure modes	14
CHAPTER 3	17
EXPERIMENTAL WORK	17

3.1 General	17
3.2 Mixture preparation	17
3.2.1 Materials characteristics	17
3.2.2 Mix designation.....	18
3.2.3 Classification of mixtures	19
3.2.4 Preparation of specimens.....	19
3.2.4.1 The testing specimens for strength.....	19
3.2.4.2 Specimens the stress-strain testing.....	20
3.2.4.3 The corbel specimens.....	20
3.2.5 Mixing and casting	21
3.3 Testing procedures.....	22
3.3.1 Fresh properties testing.....	22
3.3.2 Heating regime	24
3.3.3 Loading test.....	24
3.3.3.1 Procedure of mechanical properties testing	24
3.3.3.2 The testing procedure of stress-strain curves.....	25
3.3.3.3 Mechanical behavior testing for RC-corbels.....	26
CHAPTER 4	28
COMPRESSIVE AND TENSILE STRENGTHS OF FR-SCC BEFORE AND AFTER EXPOSURE TO ELEVATED TEMPERATURES	28
4.1 General	28
4.2 Compressive strength.....	28
4.3 Splitting tensile strength.....	32
4.4 The Internal Cracks and Fiber reacting.....	34
4.5 Numerical study.....	37
CHAPTER 5	41
CONSTITUTIVE STRESS-STRAIN RELATIONSHIPS OF FR-SCC AFTER EXPOSURE TO ELEVATED TEMPERATURES.....	41
5.1 General	41
5.2 Stress-strain characteristics	41
5.2.1 Compressive strength (Peak stress).....	41
5.2.2 Modulus of elasticity	44
5.2.3 Peak strain.....	46
5.2.4 Compressive stress-strain curve.....	47

5.3 Development of the stress-strain relationship	50
5.3.1 Basic model equation	50
5.3.2 Proposed model	50
5.3.3 Verification of proposed model	52
CHAPTER 6	53
SIZE EFFECT ON RESIDUAL STRENGTH OF FR-SCC AFTER EXPOSURE TO ELEVATED TEMPERATURES.....	53
6.1 General	53
6.2 Compressive strength.....	53
6.2.1 Medium strength self-compacting concrete (FR-MSCC)	54
6.2.1.1 Conversion factor	56
6.2.2 High strength self compacting concrete (FR-HSCC).....	58
6.2.2.1 Conversion factor	59
6.3 Tensile strength	61
6.4 Theoretical analysis	63
6.4.1 Specimen size effect	63
6.4.1.1 The size effect law	63
6.4.1.2 Size effect on compressive strength.....	64
6.4.1.2.a Cubic specimens	64
6.4.1.2.b Cylindrical specimens	66
6.4.1.3 Size effect on tensile strength	67
6.4.2 Specimen shape effect	69
CHAPTER 7	72
MECHANICAL BEHAVIOR OF FR-SCC CORBELS AFTER EXPOSURE TO ELEVATED TEMPERATURES.....	72
7.1 General	72
7.2 Load-carrying capacity	73
7.3 Load-deflection behavior	76
7.3.1 Concrete Compressive Strength (CCS).....	76
7.3.2 Shear Span-to-depth Ratio (SSR).....	79
7.3.3 Steel-Reinforcement Ratio (SRR).....	82
7.4 Cracks pattern and failure modes	85
7.4.1 Concrete Compressive Strength (CCS).....	85

7.4.2 Shear Span-to-depth ratio (SSR).....	86
7.4.3 Steel-Reinforcement Ratio (SRR).....	86
7.5 Parametric study	90
CHAPTER 8	92
CONCLUSIONS AND RECOMMENDATIONS	92
8.1 General	92
8.2 Conclusions.....	92
8.3 Recommendations for future studies	96
REFERENCES	97



LIST OF TABLES

	Page
Table 3.1 Chemical analysis of cement and binder additives.....	18
Table 3.2 Properties of fibers used in the present study.....	18
Table 3.3 Mix proportions of FR-SCC mixtures.....	18
Table 3.4 Stress characteristics of steel reinforcing bars.....	19
Table 3.5 The fresh properties results of FR-SCC mixtures used.....	22
Table 4.1 Compressive and tensile strengths of FR-SCC specimens at room temperature.	30
Table 4.2 The relative loss in compressive strength of FR-SCC specimens after different temperatures.....	31
Table 4.3 Empirical constants were used in mechanical properties calculations	38
Table 5.1 The results of compressive properties of FR-SCC cylinders before and after exposure to elevated temperatures.....	42
Table 6.1 Compressive strength of FR-MSCC specimens after exposure to different temperatures	55
Table 6.2 Compressive strength of FR-HSCC specimens after exposure to different temperatures	58
Table 6.3 Tensile strength of FR-MSCC specimens after exposure to different temperatures	62
Table 6.4 Tensile strength of FR-HSCC specimens after exposure to different temperatures	63
Table 7.1 Mechanical characteristics of test specimens after exposure to elevated temperatures.....	75
Table 7.2 Results of flexural tests for corbels with different values of concrete compressive strength (CCS) ^ψ	77
Table 7.3 Results of flexural tests for corbels with different values of shear span-to-depth ratio (SSR) ^ψ	80
Table 7.4 Results of flexural tests for corbels with different values of steel reinforcement ratio (SRR) ^ψ	83

LIST OF FIGURES

Page

Figure 2.1 Effects of different fibers on the compressive strength of SCHPC after exposure to elevated temperatures (Ding et al. 2012).	7
Figure 2.2 Effects of temperature on the compressive strength of FR-SCC (Khaliq and Kodur, 2011).	7
Figure 2.3 Compressive strength of fiber-reinforced HSC subjected to high temperatures (Pliya et al., 2011).	7
Figure 2.4 Compressive strength of HFRHSC after exposure to elevated temperatures (Chen and Liu, 2004).	7
Figure 2.5 Relative residual compressive strength of FR-HPC after exposure to high temperatures (Poon et al., 2004).	8
Figure 2.6 Effect of hybrid fibers on the compressive strength of RPC after high temperatures (Zheng et al.,2012).	8
Figure 2.7 Effects of temperature on the splitting tensile strength of FR-SCC (Khaliq et al., 2011).	9
Figure 2.8 Residual splitting tensile strength of hybrid fiber-reinforced HSC after exposure to elevated temperatures (Chen and Liu, 2004).	9
Figure 2.9 Tensile strength of steel-fiber reinforced RPC at different temperatures (Zheng et al., 2013).	9
Figure 2.10 Tensile strength of hybrid fiber-reinforced RPC after exposure to elevated temperatures (Li and Liu, 2016).	9
Figure 2.11 Modulus of elasticity of steel-fiber reinforced RPC after exposure to elevated temperatures (Tai et al., 2011).	10
Figure 2.12 Modulus of elasticity of steel-fiber reinforced recycled aggregate concrete after different temperatures (Chen et al., 2014).	10
Figure 2.13 Peak strain of steel-fiber reinforced RPC after exposure to high temperatures (Tai et al., 2011).	11

Figure 2.14 Effect of temperature on peak strain of steel fiber-reinforced RPC (Zheng et al., 2012).	11
Figure 3.1 Steel and polypropylene fibers.....	19
Figure 3.2 The specimens were cast in one batch.....	20
Figure 3.3 Geometry and reinforcement details of RC-corbels.....	21
Figure 3.4 Preparing the specimens after heating treatment.....	22
Figure 3.5 The fresh tests for SCC used.....	23
Figure 3.6 Arrangement the specimens inside the electric furnace.	23
Figure 3.7 Mechanical testing of concrete specimens used.....	25
Figure 3.8 Load capacity testing for RC-corbels	27
Figure 4.1 Compressive strength of FR-SCC specimens before and after exposure to elevated temperatures.....	30
Figure 4.2 Relative residual compressive strength of FR-SCC specimens after exposure to elevated temperatures.....	31
Figure 4.3 Splitting tensile strength of FR-SCC specimens exposed to elevated temperatures	33
Figure 4.4 Relative residual tensile strength of FR-SCC exposed to elevated temperatures	34
Figure 4.5 Thermal cracks between matrix and SF after exposure to 750°C.....	35
Figure 4.6 Micro channels formed by melting of PP fibers.	35
Figure 4.7 The oxidation and carbonation of SF after exposure to 750°C.....	36
Figure 4.8 Shape the SF after exposure to different temperature.	36
Figure 4.9 Comparison between experimental and calculated compressive strength of FR-SCC specimens.....	40
Figure 4.10 Comparison between experimental and calculated tensile strength of FR-SCC specimens.	40
Figure 4.11 Comparison of proposed models against experimental test results for residual compressive strength.....	40
Figure 5.1 Effect of temperature on the compressive strength of FR-SCC. (R.T = room temperature)	43
Figure 5.2 Effect of temperature on the elastic modulus of FR-SCC.	45
Figure 5.3 Effect of temperature on the peak strain of FR-SCC. (R.T = room temperature).....	46

Figure 5.4 Stress-strain curves of FR-SCC with various steel fiber content exposure to different temperatures.	48
Figure 5.5 Normalized stress-strain curves for FR-SCC specimens after exposure to different temperatures.	49
Figure 5.6 Compressive failure modes for cylinders of FR-SCC with various steel fiber content after different temperatures.....	50
Figure 5.7 Comparison of proposed stress-strain curves with experimental results for FR-SCC cylinders before and after exposure to elevated temperature.	52
Figure 6.1 Compressive strength of FR-MSCC specimens before and after exposure to elevated temperatures.....	55
Figure 6.2 Conversion factor for FR-MSCC specimens before and after exposure to elevated temperatures.....	57
Figure 6.3 Compressive strength of FR-HSCC specimens before and after exposure to elevated temperatures.....	59
Figure 6.4 Conversion factor for FR-HSCC specimens before and after exposure to elevated temperatures.....	60
Figure 6.5 Shape of failure for different FR-SCC specimens under compression test, after exposure to temperature 750°C.....	61
Figure 6.6 Tensile strength of FR-SCC specimens before and after exposure to elevated temperatures.....	62
Figure 6.7 Comparison between experimental and calculated compressive strength of FR-SCC cubes.....	65
Figure 6.8 Size effect on compressive strength for FR-SCC cubes before and after exposure to elevated temperatures.....	65
Figure 6.9 Comparison between experimental and calculated compressive strength of FR-SCC cylinders	66
Figure 6.10 Size effect on compressive strength for FR-SCC cylinders before and after exposure to elevated temperatures.....	67
Figure 6.11 Comparison between experimental and calculated tensile strength of FR-SCC cylinders.....	68
Figure 6.12 Size effect on tensile strength for FR-SCC cylinders before and after exposure to elevated temperatures.....	69

Figure 6.13 Relationship between compressive strengths of the 100 × 200 mm cylinder and cubic specimens before and after exposure to elevated temperatures.	70
Figure 6.14 Relationship between compressive strengths of the 150 × 300 mm cylinder and cubic specimens before and after exposure to elevated temperatures.	71
Figure 7.1 Load-deflection curves for corbels with the different values of concrete compressive strength (CCS).....	78
Figure 7.2 Load-deflection curves for corbels with the different values of shear span-to-depth ratio (SSR).....	81
Figure 7.3 Load-deflection curves for corbels with the different values of the steel reinforcement ratio (SRR).....	84
Figure 7.4 Failure modes for RC-corbels with the different values of concrete compressive strength (CCS).....	87
Figure 7.5 Failure modes for RC-corbels with the different values of shear span ratio (SSR).....	88
Figure 7.6 Failure modes for RC-corbels with the different values of the steel reinforcement ratio (SRR).....	89
Figure 7.7 Interaction effect between the main effects and the corbel's parameters on the maximum loads (mean values).....	91

LIST OF SYMBOLS AND ABBREVIATIONS

f_c'	Compressive strength of concrete without steel fiber at room temperature
$f_{c,T}$	Stress at a random point located on the stress-strain curve of FR-SCC after different temperatures (T) : MPa.
$f_{c,T}'$	Stress at peak point on the stress-strain curve of FR-SCC after different temperatures.
$\varepsilon_{c,T}$	Strain at a random point located on the stress-strain curve of FR-SCC after different temperatures.
$\varepsilon_{c,T}'$	Strain at peak point on the stress-strain curve of FR-SCC after different temperatures (peak strain).
$E_{c,T}$	Modulus of elasticity at 40% of peak stress after different temperatures.
$E_{p,T}$	Modulus of elasticity at peak stress after different temperatures.
$\sigma_N(d)$	The nominal strength.
d	Specimen dimension: cm.
f_{ct}	Direct tensile strength.
f_{cu}	Compressive strength with the size of the general cube for FR-SCC with or without steel fiber before and after exposure to elevated temperature: MPa.
f_{cs}	Compressive strength of the standard cylinder with the size of 150×300mm for FR-SCC with or without steel fiber before and after exposure to elevated temperature: MPa.
d_a	Maximum aggregate size.
$R.I$	Fiber reinforcing index.
d_f	Diameter of steel fiber.

l_f	Length of steel fiber (in mm).
f_{cy}	Compressive strength with the size of the general cylinder for FR-SCC with or without steel fiber before and after exposure to elevated temperature (in MPa).
f_t	Tensile strength with the size of the general cylinder for FR-SCC with or without steel fiber before and after exposure to elevated temperature (in MPa).
f_{ts}	Tensile strength of the standard cylinder with the size of 150×300mm for FR-SCC with or without steel fiber before and after exposure to elevated temperature (in MPa).
V_f	Steel fiber ratio.
a	Shear span of the corbel.
CCS	Concrete compressive strength
CR	Corbel.
D.S	Diagonal splitting.
F	Flexure.
FR-HSCC	Fiber-reinforced high self-compacting concrete.
FR-MSCC	Fiber-reinforced medium self-compacting concrete.
FR-SCC	Fiber-reinforced self-compacting concrete
h	Corbel depth.
LVDT	Linear variable displacement transducer.
PP	Polypropylene fiber
R^2	The correlation coefficient
S	Shear.
SCC	Self-compacting concrete
SF	Steel fiber
SRR	Steel reinforcement ratio
SSR	Shear span-to-depth ratio

T	Temperature degree ($^{\circ}C$).
ρ	Reinforcement ratio
α	Empirical constant
β	Empirical constant
γ	Empirical constant
η	Empirical constant
λ	Empirical constant
μ	Empirical constant



CHAPTER 1

INTRODUCTION

1.1 General

Self-compacting concrete (SCC) has been widely used in industrial structures throughout the world since it has the ability to flow and fill all sections of forms with little or no vibration as well as resist bleeding or segregation (Aslani and Shami, 2013). SCC is ideally suited for structural applications, especially when pouring the concrete into restricted and heavily reinforced areas (Okamura and Ouchi, 2003). SCC has a dense microstructure and is manufactured by modifying the traditional mix design to attain cohesiveness and high fluidity. This modification includes a reduction of the water-cement ratio through increase dosages of the chemical admixture. These admixtures have been used to improve the properties of SCC representing the workability in a fresh state as well as the required strength of hardened concrete (Sahmaran et al., 2005). Reduced amounts of water used lead to increases in the density and reduction in the porosity. Therefore, the concrete becomes more brittle and less fire resistance (Noumowé et al., 2006).

1.2 Temperature effect on concrete behavior

Fire is one of the most disastrous risks for reinforced concrete structures. In general, loss of strength and spalling are the main causes of failure in the concrete elements when exposed to high temperatures. Spalling occurs due to increase the internal pore pressure triggered by the vaporization of free and chemically bound water (Bakhtiyari et al., 2011). Persson (2004) observed that high moisture content, low water-cement ratio, and rapid rate of temperature exposure were the main causes of spalling. The SCC can also be affected by these factors, due to the low water-cement ratio, dense microstructure, and the kind of powder used in its production (Bakhtiyari et al., 2011, Pathak and Siddiqui, 2012). Some respective studies concluded that the residual mechanical properties of SCC are somewhat similar to conventional high-strength concrete (HSC) properties, yet SCC has been more

affected by spalling risk (Bakhtiyari et al., 2011, Sideris and Manita, 2013).

1.3 The fiber's effects on characteristics of heated concrete

It is worth mentioning that the addition of fibers to concrete mixture contributes to the mitigation of the negative effect of high temperature on concrete behavior. Therefore, the presence of steel fiber (SF) in concrete is to enhance the properties such as toughness and ductility of the concrete. This effect is attributed to bridging ability of the SFs in reduce or prevent the development of the cracks, thus improve the post-cracking behavior (Ding et al., 2012). Therefore, it can be used the SF in improving the ductile behavior and enhancing the residual mechanical properties of concrete when exposed to high temperatures.

The risk of fire-induced spalling on the other hand is usually prevented by the provision of polypropylene (PP) fibers, that used to mitigate explosive spalling in concrete during the heating processes (Okamura and Ouchi, 2003, Sideris and Manita, 2013, Chan et al., 2000, Kalifa et al, 2000, Noumowe, 2005). This effect is attributed to release the high vapor pressure through the randomly oriented micro-channels formed by the melting of PP fibers at relatively low temperature (about 167-170°C) (Kalifa et al. 2001).

Related studies (Ding et al. 2012, Khaliq and Kodur, 2011, Pliya et al., 2015, Chen and Liu, 2004, Poon et al., 2004, Zheng et al., 2012, Sukontasukkul et al., 2010, Shaikh and Hosan, 2016, Dong et al., 2008) recommended using the hybrid (SF and PP) fibers in reducing the strength loss and mitigating the risk of explosive spalling for concrete at high temperatures. Thus, steel and polypropylene fibers can be combined in order to obtain fire-resistance concrete.

1.4 Behavior of fiber-reinforced SCC after exposure to elevated temperatures

Based on the above mentioned, fiber-reinforced SCC (FR-SCC) can be used as a high-performance building materials that combines the benefits of fresh properties of SCC as well as improving the characteristics of the concrete in the hardened state due to adding fibers. Many studies were implemented to predict the properties of SCC at room temperature. However, the mechanical behavior of FR-SCC after exposure to high temperatures has been little taken into consideration so far.

1.5 Aim of the study

The present study aims to understand the mechanical behavior of SCC with hybrid fibers after exposure to high temperatures. In the experimental program of the current study, the following topics will be studied in details:

- The steel fiber's effect on the mechanical properties which include compressive strength and splitting tensile strength of FR-SCC after different temperatures.
- Characteristics of the stress-strain curves including peak stress, modulus of elasticity, and peak strain of the FR-SCC specimens before and after exposure to elevated temperatures.
- Size effect on compressive strength and tensile strength of different FR-SCC specimens when exposed to elevated temperatures.
- None of the previous studies have explored the mechanical behavior of fiber-reinforced concrete (FRC) corbels subjected to elevated temperatures. For this reason, the main aim of the present study is to investigate the steel fiber effect on the mechanical behavior of FR-SCC corbels before and after exposure to elevated temperatures.

1.6 Layout of the thesis

The present study focuses on the investigation of mechanical behavior of FR-SCC corbels after exposure to elevated temperatures.

This thesis consists of eight chapters and is organized as follows:

- Chapter 1 presents a brief introduction, contribution, and the aim of the study.
- Chapter 2 reviews the literature studies related to the mechanical properties of FRCs subjected to elevated temperatures.
- In chapter 3, materials used and steps followed in the practical program to produce the FR-SCC mixtures are described in detail. Also the test procedures according to corresponding specifications have been mentioned.
- Chapter 4 presents the results of compressive and tensile strengths of standard

cylindrical specimens for concrete used before and after exposure to elevated temperatures. Also, it has benefited from the test results in proposing equations to predict these mechanical properties in terms of compressive strength at room temperature, steel fiber ratio, and temperature levels.

- Chapter 5 discusses the characteristics of stress-strain curves of SCC with or without SF after exposure to different temperatures. The constitutive relationships for stress-strain are studied in detail for the concrete used.
- After obtaining the desired data for the effect of temperature on the different specimens, a program is implemented in chapter 6 to predict the effect of specimen size on residual strengths (compressive and tensile strengths) of FR-SCC mixtures.
- Chapter 7 presents the results of the tests and discusses the main purpose of this thesis, which is the mechanical behavior of FR-SCC corbels subjected to elevated temperatures.
- Finally, chapter 8 presents a summary of the conclusions that can be reached through the present study, as well as the most important recommendations for the future studies.

CHAPTER 2

LITERATURE REVIEW

2.1 Mechanical properties of FRC after exposure to elevated temperatures

2.1.1 Compressive strength

Ding et al. (2012) has analyzed the effect of different fibers on the mechanical properties of self-compacting high-performance concrete (SCHPC) subjected to high temperatures. It has been shown that the polypropylene fiber (PP fiber) significantly prevents the spalling of the SCHPC specimens while the steel fiber (SF) improves the residual strength of SCHPC specimens after exposure to elevated temperatures. It was found that the compressive strength of hybrid-fiber reinforced SCHPC were better than that of mono-fiber reinforced SCHPC after exposure to same temperatures as shown in Figure 2.1. Therefore, the use of hybrid fiber (SF+PP fiber) can be more effective in improving the characteristics of SCC after exposure to elevated temperatures. On the other hand, the failure mode of SFs changed from the pullout at relatively low temperature to break down at a temperature higher than 800°C.

Khaliq and Kodur (2011) studied the temperature effect on the mechanical behavior of FR-SCC as shown in Figure 2.2. It has been proved that the strength retention level in SCC is higher than in conventional (HSC). It might due to the superior microstructure for the SCC, thus it exhibits higher strength even at high temperatures.

Pliya et al. (2011) proved that using steel and polypropylene fibers as a cocktail significantly improve the behavior of high strength concrete (HSC) after exposure to high temperatures as shown in Figure 2.3. The micro-channels generated by the polypropylene melting reduce the risk of explosion during the heating process, while steel fiber contributes to mitigating the heating damages and slightly reduces the rate of degradation of residual strengths of HSC subjected to high temperatures.

Chen and Liu (2004) investigated the compressive strength of hybrid-fiber-reinforced HSC (HFRHSC) when exposed to high temperatures. It has been shown that mixing steel fibers (SF) and polypropylene (PP) fibers greatly improve the characteristics of HSC subjected to elevated temperatures as shown in Figure 2.4. For instance, melting the PP fiber create micro channels in structure of concrete. The channels release the high vapor pressure after melting temperature (170 °C). Thus, reducing the risk of spalling failure at high temperatures.

Poon et al. (2004) examined the compressive properties of fiber-reinforced high-performance concrete after exposure to elevated temperatures. The concrete mixtures were reinforced with either SF or PP fiber, or both. It was noticed that the average of relative residual strengths was 45% and 23% after exposure to 600°C and 800°C respectively as shown in Figure 2.5. The fibers were effective in mitigating the temperature effect on the degradation of residual strength. Therefore, the combination of SF and PP fiber can show further improvements to the concrete properties compared with the use of SF only. Despite the effectiveness of PP fiber in preventing the explosive spalling, it has a negative effect on the compressive strength of SCC subjected to high temperatures (Sideris and Manita, 2013).

Al Qadi and Al-Zaidyeen (2014) studied the contribution of different contents of PP fiber in preventing the spalling of SCC when exposed to elevated temperatures. It can be concluded that the 0.1% of PP fiber was a superior performance during heating in comparison with the other percentages of PP fibers.

Bakhtiyari et al. (2011) proved that the SCC is susceptible to spalling more than the normal strength concrete (NSC). However, the NSC suffered compressive strength loss greater than the SCC at elevated temperatures.

Zheng et al. (2012) reviewed the influence of hybrid fibers on the compressive strength of reactive powder concrete (RPC) after high temperatures. After exposure to temperatures not higher than 300°C, the compressive strength slightly increased compared with the original unheated value as shown in Figure 2.6. This attributed to cement hydration reaction more fully, undergoing "high-temperature curing". After exposure to temperature higher than 300°C, the heating damage within the RPC specimens is gradually increasing as a temperature rises.

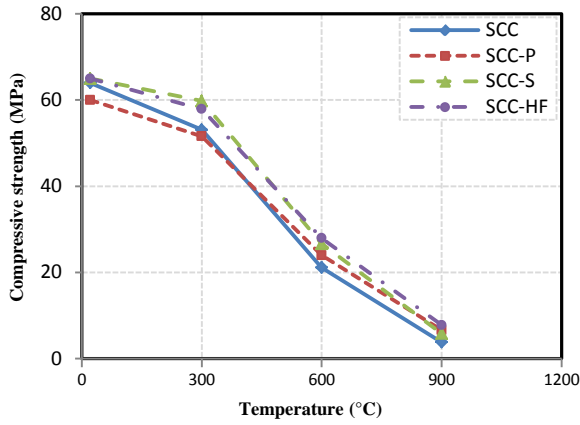


Figure 2.1 Effect of different fibers on the compressive strength of SCHPC after exposure to high temperatures (Ding et al. 2012).

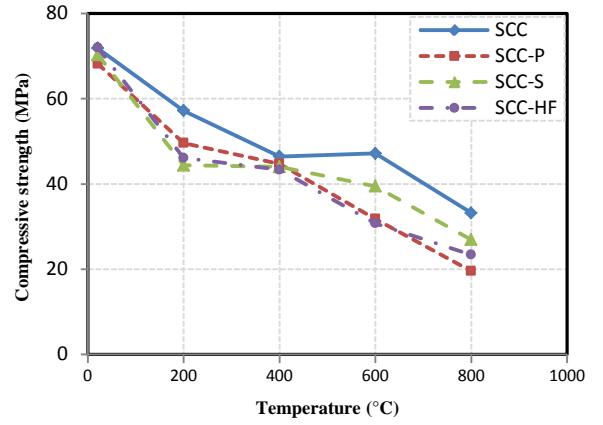


Figure 2.2 Effects of temperature on the compressive strength of FR-SCC (Khaliq and Kodur, 2011).

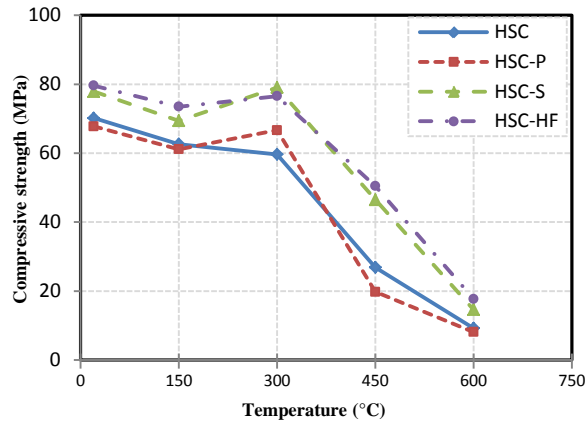


Figure 2.3 Compressive strength of fiber-reinforced HSC subjected to high temperatures (Pliya et al., 2011).

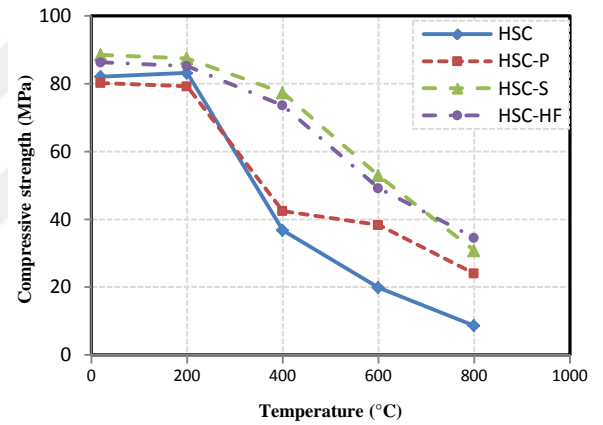


Figure 2.4 Compressive strength of HFRHSC after exposure to elevated temperatures (Chen and Liu, 2004).

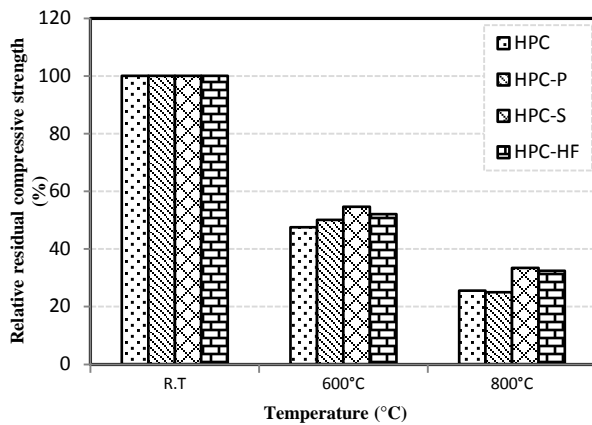


Figure 2.5 Relative residual compressive strength of FR-HPC after exposure to elevated temperatures (Poon et al., 2004).

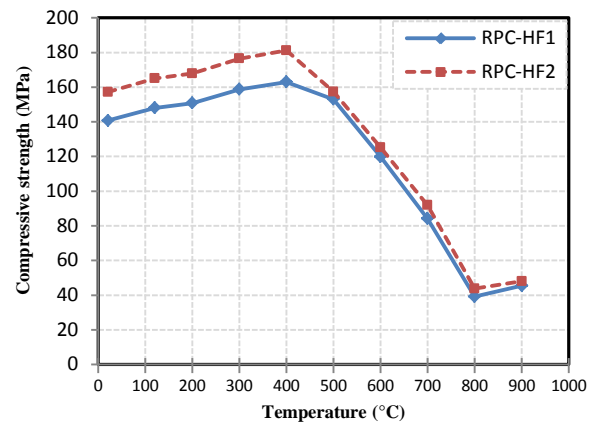


Figure 2.6 The hybrid fibers effect on the compressive strength of RPC after high temperatures (Zheng et al., 2012).

The decomposition of calcium hydroxide to calcium oxide between 400 and 600°C, resulting in accelerating the degradation of residual compressive strength. The sharp loss in compressive strength after 600°C may be also caused by quartz transforming from α -form to β -form (Zheng et al., 2015). Therefore, the addition of steel fiber to concrete reduces the rate of strength degradation after exposure to high temperatures (Chen et al., 2014).

2.1.2 Splitting tensile strength

Khaliq and Kodur (2011) investigated the effects of temperature on the splitting tensile strength of FR-SCC as shown in Figure 2.7. It can be observed that the incompatible in thermal stresses within the SCC matrix leads to the rapid development the micro and macro cracks during the heating process, thus resulting in sharp reductions in tensile strength under tensile testing. The effective of SF in bridging and prevent the development of the cracks under tensile loading leads to significantly improving the tensile strength of the SCC specimens.

Chen and Liu (2004) investigated the splitting tensile strength of hybrid fiber-reinforced HSC subjected to elevated temperatures. It was shown that the hybrid of SF and PP fibers greatly improve the tensile strength of concrete before and after exposure to elevated temperatures. For instance, after exposure the HSC specimens to 800°C, the hybrid fibers can award the tensile strength around 40% as an additional enhancement as shown in Figure 2.8.

In general, the appearance and development of each new crack reduce the available area for load carrying, which leads to increase the stress at the critical tips of the crack. Furthermore, the cracks tend to be close under the compression load, while expanding rapidly under tensile loading. Therefore, the reduction in tensile strength is greater than the gradual loss in compressive strength with increasing the temperature as reported by Zheng et al. (2013) as shown in Figure 2.9.

Li and Liu (2016) measured the direct and indirect tensile strength of RPC which contain both SF and PP fibers after exposure to 20-900°C. It has been shown the SF can considerably improve the performance of tensile for heated and unheated concrete, while PP fibers have no obvious influence on the residual tensile strength at elevated temperature. The deterioration in the microstructure of heated concrete

resulted in decreasing the tensile strength linearly with the temperature increase as shown in Figure 2.10.

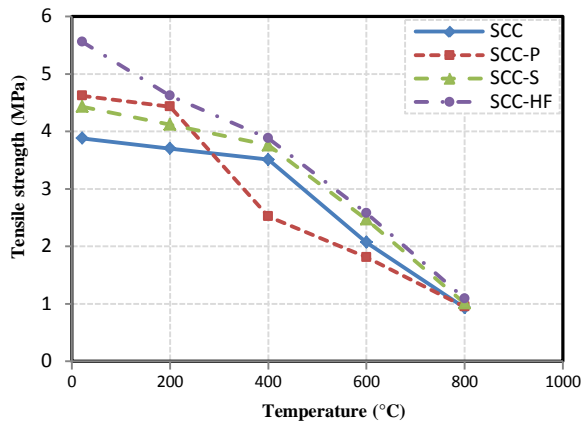


Figure 2.7 Effects of temperature on the splitting tensile strength of FR-SCC (Khaliq et al., 2011).

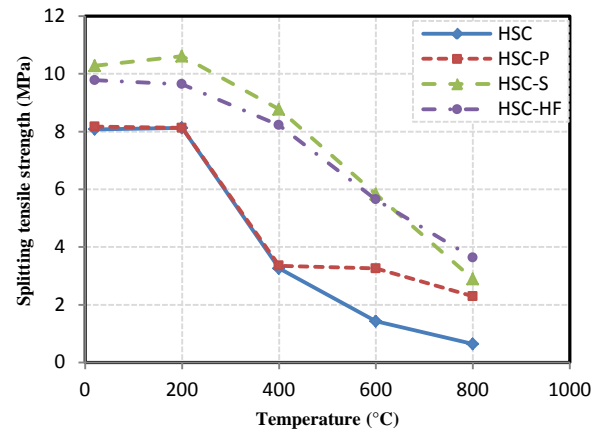


Figure 2.8 Residual splitting tensile strength of hybrid fiber-reinforced HSC after different temperatures (Chen and Liu, 2004).

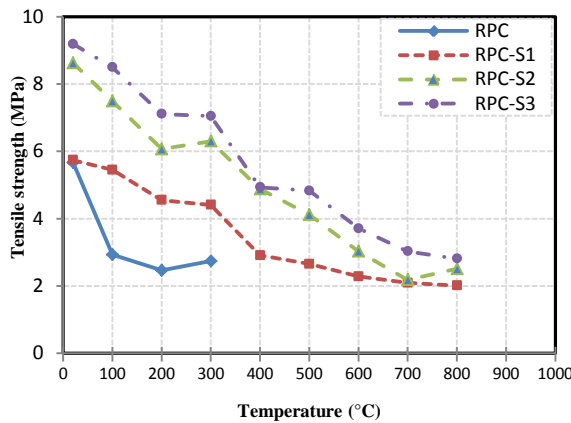


Figure 2.9 Tensile strength of steel-fiber reinforced RPC at elevated temperatures (Zheng et al., 2013).

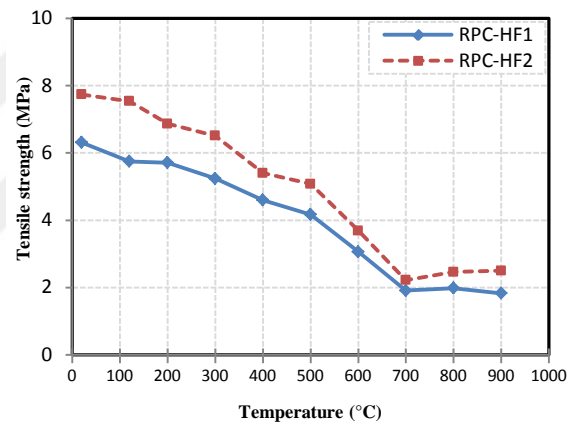


Figure 2.10 Tensile strength of hybrid fiber-reinforced RPC when exposed to high temperatures (Li and Liu, 2016).

2.1.3 Modulus of elasticity

Chang et al. (2006) studied the temperature effect on the elastic modulus of concrete. It can be seen that the compressive strength is decreasing and the peak strain is increasing with the temperature increases, this relevant with decrease the modulus of elasticity. The investigation into the effect of temperature on the elastic modulus of the concrete is important in evaluating the damage to the concrete structural members due to fire.

Tai et al. (2011) proved that the rate of declining in the elastic modulus of concrete, obviously increases after exposure to temperature higher than 500°C, this attributed to the rapid reduction in compressive strength as depicted in Figure 2.11. Moreover,

the elastic modulus can be improved by using the SF within the concrete at different temperatures.

In general, the loss in the elastic modulus of concrete is more pronounced than the reduction in the compressive strength of concrete subjected to elevated temperatures (Zheng et al., 2015).

Kim et al. (2013) observed that the relative residual elastic modulus decreases with the concrete grade increased. Degradation of the elastic modulus depends on the microstructure damage of concrete due to exposure to high temperature. For this reason, SF tends to enhance the elastic modulus particularly at high temperatures as concluded by Chen et al. (2014) as shown in Figure 2.12.

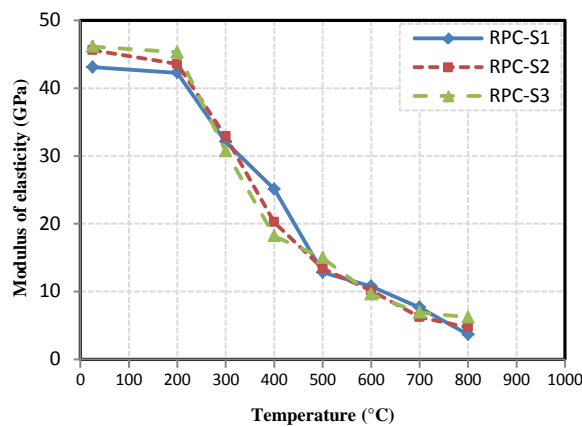


Figure 2.11 Modulus of elasticity of steel-fiber reinforced RPC after exposure to high temperatures (Tai et al., 2011).

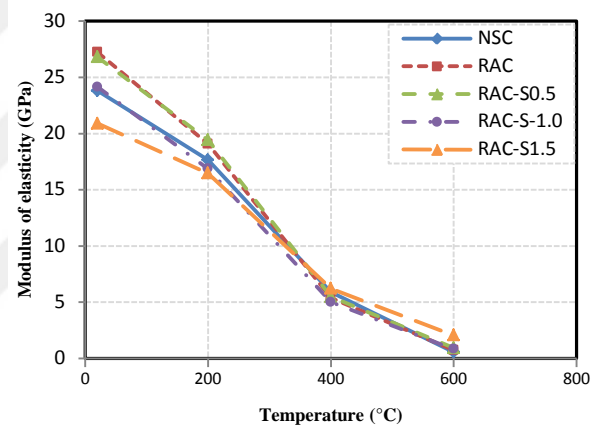


Figure 2.12 Modulus of elasticity of steel-fiber reinforced recycled aggregate concrete after different temperatures (Chen et al., 2014).

2.1.4 Peak strain

Chang et al. (2006) proved that the peak strain for concrete heated to 200°C almost equal to the original value. Beyond 200°C, the peak strain is increasing as a temperature increasing. This increase may be attributed to the cracks caused by incompatibilities in thermal stresses between cement paste and aggregate during heating and cooling processes.

Tai et al. (2011) found that the peak strain began to increase gradually after exposure to 200°C. The peak strains continued to increase, doubling after exposure to 500°C. When exposed to 700°C, the peak strains reach nearly three times of the original unheated value as shown in Figure 2.13. The cracks continue to expand as the temperature increases, subsequently causing an increase in peak strain. It was

found that addition of SFs to concrete reduce the appearance and expansion of the cracks.

Zhang et al. (2012) showed that after exposure to temperature not higher than 300°C, the peak strain slightly increases compared to the unheated value. Thereafter, the peak strain increase is in exponential shape even exposure to 600°C as shown in Figure 2.14. Beyond 600°C, the weakened the steel fibers lead to the increase the brittleness of concrete. Therefore, the peak strain is in a linear shape with the increasing temperature.

In general, the initiation and development the cracks, and decomposition of $\text{Ca}(\text{OH})_2$ and C-S-H were responsible to rapidly increase the peak strain with temperature increase after 600°C (Zheng et al., 2015).

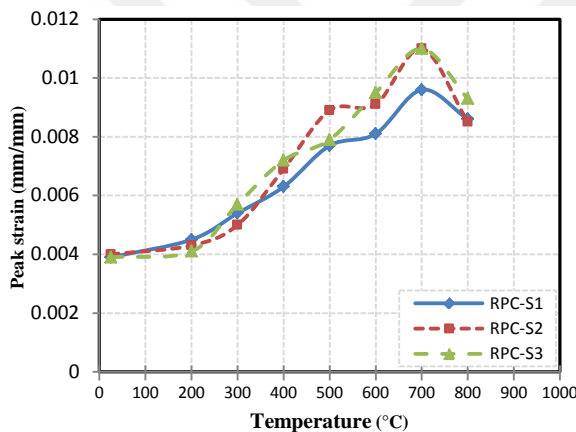


Figure 2.13 Peak strain of steel-fiber reinforced RPC after exposure to high temperatures (Tai et al., 2011).

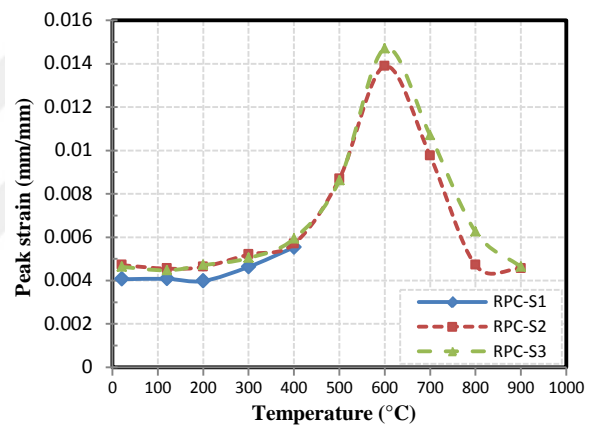


Figure 2.14 Effect of temperature on peak strain of steel fiber-reinforced RPC (Zheng et al., 2012).

2.1.5 Characteristic the stress-strain curves

Chang et al. (2006) analyzed the stress-strain relationships under the compression loading for concrete after exposure to high temperatures. The shape of the ascending curves of stress-strain of heated concrete differs for unheated concrete, it depends on the heating temperature. Also, the flatter degree of the descending curves of the stress-strain curve is increasing with the temperature increasing.

Tai et al. (2011) investigated the relationship between stress and strain of SF reinforced concrete when exposed to high temperatures. The slope of the ascending curve is decreasing and also the descending curve gradually becomes gentler with increasing temperatures.

Zheng et al. (2012) has investigated the stress-strain relationships for steel-fiber reinforced RPC subjected to temperature up to 900°C. After exposure to a temperature not exceeding 300°C, the shape of the stress-strain curve was slightly affected in comparison to the original concrete curve. After this temperature, the thermal damage within the concrete increases gradually. Therefore, the stress-strain curves become more flatter, and also the peak point on the stress-strain curve is moving to the right bottom whenever the temperature increases. In general, the descending curve of concrete without steel fiber showed more steeper, this attributed to rapid and brittle failure. However, the steel fiber contributes to enhancing the ductility of fiber-reinforced concrete, particularly after peak point. Therefore, the steel fiber can be improved the plastic deformation capacity of concrete.

Kim et al. (2013) proved that the slope of the ascending curve increased with an increase in concrete grade at the same temperature.

The ascending curve becomes nonlinear and its slope decreases as temperature rises. While the nonlinearity degree and the slope of the descending curve are also decreased gradually as temperature rises above 400°C (Zheng et al., 2015).

In general, the slope of the stress-strain curves is decreasing with the temperature increases. Also, the reduction in the slope of the descending curve is greater than that of the ascending curve for the stress-strain curves of concrete (Chen et al., 2014).

2.2 Size effect on the mechanical properties of concrete

The compressive and tensile strengths of concrete are the most important mechanical properties in the concrete structure design, which are routinely specified and tested by control specimens (Nikbin et al., 2014). The international standards and codes suggested reliance on different shapes of the test specimens of concrete. Most common shapes are the cylinder with dimensions of 150×300mm and the cube with dimensions of 150mm. These specimens are known as the standard specimens.

Yi et al. (2006) analyzed the effects of shape and size of the specimen, as well as placement direction on compressive strength based on fracture mechanics. It has been shown that the strength ratio of the cube to the cylinder decreases as the concrete grade increases.

Aslani (2013) has investigated in the effects of shape and size of different specimens on the compressive and tensile strengths of SCC specimens with and without fibers experimentally based on fracture mechanics.

Fires represent one of the most severe risks to the buildings and concrete structures. Study the temperature effects on different concrete specimens gives an indication of the affecting extent of the thermal damage for each specimen under the same conditions. Therefore, the performance of concrete structural members that have different cross-sections can be evaluated when exposed to elevated temperatures. However, no previous studies have investigated the size effect on the mechanical properties (tensile and compressive strengths) for the different specimens of FR-SCC after exposure to elevated temperatures.

2.3 Mechanical behavior of FRC corbels

2.3.1 Load-deflection behavior

Fattuhi (1987, 1988, 1994, 1994) studied the effectiveness of steel fibers in improving the mechanical behavior of RC-corbels. The test results have proven that the RC-corbels containing steel fiber exhibited considerable improvement in load-carrying capacity and maximum shear stress. The presence of steel fibers helps in increasing both toughness and ductility of RC-corbels. The steel fibers are able to raise and extend the descending portion of the load-deflection curves. In general, the shape of the load-deflection curve depends on the fiber ratio, volume of the main reinforcement, as well as shear span-to-depth ratio. However, the behavior of RC-corbels can be more ductile, when use the steel fiber as a secondary reinforcement with a relatively low volume of the main reinforcement, and tested at relatively large shear span. Therefore, it can be obtained to more gradual and ductile conduct which results in elastic-plastic behavior for the load-deflection curves of the RC-corbels.

It has been proved that the addition of steel fiber to corbel mixtures is able to change the failure mode from shear or diagonal splitting to the flexure failure, particularly when the corbel is reinforced by relatively low volumes of steel reinforcement.

Fattuhi and Hughes (1989, 1989) investigated the behavior of RC-corbels containing either stirrups or steel fibers. These secondary reinforcement enhances both shear and flexural strengths as well as a stiffness of the RC-corbels. The RC-corbels

reinforced with steel fibers usually behave more ductile and fail in flexural mode, while those reinforced with stirrups constantly fail in shear mode. When used the stirrups as a secondary reinforcement, A partial loss of corbel strength shortly after reaching maximum loads was observed. While, the improvement in ductility of the RC-corbels were more pronounced when using the steel fiber instead of the stirrups. It can be concluded that the use of the steel fibers as a shear reinforcement in corbels could be an appropriate alternative to stirrups.

Gampione et al. (2005) and Gampione et al. (2007) analyzed the steel fiber effect on flexural and shear behavior of the RC-corbels. The addition of steel fiber contributes to significantly increase in the maximum and failure loads of the RC-corbels. This improvement is proportional to the fiber content. Therefore, more toughness for load-deflection curves of the FRC corbels was observed due to increase the maximum deflection corresponding to the failure load.

Gampione (2009) studied the effect of the main reinforcement ratio on the behavior of FRC-corbels under the effect of vertical load. It was noticed that variation in the main reinforcement ratio has effectively to change the brittle to ductile behavior for the RC-corbels. The change in this property also depends on shear span-to-depth ratio and concrete strength. The presence of steel fiber somewhat helpful in improving the ductile behavior of the corbels, particularly when using relatively low percentage of main reinforcement. After that, the RC-corbels becomes more brittle as the main reinforcement ratio increase, regardless of the presence or absence of the steel fibers in the concrete used. In general, increasing the main reinforcement ratio enhance the strength, but caused an increase the brittleness of the RC-corbels.

2.3.2 Crack pattern and failure modes

From Fattuhi's studies (1987, 1988, 1994, 1994), it was identified the steel fiber effect on the crack pattern and failure modes for the RC-corbels. The presence of steel fiber is increasing the intensity of small crack which form before reaching to the maximum load of the corbels. Therefore, the RC-corbels reinforced with steel fibers can be exhibit multiple cracks at failure. The steel fiber also reduces the crack width under specific load due to bridging ability of the cracks. Therefore, the corbels reinforced by steel fibers show a smaller width of cracks under loading test. It was observed that decreasing the shear span-to-depth ratio also causes reduced width of

crack.

Fattuhi and Hughes (1989, 1989) made a comparison between the effects of steel fibers and stirrups on the failure mode of the RC-corbels. In general, the corbels containing stirrups usually fail in shear, while it is possible to change the mode of failure from shear to flexural by using sufficient volume of steel fibers. When using steel fibers as a secondary reinforcement instead of stirrups, achieve to the flexural failure can be more possible, also enhance the ductility and safety of the corbels.

Foster et al. (1996) investigated the effects of concrete grade and shear span-to-depth ratio on the crack pattern of RC-corbels. It has been proved that the first crack being to appear at the corbel-column junction from the loading face and extend toward the top junction of the corbel. The RC-corbels cracked earlier with increase the shear span-to-depth ratio and decrease the concrete strength. The number of main bars and the presence of secondary reinforcement did not effect on the first cracking load. However, an increase in the shear span-to-depth ratio cause reductions in the first cracking load.

The presence of steel fibers in the corbel mixture able to control the opening and extension of cracks during loading. Therefore, the random distribution of steel fibers within the concrete specimen reduce or somewhat prevent the cracks in all directions for the RC-corbels (Campione et al., 2005).

Gampione (2009) studied the effect of the variation in the main reinforcement ratio on the modes of failure of the RC-corbels. The variation in the main reinforcement ratio represents the main guarantor to yielding of steel reinforcement before concrete crushing in addition to the other effects such as fiber content, concrete strength, and shear span-to-depth ratio. In the presence of steel fibers, the moderate ratio of the main reinforcement increase possibility of yielding the main reinforcement of the corbel, particularly when tested at relatively wide shear span and has been produced from ordinary strength concrete. Contrarily, when using the high percentage of main reinforcement, the crushing of concrete occurs in the compressed regions, regardless of the other auxiliary factors. On the other hand, when using a high percentage of reinforcing steel, although the addition of steel fiber contributed to greatly improve in strength of corbels, but it becomes unable to change the mode of failure from brittle (concrete crushing) to more ductile (yielding of the steel reinforcement). In

general, yielding of steel reinforcement did not occur in the corbel which contains a relatively large percentage of main reinforcement. This attributed to the premature crisis for the concrete.



CHAPTER 3

EXPERIMENTAL WORK

3.1 General

A total of six SCC mixtures were prepared as follows: two concrete grades (50MPa and 80MPa) and three steel fiber (SF) ratios of 0%, 0.5% and 1% were prepared for each desired temperature. Each mixture contains of 0.1% polypropylene fiber (PP) as a volume fraction. The specimens are tested at room temperature (R.T) and after exposure to elevated temperatures 250, 500, 750°C in the experimental program.

3.2 Mixture preparation

3.2.1 Materials characteristics

Portland cement (ASTM type II) with a fineness of 295 m²/kg and specific gravity of 3.12 was used in all mixtures. Locally available crushed stone and crushed sand (from the same source) with a specific gravity of 2.65 were used as a coarse and fine aggregate, and have water absorptions of 0.8% and 1.4%, respectively. The maximum aggregate size was 11mm. Silica fume and fly ash (type F) were used in the concrete mixtures as binder additives to satisfy the SCC requirements. The chemical compositions of cement, silica fume, and fly ash are inserted in Table 3.1. A high-performance super-plasticizer was added to the mixture to obtain the required workability for the SCC.

Figure 3.1 shows the hooked-end steel fiber (SF) and polypropylene fiber (PP) that used to produce FR-SCC. The properties of the SF and PP fibers utilized in the study are shown in Table 3.2, and the proportions of the FR-SCC mixtures are listed in Table 3.3. The stress characteristics of reinforcing steel used in corbel reinforcement were presented in Table 3.4.

Table 3.1 Chemical analysis of cement and binder additives

Oxide (%)	Cement	Silica fume	Fly ash
SiO ₂	20.4	93.2	56.2
Fe ₂ O ₃	3.9	1.5	6.69
CaO	63.0	0.4	4.24
Al ₂ O ₃	4.9	0.7	20.17
MgO	1.7	0.1	1.92
SO ₃	2.0	0.1	0.49
Na ₂ O+ K ₂ O	0.9	1.4	2.36

Table 3.2 Properties of fibers used in the present study

Properties	Steel Fiber (SF)	Polypropylene fiber (PP)
Length (mm)	30	12
Diameter (mm)	0.75	0.02
Density (g/cm ³)	7.8	0.91
Tensile strength (MPa)	1200	450

3.2.2 Mix designation

The preparation of SCC has differed from that of conventional concrete due to the difference in placing and filling manner. To obtain the desired properties of SCC, it is required to fulfill three essential criteria, namely the passing and the filling ability without using vibration as well as segregation resistance. Hence, the basic experiments such as slump flow, V-funnel, and L-box are performed to measure the fresh properties of concrete used. In this study, these experiments are conducted in accordance with the EFNARC guidance (2002). The content of super-plasticizer and water-binder ratio (w/b) were 1.0%, 0.34 for FR-MSCC and 1.2%, 0.3 for FR-HSCC respectively.

Table 3.3 Mix proportions of FR-SCC mixtures.

Materials	Mix code					
	FR-MSCC			FR-HSCC		
	FR-MSCC-S0	FR-MSCC-S5	FR-MSCC-S10	FR-HSCC-S0	FR-HSCC-S5	FR-HSCC-S10
Cement (kg/m ³)	250			450		
Fine Aggregate (kg/m ³)	1000			1000		
Coarse Aggregate (kg/m ³)	667			667		
Fly ash (kg/m ³)	215			50		
Silica fume (kg/m ³)	35			35		
Water (l/m ³)	170			160		
Superplasticizer (% volume of binder)	1.0			1.2		
Steel fiber (SF) (kg/m ³)	0	39	78	0	39	78
Polypropylene fiber (PP) (kg/m ³)	0.91			0.91		
w/c*	0.68			0.36		
w/b*	0.34			0.30		

*w/c = water/cement ratio, w/b = water/binder ratio, binder content= cement+fly ash+silica fume.

Table 3.4 Stress characteristics of steel reinforcing bars

Diameter (ϕ) mm	Yield stress (MPa)	Ultimate strength (MPa)
8	550	640
10	455	588
14	480	595



Figure 3.1 Steel and polypropylene fibers.

3.2.3 Classification of mixtures

Classification of mixtures is based on their compressive strength class and the SF ratio as shown in Table 3.3. The first two letters (FR) denote that the mixture contains 0.1% of PP fiber, while the compressive strength class is represented by M for medium strength and H for high strength, followed by the SCC abbreviation of self-compacting concrete, and finally the steel fiber (SF) volume fraction. For example, FR-HSCC-S10 refers to a high-strength SCC mix with an SF ratio of 1%.

3.2.4 Preparation of specimens

3.2.4.1 The testing specimens for strength

Six mixtures were prepared for each desired temperature, resulting in 24 mixtures in total. As shown in Figure 3.2, each batch included eighteen specimens composed of six cylinders with dimensions of 150×300mm (S-150), six cylinders with dimensions of 100×200mm (S-100), three cubes with sizes of 100mm (C-100), and three cubes with sizes of 150mm (C-150). Three specimens of each type were adopted to evaluate the compressive strength, while the remaining cylindrical specimens were used to determine the tensile strength of the concrete used. All measurements are taken as the average of three readings.

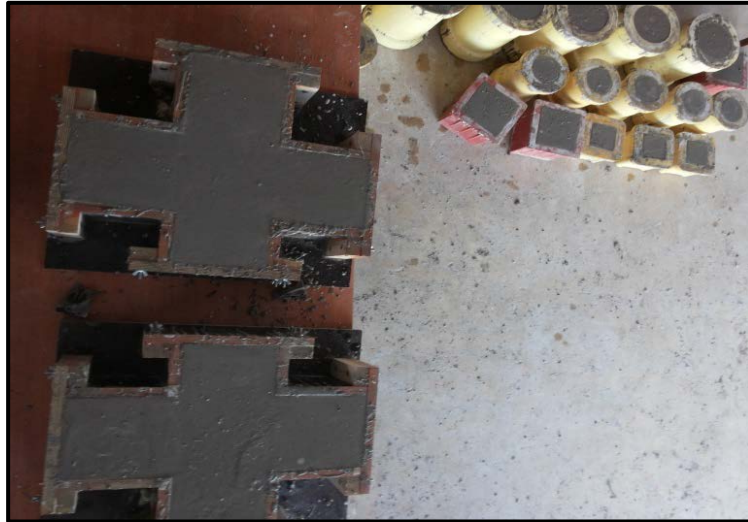


Figure 3.2 The specimens were cast in one batch.

3.2.4.2 Specimens the stress-strain testing

36 additional cylindrical specimens with dimensions of 150mm in diameter and 300mm in height were cast to study the stress-strain characteristics for concrete used such as peak stress, modulus of elasticity, and peak strain.

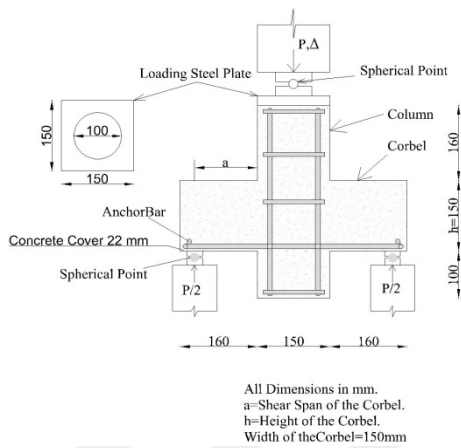
3.2.4.3 The corbel specimens

48 reinforced concrete corbels (RC-corbels) having the geometry and steel reinforcement details shown in Figure 3.3, were produced and tested in the present thesis. The height, and length of each corbel were 150 and 160mm, respectively. The details of the corbel and supporting column are shown in Figure 3.3. The RC-corbel was reinforced at the bottom (tension zone) with two longitudinal steel bars having a diameter of either 10 or 14mm. To provide additional anchorage; a cross bar of compatible diameter was welded to the longitudinal bars, close to the end of each corbel. The concrete cover for all RC-corbels were 22mm (Since the diameter of the reinforcing bars is different, the distance from the reinforcement edge to the face of the concrete has been fixing). The column segment was reinforced with four bars of 10mm in diameter confined with 8mm diameter stirrups placed on a pitch of 100mm.

The 48 RC-corbels were divided into two groups based on the grades of SCC mixtures; medium strength corbels (FR-MSCC) and high strength corbels (FR-HSCC). The FR-MSCC group is further divided into two groups to study the influence of the shear span-to-depth ratio (a/h) using $a=90$ ($a/h=0.6$) and $a=120$ mm ($a/h=0.8$). The FR-HSCC group is also further divided into two groups to study the steel reinforcement ratio (ρ) parameter. Where the first part includes corbels

reinforced with bars of $2\text{Ø}10\text{mm}$ ($\rho=0.0082$) as a main reinforcement, while the second part have been reinforced by $2\text{Ø}14\text{mm}$ ($\rho=0.016$). RC-corbels with main longitudinal bars without horizontal stirrups have been adopted on the steel fibers (SF) as a secondary reinforcement.

In this experimental program, parameters which were studied Concrete Compressive Strength (CCS), Shear Span-to-depth Ratio (SSR), and Steel Reinforced Ratio (SRR). The main aim of the present thesis is to investigate the effects of using these parameters on the mechanical behavior of FR-SCC corbels with and without SF, before and after exposure to elevated temperatures.



(a) Dimension of corbels and reinforcement details



(b) Geometry of RC-corbel

Figure 3.3 Geometry and reinforcement details of RC-corbels

3.2.5 Mixing and casting

According to the mix proportions shown in Table 3.3, the quantities of required materials for one batch have been weighted. The fine and coarse aggregates with the fibers were firstly mixed in dry conditions for 2min. Then, the binder materials containing cement, fly ash, and silica fume were added with the half amount of the water and have mixed for 1min. Finally, the remaining water and superplasticiser were pre-mixed and poured into the mixture with another 2min of mixing to consist the mixture contents. After the mixing procedure was complete, the desired experiments in fresh state are conducted to determine the fresh properties for the SCC mixture. The test specimens are cast immediately without compaction.

The specimens are covered and left for 24h in the casting room. Thereafter, they are demoulded and cured in water tank with heating control at $21\pm 1^\circ\text{C}$ until the 28 days

as shown in Figure 3.4.



Figure 3.4 Preparing the specimens after curing treatment.

3.3 Testing procedures

3.3.1 Fresh properties testing

Slump flow, V-funnel, and L-box tests were conducted to determine the fresh properties of the considered mixtures as shown in Figure 3.5. Fresh test results of the produced mixtures are inserted in Table 3.5. As can be seen in Table 3.5, the test results of Slump and L-box for the mixtures were found to be within the range recommended by EFNARC (2002). However, the V-funnel results for SCC containing steel fibers have exceeded EFNARC limits, it may be attributed to the fact that EFNARC's limits are proposed are for plain SCC. As expected, presence of fibers had a negative effect on the workability and thus leads to higher flow time.

Table 3.5 The fresh properties results of FR-SCC mixtures used.

Specimen	SF ratio (%)	Slump-flow (mm)	T500mm (s)	V-funnel flow (s)	Blocking ratio (H_2/H_1)
FR-MSCC-S0	0	700	2.62	8.22	0.93
FR-MSCC-S5	0.5	665	3.45	14.64	0.87
FR-MSCC-S10	1.0	610	4.34	19.16	0.83
FR-HSCC-S0	0	670	3.17	12.71	0.88
FR-HSCC-S5	0.5	615	4.10	18.54	0.83
FR-HSCC-S10	1.0	570	4.92	23.87	0.80
Limitation EFNARC		520-700	2-5	≤ 10	≥ 0.75



a) Slump flow for 0% SF



b) Slump flow for 1% SF



c) V-funnel test



d) L-box test

Figure 3.5 The fresh tests for SCC used.



Figure 3.6 Arrangement the specimens inside the electric furnace.

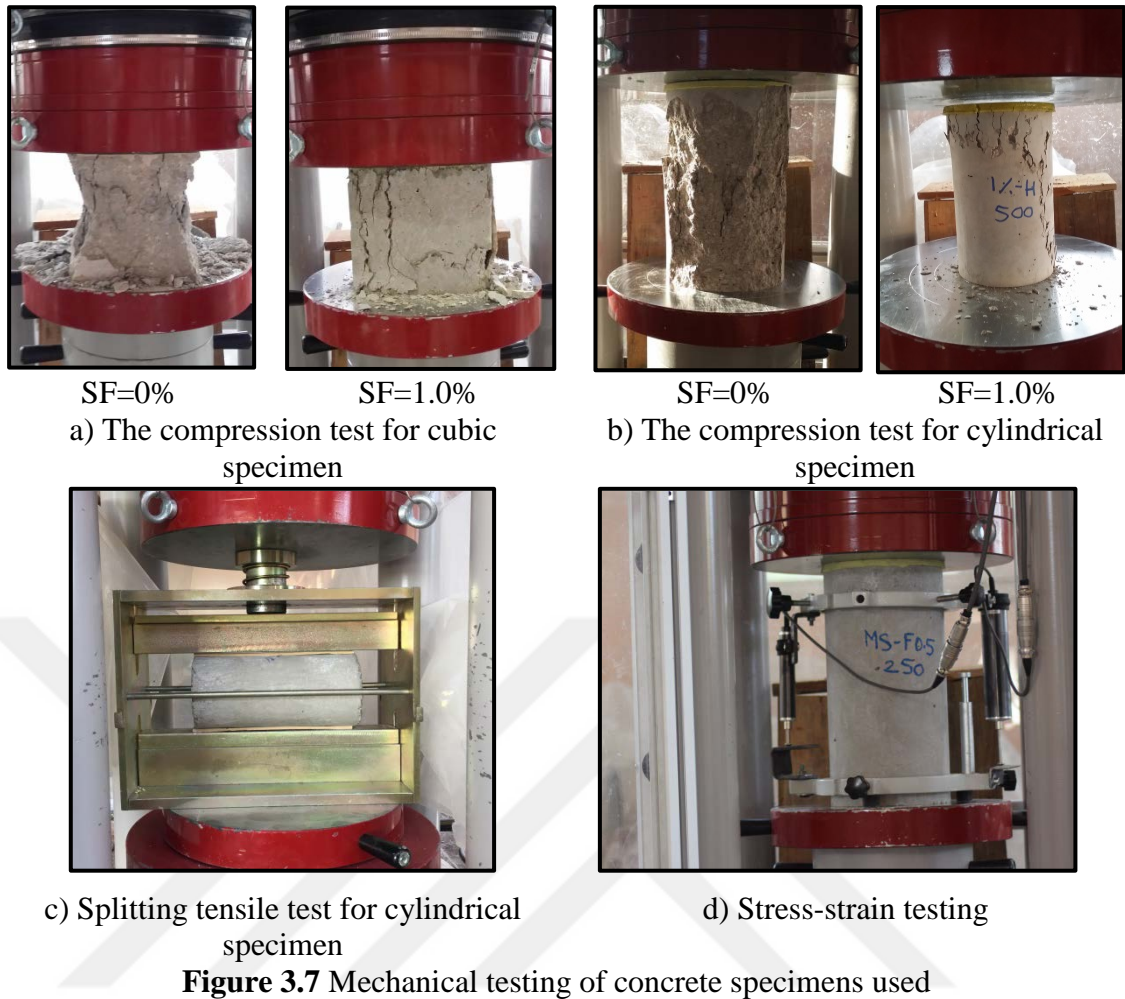
3.3.2 Heating regime

After the 28 ± 1 days of water curing process, the specimens (for one batch as shown in Figure 3.6) were placed in electrical furnace and dried at $105 \pm 5^\circ\text{C}$ for 24 hours to reduce the moisture content in order to mitigate spalling-induced explosion as reported by Jansson and Bostrom (2013). The specimens were heated at a rate of $5^\circ\text{C}/\text{min}$ until the desired temperatures of 250°C , 500°C , and 750°C , respectively. The specimens were maintained at the desired temperature for 60 minutes in order to ensure that the specimens were homogeneously heated as recommended in studies by Lau and Ansoon (2006), and Pliya et al. (2011). The specimens were then naturally cooled down to room temperature in the span of a 24 hours prior to loading tests.

3.3.3 Loading test

3.3.3.1 Procedure of mechanical properties testing

Cubic (C-100 and C-150) and cylindrical (S-100 and S-150) specimens were tested in universal testing machine with 3000 kN-capacity. Compressive strength was determined in accordance with ASTM (2004) and BS1881 (2002) standards for cylindrical and cubic specimens, respectively as shown in Figure 3.7 (a and b). According to the specification, the loading rate for C-100, C-150, S-100 and S-150 are 2, 4.5, 1.5 and 3.5 kN/s, respectively. Splitting tensile test was performed on two different sizes of cylindrical specimens (S-100 and S-150) and was conducted as per ASTM (2004) as shown in Figure 3.7 c. S-100 and S-150 cylindrical specimens were loaded with a rate of 1.0 and 1.5 kN/s, respectively, for splitting tensile strength test. Test results represent the average of three readings for corresponding specimens measurements of each mechanical parameter.



3.3.3.2 The testing procedure of stress-strain curves

Stress-strain tests were performed on the standard cylindrical specimens with reference to ASTM (2004), using a universal 3000 kN-capacity testing machine. This machine was operated in a displacement controlled mode with a slow rate of 0.2mm/min. Axial displacement of the cylinders under compression were measured by two linear variable displacement transducers (LVDT). The LVDTs were set at two opposite locations in the mid-height region of the cylinders. The vertical distance of the LVDT was 225mm as shown in Figure 3.7 d. All strain values were calculated by averaging the two LVDT readings.

The test was terminated when a sudden decrease in load around 20% of the peak stress was observed. Corresponding stress data was collected using a computerized data-logging system. The stress-strain data were obtained by averaging the results of three specimens for the same mixture. In addition to predicting the stress-strain behavior of the cylindrical specimen, important compressive properties such as

compressive strength (peak stress), modulus of elasticity, and peak strain were obtained. Each value indicates the average results of corresponding measurements for a sample set consisting of three specimens.

3.3.3.3 Mechanical behavior testing for RC-corbels

The load carrying capacity tests of RC-corbels were performed using a 500kN-capacity hydraulic servo-controlled testing machine. After cooling the RC-corbels, they were painted and marked, such that any cracking could be clearly traced; the loads at which the formation and propagation of cracks initiated were recorded. The RC-corbels were tested in an inverted position, and were vertically loaded only at the top end of the corbel's column. The load scheme is shown in Figure 3.8. Since the dimensions of bearing plate has a significant impact on load-capacity for the corbel (Kriz and Rath, 1965), the same supports and loading plates were used in all tests to achieve smooth comparison. Loading tests were implemented according to the configuration which was proposed by many researchers for double-sided corbels [Fattuhi (1987), Fattuhi and Hughes (1989a), Fattuhi and Hughes (1989b), Fattuhi (1988), Fattuhi (1994)]. All corbels were placed on two supports and the load was applied to the column and then transferred to the corbels by reaction forces existing on the supports. Width of the supports (w) is 20 mm and the contact length of the supports is equal to the width of the corbels. The dimensions of the loading plate are shown in Figure 3.3. The machine was operated in a displacement controlled mode with a displacement rate of 0.2 mm/min to identify and observe the post-peak behavior of the corbels in detail. The deflection was measured using two LVDTs. These were placed at two opposite sides of the corbel-column junction at the tension side of the corbel's beams. The corbels were loaded on two supports; one being a roller support, and the other being a pin which allows free rotation, while preventing translational motion in horizontal and vertical direction. These supports are placed at a distance ($a=90\text{mm}$ or 120mm) from the face of the column as shown in Figure 3.8. The deflection value was obtained as average values of two LVDT readings for each specimen. In addition to the load-deflection curves, the first cracking load, maximum load, and failure load were recorded for all RC-corbels. The first cracking load is the load value that is recorded when the first crack appeared in the corbels during testing. Maximum load represents the highest load which the corbel can withstand without failure during the test. Failure load is the final load value that is recorded when the

specimen fails. During testing, cracks were marked with corresponding loads and the crack patterns were diagnosed to identify the failure modes for each RC-corbel.



a) Computerized data-logging system



b) Adjusting the LVDT during the testing

Figure 3.8 Load capacity testing for RC-corbels

CHAPTER 4

COMPRESSIVE AND TENSILE STRENGTHS OF FR-SCC BEFORE AND AFTER EXPOSURE TO ELEVATED TEMPERATURES

4.1 General

The studies on the mechanical properties of fiber-reinforced self-compacting concrete (FR-SCC) exposed to elevated temperatures is very limited. Limited information has been reported on the residual strengths of SCC with hybrid fibers. In this chapter, emphases were placed on understanding the behavior and modeling the compressive and tensile strengths of SCC with hybrid fibers before and after subjected to elevated temperatures.

4.2 Compressive strength

The mean value of compressive strength results for FR-SCC used (6 mixtures) at room temperature (21°C) have been listed in Table 4.1. Each value was obtained by averaging the result of three corresponding specimens. It can be seen that the target compressive strength of both types of SCC were achieved satisfactorily after 28 days. The addition of SF generally did not improve the compressive strength for concrete specimens at room temperature. This may be attributed to that the SFs contributed to reduce the workability of concrete.

Figure 4.1 illustrates the compressive strength of FR-SCC with and without SF, before and after subjected to elevated temperatures. A general tendency is the reduction in compressive strength with the temperature increases. However, a slight increase in strength is observed after exposure to 250°C, which can be attributed to fully complete hydration (Zheng et al. 2012), followed by water migration towards the pores (Fares et al. 2010, Dias et al., 1990). Once the temperature increases further, the generated water increases the internal pressure, which causes thermal cracks to form, followed by a significant reduction in the compressive strength. Beyond 500°C, it was observed that the compressive strength, drop sharply with the

increase in temperature for both SCC types (FR-MSCC and FR-HSCC), therefore, It can be concluded that the 500°C represent the critical temperature for SCCs when exposed to elevated temperatures.

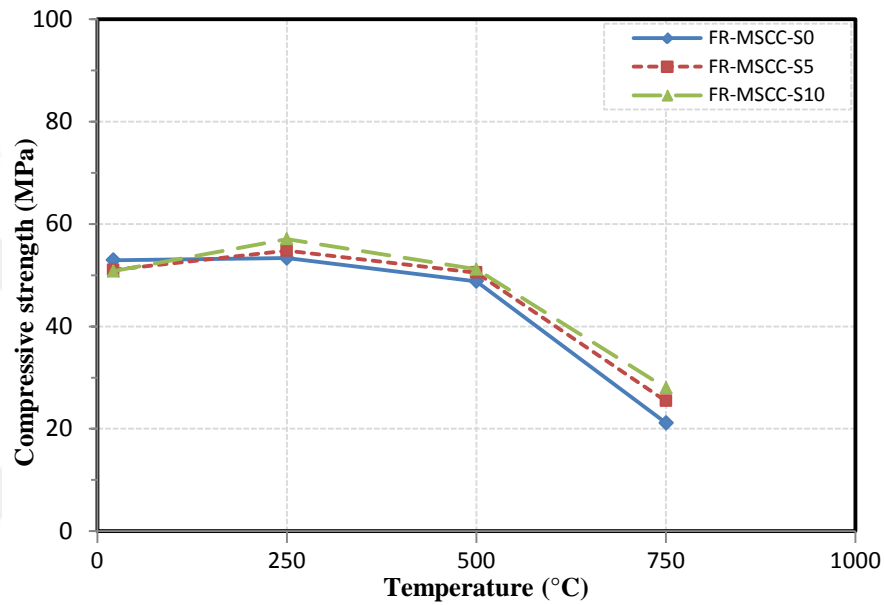
Furthermore, the contraction in the cement paste and the expansion of aggregate result in weaker bonding within concrete mixtures (Bakhtiyari et al., 2011, Fares et al., 2010). No spalling was observed for SCC specimens at any temperature level, it can be controlled by use of polypropylene fibers (PP).

Figure 4.2 shows the relative residual compressive strength for FR-SCC specimens after exposure to 250, 500, and 750°C. When concrete specimens are exposed to the same temperature, the results indicated that the relative residual strength decreases as the concrete grade increases. Therefore, the residual strength of FR-MSCC specimens were ranged 39-53% of the original strength after exposure to 750°C. While the residual strength of FR-HSCC specimens ranged 34-50% for the same condition. It can be concluded that level of deterioration and degree of affectedness for heated concrete are increasing with increase the degree of concrete. For all SCC mixtures, there was retaining a level of compressive strength about 44% on average after exposure to 750°C. Therefore, the level of preservation is much higher than that for conventional HSC, which has not greater than 25% when exposed to the same temperature (Khaliq and Kodur, 2011). This high performance in compressive strength for SCC proves that it has superior microstructure even at high temperatures (Sideris at al., 2007).

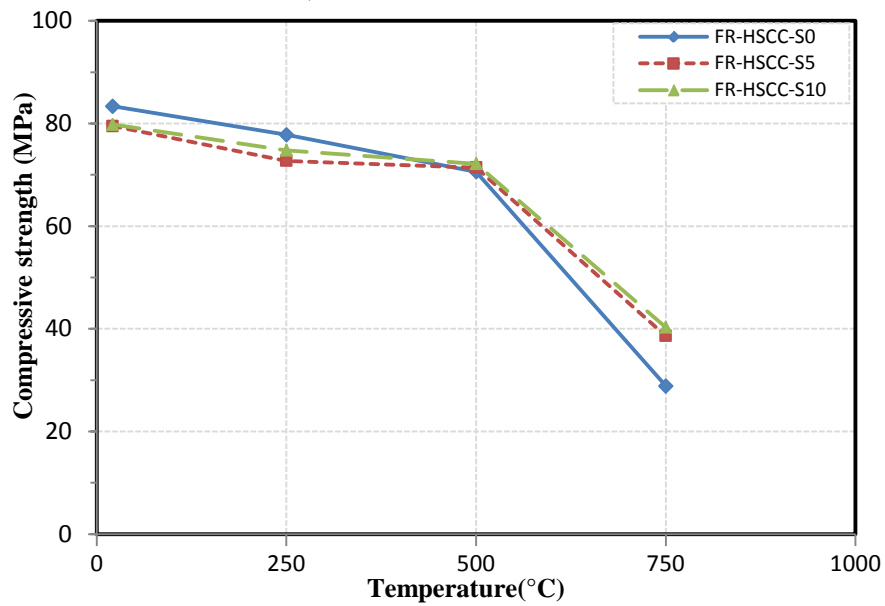
Table 4.2 shows the loss in compressive strength for both SCC mixtures after exposure to elevated temperatures up to 750°C. It was observed a severe loss in compressive strength after the temperature is increasing more than 500°C. This attributed to decompose the calcium hydroxide in a concrete matrix (Zheng et al. 2013). With the addition of steel fiber to concrete mixtures, there was a noticeable improvement of compressive strength, particularly after exposure to high temperatures. Thus, when adding 1% of SF, it can be reduced loss of strength by 25% for the specimens exposed to 750°C. On the other hand, the loss in the strength is increasing with increase the rigidity of concrete.

Table 4.1 Compressive and tensile strengths of FR-SCC specimens at room temperature.

Mix code	SF %	Compressive strength (MPa)	Tensile strength (MPa)
FR-MSCC-S0	0	52.9	4.6
FR-MSCC-S5	0.5	51.1	6.4
FR-MSCC-S10	1.0	50.8	6.3
FR-HSCC-S0	0	83.4	4.3
FR-HSCC-S5	0.5	79.5	8.2
FR-HSCC-S10	1.0	79.8	9.2

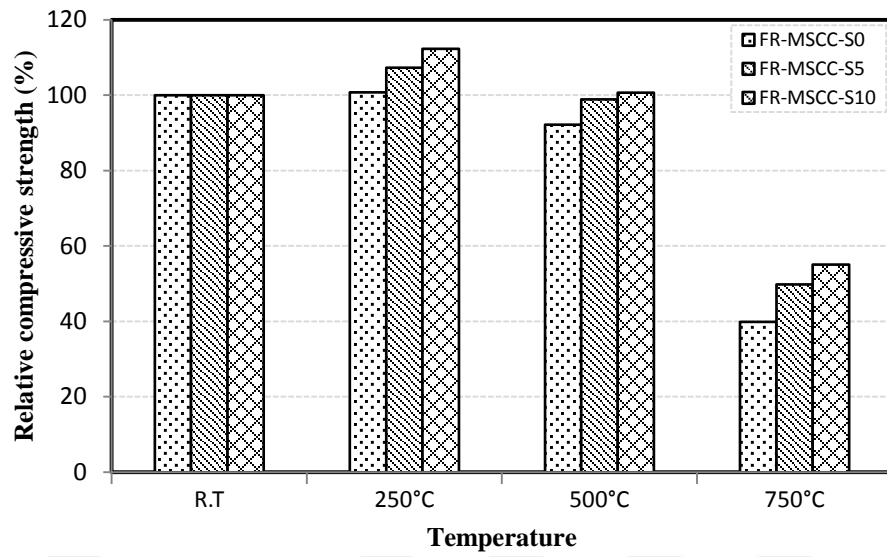


a) FR-MSCC mixtures

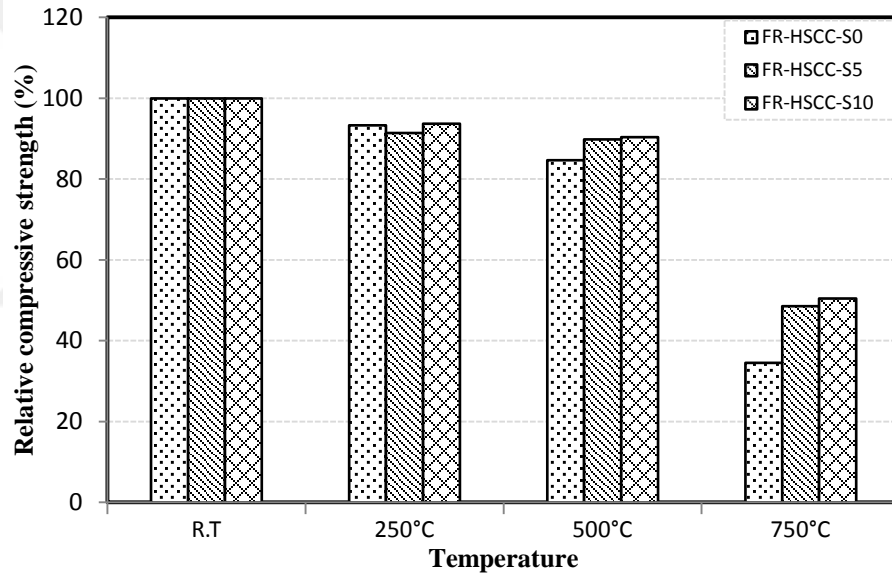


b) FR-HSCC mixtures

Figure 4.1 Compressive strength of FR-SCC specimens before and after exposure to elevated temperatures



a) FR-MSCC mixtures



b) FR-HSCC mixtures

Figure 4.2 Relative residual compressive strength of FR-SCC specimens after exposure to elevated temperatures

Table 4.2 The relative loss in compressive strength of FR-SCC specimens after different temperatures.

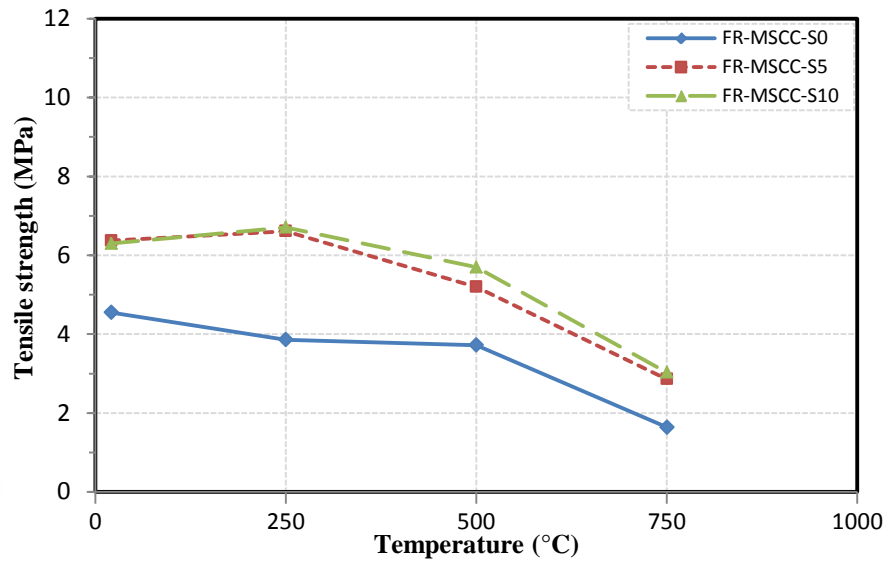
Relative loss $\left(\frac{f'_c - f'_{c,T}}{f'_c}\right)$ (%)	21°C	250°C	500°C	750°C
FR-MSCC-S0	----	-0.76*	7.78	60.09
FR-MSCC-S5	----	-7.35*	1.06	50.21
FR-MSCC-S10	----	-8.11*	3.12	46.96
FR-HSCC-S0	----	6.69	15.33	65.42
FR-HSCC-S5	----	8.54	10.18	51.44
FR-HSCC-S10	----	6.29	9.56	49.5

*greater than unheated original strength.

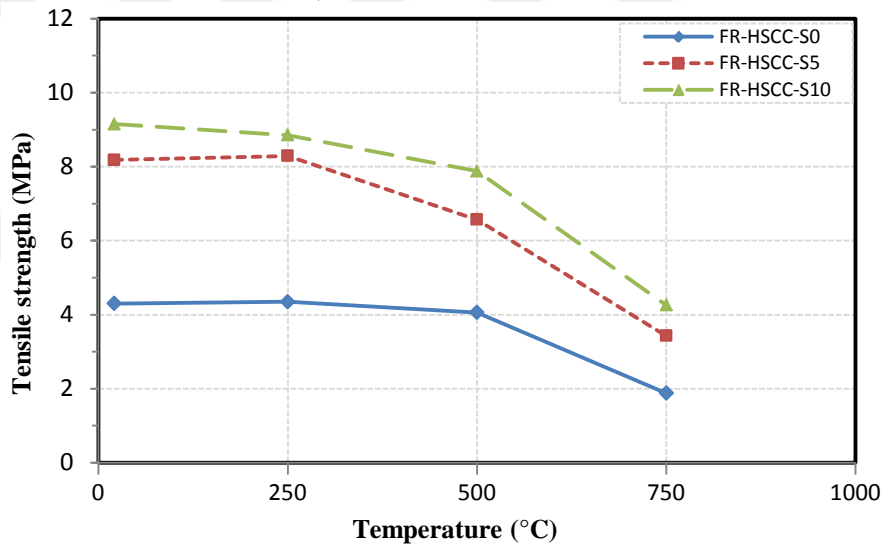
4.3 Splitting tensile strength

Figures 4.3 and 4.4 show the results of absolute and relative splitting tensile strength for both concrete classes (FR-MSCC and FR-HSCC) after different temperatures. It was observed that the reduction in the tensile strength was sharper than the loss of the compressive strength for both FR-SCC types with increasing the temperature. The addition of SF, however, led to significant improvement in the tensile strength, as evidenced in Figure 4.3. The results indicated that when the concrete grade increases the tensile strength is increasing, but the loss in the tensile strength is also increased after exposure to the same temperature.

It can be seen that the presence of SF results in considerable improvement in tensile strength, whereas this efficiency decreases relatively with the increase in concrete grade after exposure to the same temperature. The enhancement of SFs for tensile strength can be attributed to their influence on bridging of cracks, thus reduce or prevent develop the cracks under tensile loading. It is worth mentioning that the efficiency of SF is decreasing due to oxidation after exposure to temperature higher than 500°C (Ding et al., 2012), in addition to rapid development for the thermal cracks under loading effect. These causes may be contributed to sharp losses in tensile strength of FR-SCC after exposure to 750°C.

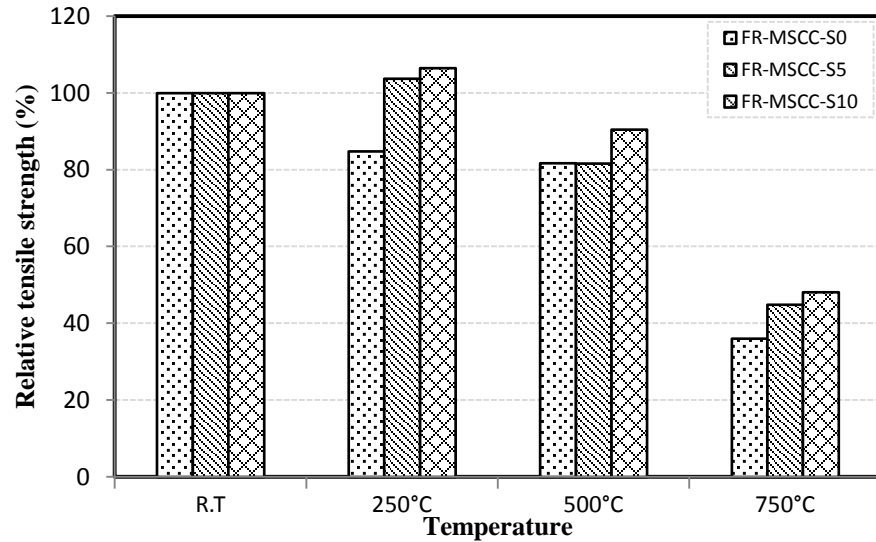


a) FR-MSCC mixtures

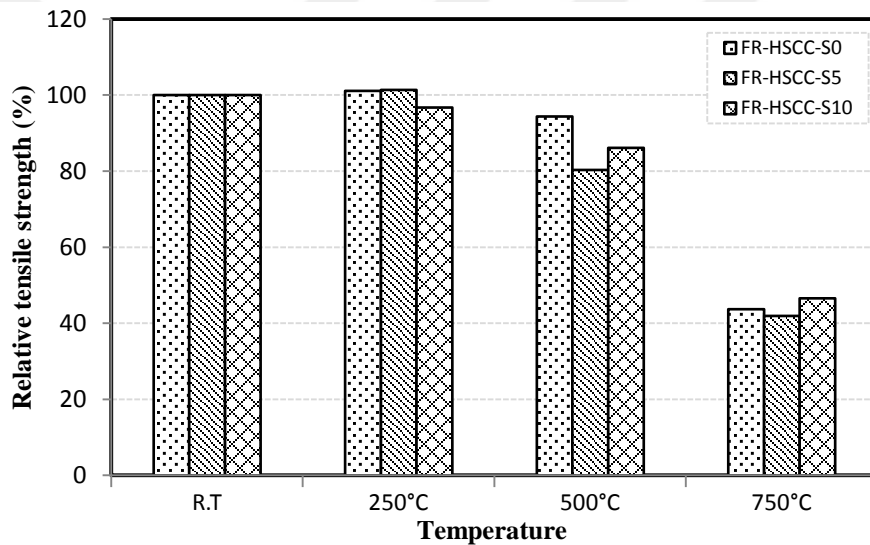


b) FR-HSCC mixtures

Figure 4.3 Splitting tensile strength of FR-SCC specimens exposed to elevated temperatures



a) FR-MSCC mixtures



b) FR-HSCC mixtures

Figure 4.4 Relative residual tensile strength of FR-SCC exposed to elevated temperatures

4.4 The Internal Cracks and Fiber reacting

The ability of PP fibers in reducing or preventing the spalling of the SCC specimens and SFs in improving the residual mechanical properties can be a precondition for using hybrid fibers as fire resistance materials. SF can reduce the thermal expansion in a concrete matrix induced by rapid change in temperature (Ding et al. 2010). Within reason of the SF having a higher heat transfer coefficient, it can mitigate the large temperature gradient and restrict the crack development in SCC via the bridging effect (Ding et al., 2012, Chan et al., 2000).

The images taking by scanning electron microscope (SEM) show that some macro cracks have been controlled on their extension by using SFs.

The difference in thermal expansion between SF and concrete can result in various thermal strains during heating and cooling processes. However, the thermal expansion of SF is assumed to be mainly along the fiber length (Chan et al., 2000, Poon et al. 2004, Lau and Anson, 2006). Yet, for concrete, a three-dimensional thermal field must be considered. Thus, the thermal cracks may occur parallel or transverse to the fiber axis (Ding et al.,2012). Higher SF content may result in a reduction in the difference of thermal stresses in the FR-SCC matrix as a result of high heat transfer coefficient of SFs. One of the concerns is that the bond behavior might be affected negatively by the strains transverse to the fiber axis. The various parallel strains, on the other hand, may also occur during heating and cooling processes as shown in Figure 4.5.

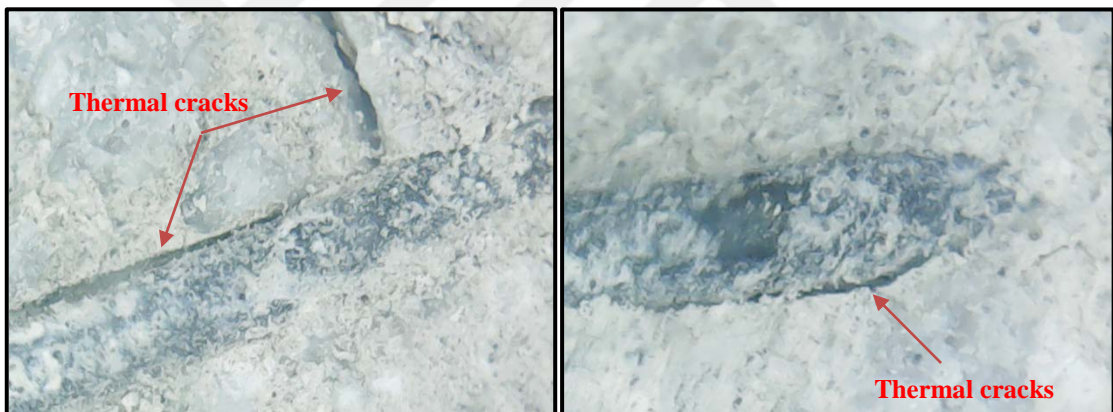


Figure 4.5 Thermal cracks between matrix and SF after exposure to 750°C.



Figure 4.6 Micro channels formed by melting of PP fibers.

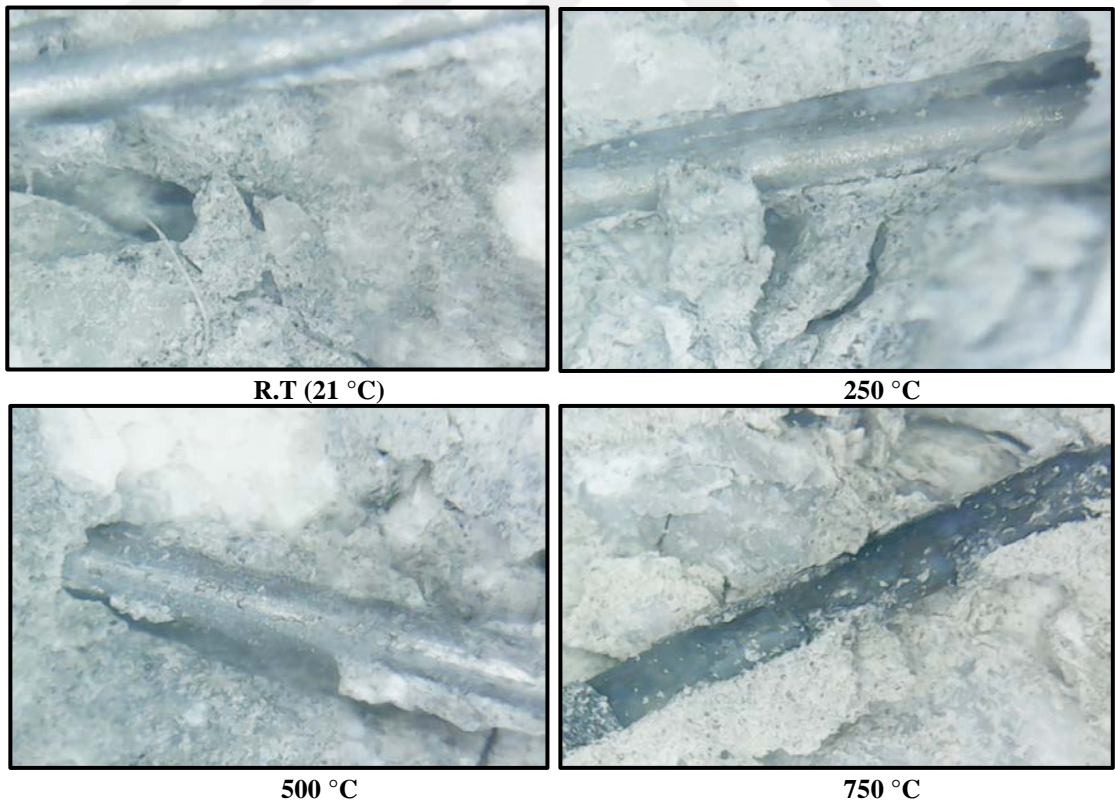
Traces of melted PP fibers can act as micro-channels as shown in Figure 4.6, allowing release of the water vapor to disperse within the channels and reduce the internal pressure, followed by a mitigation of spalling risk.



FR-MSCC-S10 mixture

FR-HSCC-S10 mixture

Figure 4.7 The oxidation and carbonation of SF after exposure to 750°C.



R.T (21 °C)

250 °C

500 °C

750 °C

Figure 4.8 Shape the SF after exposure to different temperature.

On the other hand, the high fly ash content increases the porosity of concrete at elevated temperatures (Pathak and Siddique, 2012, Sahmaran et al. 2005). This causes the expansion of pores and thus leads to greater permeability after exposure to elevated temperatures. Consequently, there is greater permeability available to initiate oxidation in the SF at elevated temperatures. Comparing the FR-SCC mixtures after exposure to 750°C, the oxidation of SF in FR-MSCC is more than that of FR-HSCC counterparts, as shown in Figure 4.7.

Figure 4.8 compares the SF shapes after different temperature levels (21, 250, 500, 750°C). It can be concluded that the SFs were not exhibit corrosion even after exposure to 500°C.

4.5 Numerical study

An experimental results database of the present study is an effective tool to utilize the mechanical property relationships for different classes of FR-SCCs after exposure to elevated temperatures. The mechanical properties include compressive strength and tensile strength of SCC. Non-linear regression analyses were carried out to propose these relationships by using the experimental data of the present study. The dependent parameters of the proposed model consisted of the compressive strength (f'_c) at room temperature, steel fiber ratio (V_f) and temperature degree (T), to obtain the compressive strength and tensile strength of FR-SCC after exposure to elevated temperatures.

By using the following formulas, the compressive strength (f_c) and splitting tensile strength (f_t) after exposure to elevated temperatures (T) can be estimated for all classes of SCCs with and without steel fibers (V_f):

i) Compressive strength (f_c):

$$\begin{aligned}
 f_{c(f'_c, V_f, T)} &= f(f'_c, V_f, T) \\
 \Rightarrow f_{c(f'_c, V_f, T)} &= f(f'_c, V_f) \times f(T, V_f) \\
 \Rightarrow f_{c(f'_c, V_f, T)} &= f(f'_c, V_f) \times \left[1 + \left(\frac{T \times V_f}{\alpha} \right) + \left(\frac{T}{\beta} \right)^2 + \left(\frac{T}{\gamma} \right)^4 - \left(\frac{T}{\lambda} \right) - V_f \times \left(\frac{T}{\eta} \right)^3 - \left(\frac{T}{\mu} \right)^3 \right] \quad (1)
 \end{aligned}$$

ii) Tensile strength (f_t):

$$ft_{(f'_c, V_f, T)} = f(f'_c, V_f, T)$$

$$\Rightarrow ft_{(f'_c, V_f, T)} = f(f'_c, V_f) \times S(T, V_f)$$

$$\Rightarrow ft_{(f'_c, V_f, T)} = f(f'_c, V_f) \times \left[\frac{1}{15.67} + \left(\frac{V_f}{\alpha} \right) + \left(\frac{T}{\beta} \right)^2 + \left(\frac{T}{\gamma} \right)^4 - \left(\frac{T}{\lambda} \right)^3 - \left(\frac{V_f}{\eta} \right)^2 - V_f \times \left(\frac{T}{\mu} \right)^2 \right] \quad (2)$$

Where $f_{(f'_c, V_f)}$ is a common term used in all proposed formulas, which is a function of compressive strength (f'_c) at room temperature and steel fiber ratio (V_f), and equal to:

$$f(f'_c, V_f) = f'_c \times f(V_f) = f'_c \times \left(1 - \frac{V_f^{0.9251}}{25.24} \right) \quad (3)$$

Where:

f'_c is the normal compressive strength without fibers at room temperature.

$f_{(f'_c, V_f, T)}$ is the compressive strength of SCC with SF% (V_f), and after exposure to temperature (T).

$ft_{(f'_c, V_f, T)}$ is the tensile strength of SCC with SF% (V_f), and after exposure to temperature (T).

The $\alpha, \beta, \gamma, \lambda, \eta,$ and μ are empirical constants used in above mentioned proposed relationships, shown in Table 4.3.

Table 4.3 Empirical constants were used in mechanical properties calculations

Mechanical properties	α	β	γ	λ	η	μ
Compressive strength (f_c)	3454.2	326.6	565.3	619.6	1927.2	378.2
Tensile strength (f_t)	10.48	2056.1	1219.6	1101.6	26.75	4939.4

By use of the proposed formulas, the numerical values of the mechanical properties of fiber-reinforced self-compacting concrete before and after exposure to elevated temperatures can be calculated easily and practically (just by substituting the f'_c , SF% (V_f), and T). The range of SF is from 0 to 1.0% and the highest permissible temperature is 1000°C.

The correlation coefficients (R^2) for Eqs. (1) and (2) are 0.97 and 0.92, as shown in

Figures 4.9 and 4.10 respectively.

Determination of the compressive strength at an elevated temperature is illustrated by the following example, in order to show the effectiveness of the formulas;

Example: If $f'_c=65$ MPa (Compressive strength at room temperature), SF ratio (V_f) =0.5% and the compressive strength at temperature (T) =750°C is required;

Solution:

1st stage: calculate $f_{(f'_c, V_f)}$:

Substitute the $f'_c= 65$ and $V_f= 0.5$ in the Eq. 3 (to take the SF effect into account) :

$$f_{(f'_c, V_f)} = f_{(65, 0.5)} = f'_c \times \left(1 - \frac{V_f^{0.9251}}{25.24} \right) = 65 \times \left(1 - \frac{(0.5)^{0.9251}}{25.24} \right) = 63.644 \text{ MPa.}$$

2nd stage: calculate $f_{(T, V_f)}$: substitute the $V_f= 0.5$ and $T=750^\circ\text{C}$ in the second part of

$$\text{Eq. 1.: } f_{(T, V_f)} = f_{(750, 0.5)} = 1 + \left(\frac{T \times V_f}{\alpha} \right) + \left(\frac{T}{\beta} \right)^2 + \left(\frac{T}{\gamma} \right)^4 - \left(\frac{T}{\lambda} \right) - V_f \times \left(\frac{T}{\eta} \right)^3 - \left(\frac{T}{\mu} \right)^3$$

when:

$\alpha = 3454.2, \beta = 326.6, \gamma = 565.3, \lambda = 619.6, \eta = 1927.2, \mu = 378.2$ (from table 4.3),

therefore:

$$f_{(T, V_f)} = 1 + \left(\frac{750 \times 0.5}{3454.2} \right) + \left(\frac{750}{326.6} \right)^2 + \left(\frac{750}{565.3} \right)^4 - \left(\frac{750}{619.6} \right) - 0.5 \times \left(\frac{750}{1927.2} \right)^3 - \left(\frac{750}{378.2} \right)^3 = 0.4417$$

3rd stage: Calculate the compressive strength (after 750°C and with SF=0.5%):

$$f_{c(65, 0.5, 750)} = f_{(f'_c, V_f)} \times f_{(T, V_f)} = f_{(65, 0.5)} \times f_{(750, 0.5)} = 63.644 \times 0.4417 = 28.11 \text{ MPa.}$$

Another mechanical properties can be calculated (tensile strength) by using corresponding equations (Eqs. 2).

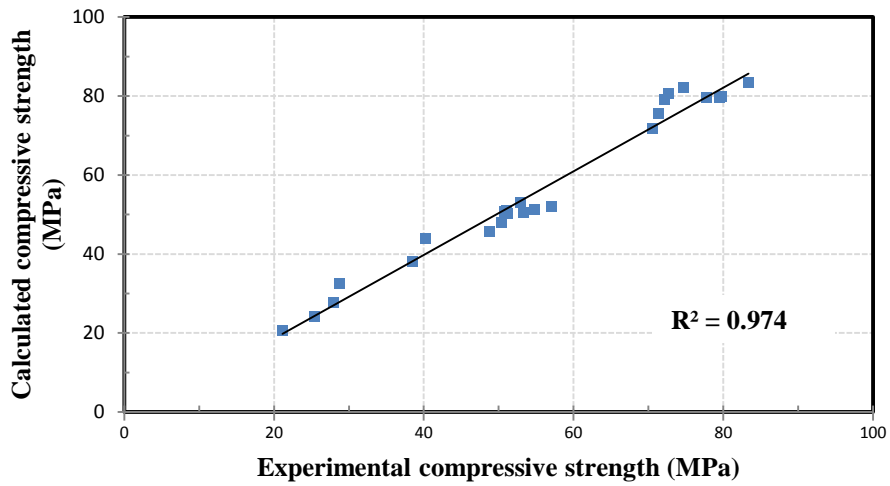


Figure 4.9 Comparison between experimental and calculated compressive strength of FR-SCC specimens.

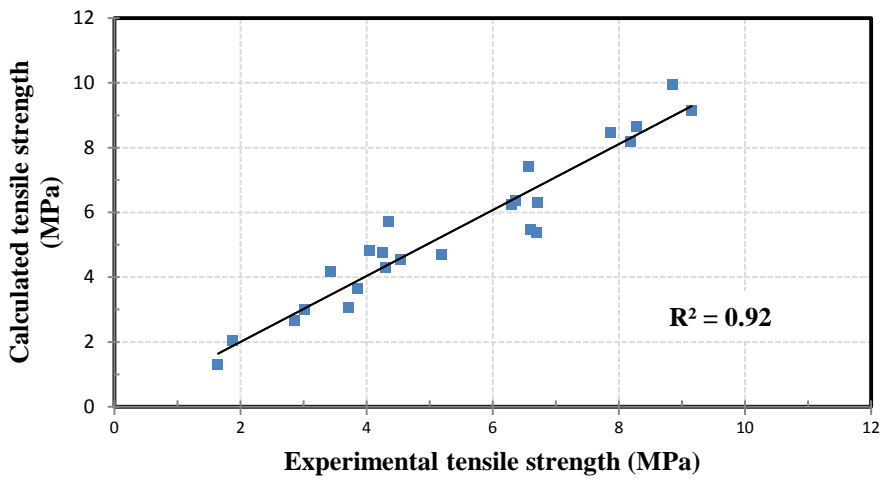


Figure 4.10 Comparison between experimental and calculated tensile strength of FR-SCC specimens.

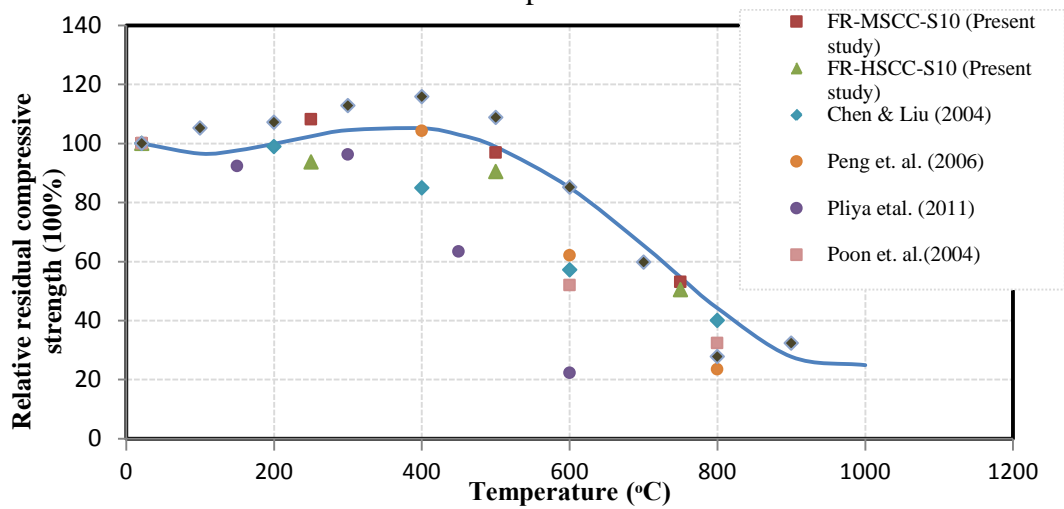


Figure 4.11 Comparison of proposed models against experimental test results for residual compressive strength.

CHAPTER 5

CONSTITUTIVE STRESS-STRAIN RELATIONSHIPS OF FR-SCC AFTER EXPOSURE TO ELEVATED TEMPERATURES

5.1 General

Investigation of the temperature effect on the compressive behavior of SCC is essential to evaluate and repair the damaged concrete structures due to fire (Poon et al., 2004). Therefore, development of a realistic stress-strain relation under compressive loading is crucial for predicting the behavior of structural members at elevated temperatures (Zheng et al., 2012). Although numerous studies focusing on the mechanical properties of SCC at room temperature are available, the study covering the compressive behavior of SCC subjected to high temperatures is very limited (Aslani and Samali, 2015). This chapter aims to understand the compressive behavior of FR-SCC specimens before and after exposure to elevated temperatures up to 750°C. The effect of the SF ratio (0%, 0.5%, 1.0%) and temperature level (room temperature, 250°C, 500°C and 750°C) on various mechanical properties including, elastic modulus, peak strain, peak stress, and stress-strain behavior of SCC, is investigated. The novelty of this study lies within the facts that (i) it analyses the effect of SF on the compressive behavior of SCC exposed to elevated temperatures, and (ii) it proposes a constitutive model to predict the stress-strain behavior of fire-exposed FR-SCC specimens, for the first time in literature.

5.2 Stress-strain characteristics

5.2.1 Compressive strength (Peak stress)

Table 5.1 and Figure 5.1 show the compressive strength ($f'_{c,T}$) of fiber-reinforced self-compacting concrete (FR-SCC) specimens with and without SF, and before and after exposure to elevated temperatures. As shown in Figure 5.1, despite the slight increase after exposure to temperatures below 250°C, the compressive strength of FR-SCC decreases in general as temperature rises. When the FR-SCC specimens

were heated to 250°C, the compressive strength increased by nearly 10%.

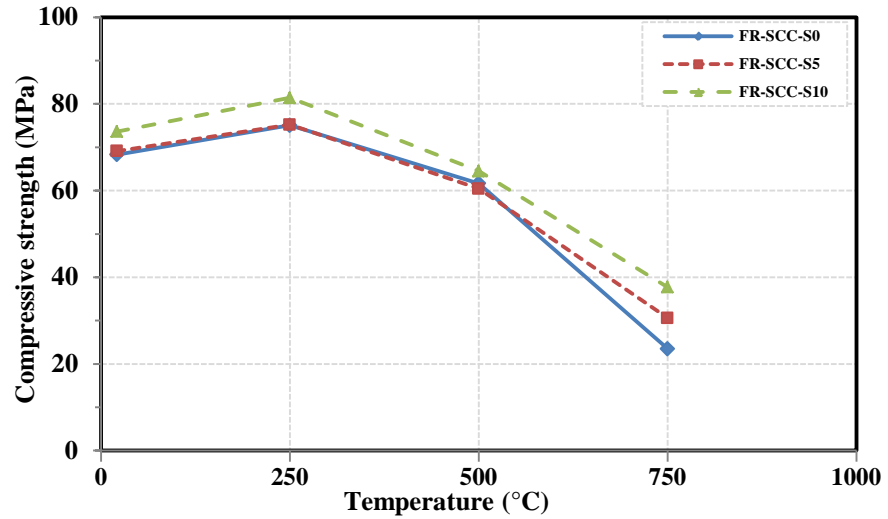
Beyond this temperature, thermal cracks start to appear in the FR-SCC specimens due to the incompatibility of thermal stresses between cement paste and aggregate. These cracks develop rapidly with the temperature increase. During the compression test, extension and width of the thermal cracks propagate quickly, thus resulting in a decline in the compressive strength. Therefore, when FR-SCC-S0, FR-SCC-S5 and FR-SCC-S10 specimens were exposed to 500°C, their residual strengths were 90%, 87%, and 88%, respectively, of the unheated compressive strength. It is noteworthy that the compressive strength of the FR-SCC specimens suffers a quicker loss after exposure to temperatures higher than 500°C. This can be attributed to the decomposition of calcium hydroxide between 400 and 600°C (Zheng et al., 2013). This confirms that the critical temperature for FR-SCC specimens is 500°C. The compressive strength of FR-SCC-S0, FR-SCC-S5, and FR-SCC-S10 specimens decreased by about 66%, 56%, and 49%, retaining more than 35% of its original strength after exposure to 750°C. Thus, the compressive strength drops abruptly with temperatures higher than 500°C, resulting in a potential severe damage in the concrete structure.

The effectiveness of SF on the residual compressive strength is shown in Figure 5.1 (b). The FR-SCC specimens reinforced with SF of 1% have higher compressive strength before and after subjected to elevated temperatures. In particular, after exposure to 750°C, the residual strength of FR-SCC-S10 (reinforced with SF of 1%) was 1.5 times greater than FR-SCC-S0 (without SFs). It can be concluded that SF has a significant contribution to reduce the negative effect of elevated temperature on the residual compressive strength of SCCs.

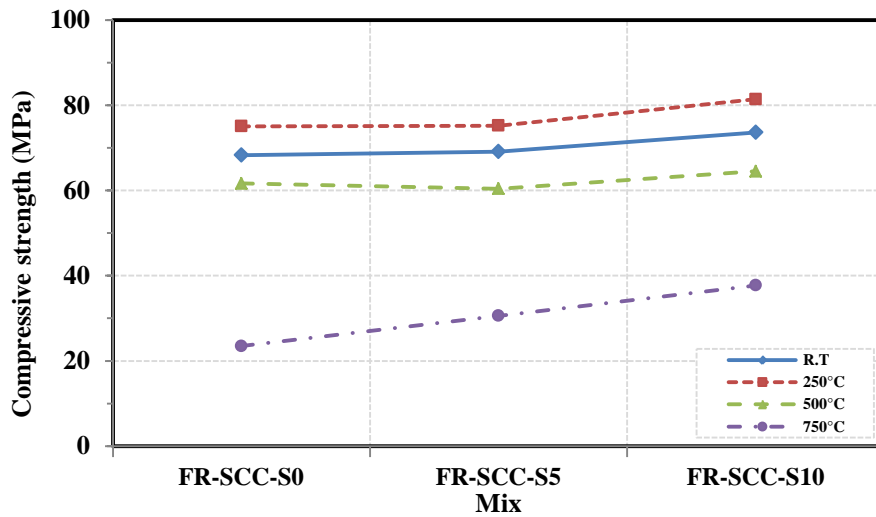
Table 5.1 The results of compressive properties of FR-SCC cylinders before and after exposure to elevated temperatures

Temperature (°C)	Compressive strength ($f'_{c,T}$) (MPa)			Elastic modulus ($E_{c,T}$) (GPa)			Peak strain ($\epsilon'_{c,T}$) ($\times 10^{-3}$ mm/mm)		
	FR-SCC-S0	FR-SCC-S5	FR-SCC-S10	FR-SCC-S0	FR-SCC-S5	FR-SCC-S10	FR-SCC-S0	FR-SCC-S5	FR-SCC-S10
21	68.3 (1.0)*	69.1 (1.0)	73.6 (1.0)	42.0 (1.0)	41.1 (1.0)	35.2 (1.0)	2.2 (1.0)	2.7 (1.0)	2.7 (1.0)
250	75.1 (1.10)	75.2 (1.09)	81.4 (1.11)	34.0 (0.81)	30.0 (0.73)	32.9 (0.94)	2.8 (1.27)	2.7 (1.01)	3.0 (1.1)
500	61.6 (0.90)	60.4 (0.87)	64.5 (0.88)	15.1 (0.36)	12.8 (0.31)	18 (0.51)	4.1 (1.84)	5.2 (1.92)	5.0 (1.85)
750	23.5 (0.34)	30.6 (0.44)	37.7 (0.51)	5.3 (0.13)	6.2 (0.15)	7.8 (0.22)	5.3 (2.39)	6.2 (2.28)	6.3 (2.33)

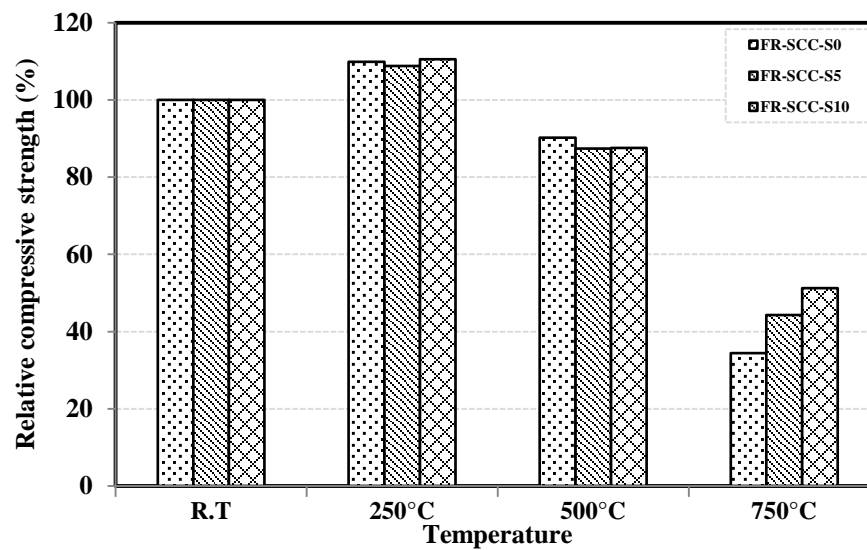
*The value between two brackets represents the relative residual value.



(a) Effect of temperature level on compressive strength



(b) Effect of steel fiber content on compressive strength



(c) Effect of temperature level on relative compressive strength

Figure 5.1 Effect of temperature on the compressive strength of FR-SCC. (R.T = room temperature)

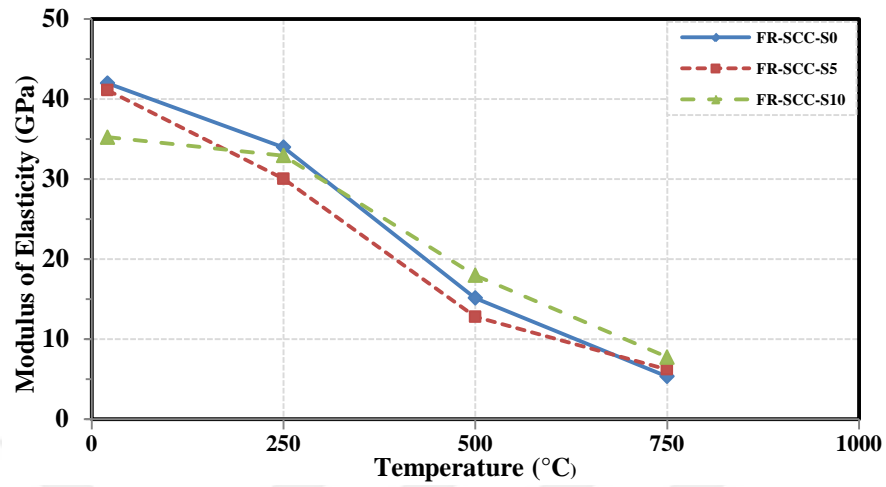
It is observed that the strength retention level of SCC reinforced by 1% SF was 51%, even after exposure to 750°C, while the residual strength of conventional high-strength concrete (HSC) at the same conditions were about 31%, 34% and 44% (Poon et al., 2004, Lau and Anson, 2006, Peng et al., 2006), respectively. In general, the SF performance with the SCC is more efficient than with the conventional HSC. In this study, no explosive spalling was observed at any temperature because specimens underwent heat treatment to minimize the water content and PP fibers were added to the SCC mixtures.

5.2.2 Modulus of elasticity

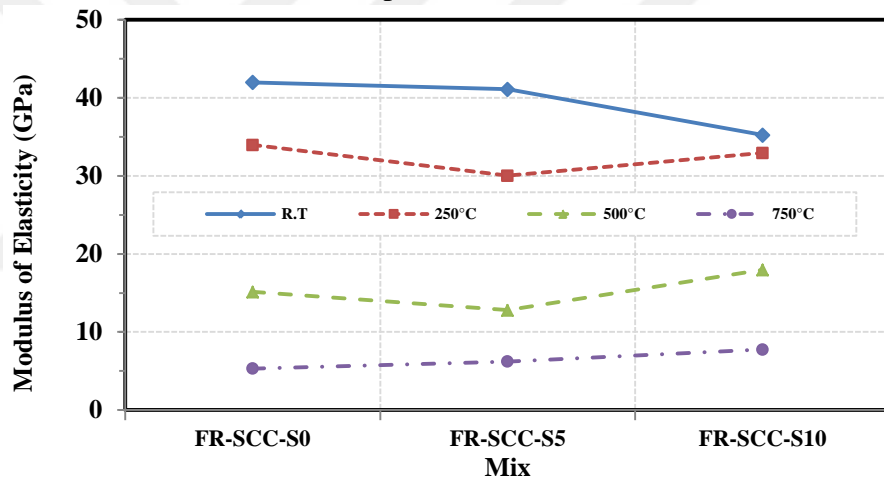
Investigation of the temperature effect on the elastic modulus of concrete is also significant for the evaluation and rehabilitation of concrete structures subjected to fire damage. Elastic modulus of heated and unheated SCC specimens is calculated depending on the secant modulus which corresponds to 40% of the maximum stress obtained from stress-strain graphs. The variation of elastic modulus ($E_{c,T}$) of FR-SCC is illustrated in Table 5.1 and Figure 5.2 for different SF ratios before and after exposure to elevated temperature levels. In general, after heating the specimens, thermal cracks initiate and develop due to loading resulting in a decrease in the compressive strength (peak stress) and increase in the corresponding strain (peak strain), thereby declining the ascending slope of the stress-strain curve and resulting in reduction of the elastic modulus. When exposed to temperatures not higher than 250°C, the elastic modulus yield comparable decreases by 17% for all FR-SCC specimens. Thereafter, the elastic modulus continues to quickly decrease with temperature increase. After exposure to 500°C, the elastic modulus of FR-SCC-S0, FR-SCC-S5, and FR-SCC-S10 decreased to 64%, 69% and 51%, of its original value, respectively. After exposure to temperatures higher than 500°C, the thermal cracks develop much more quickly, leading to a rapid decline for the slope of the ascending part of the stress-strain curve, which reduce the elastic modulus. Thereafter 750°C, the elastic modulus of FR-SCC-S0, FR-SCC-S5, and FR-SCC-S10 decreases by 87%, 85%, and 78%, respectively.

As shown in Figure 5.2 (b), SF has a positive effect on the enhancement of elastic modulus of FR-SCC mixtures, particularly after exposure to high temperatures. In general, the reduction in the elastic modulus is higher than the loss of the

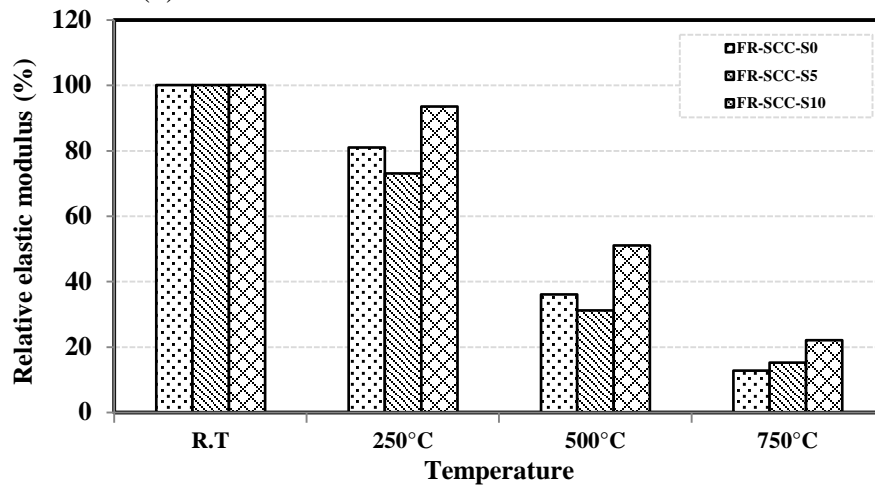
compressive strength for the FR-SCC specimens when subjected to the same temperature levels.



(a) Effect of temperature level on elastic modulus



(b) Effect of steel fiber content on elastic modulus

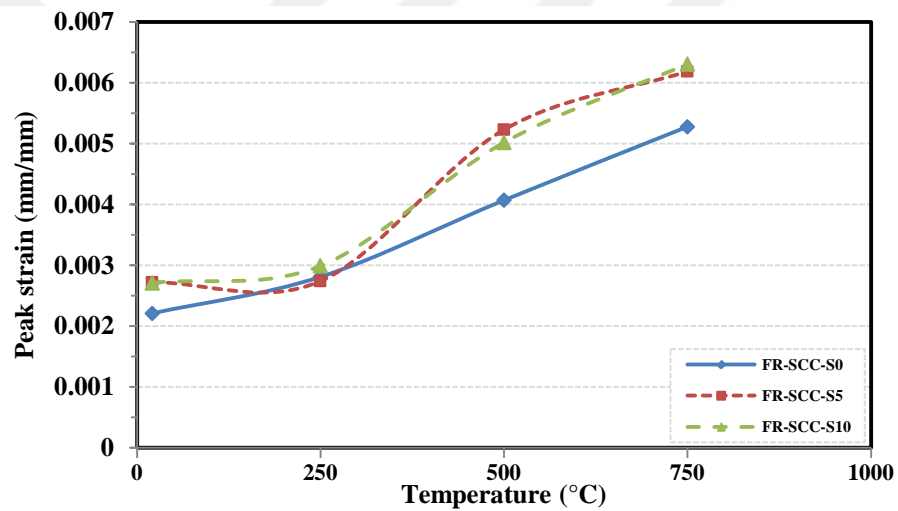


(c) Effect of temperature level on relative elastic modulus

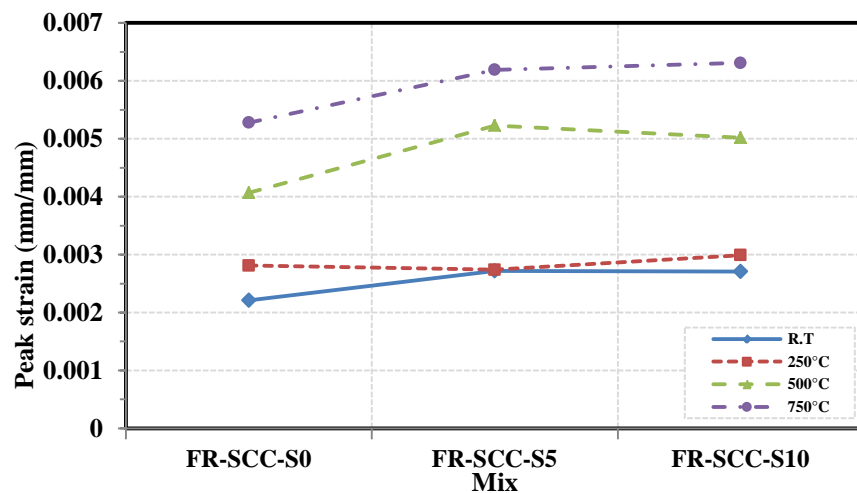
Figure 5.2 Effect of temperature on the elastic modulus of FR-SCC.

5.2.3 Peak strain

The peak strain ($\epsilon'_{c,T}$) of FR-SCC specimens with and without SF obtained from compression tests after exposure to different temperatures is shown in Table 5.1 and Figure 5.3. After exposure to 250°C, the peak strain yielded a moderate increase compared to the original unheated specimen. At temperatures higher than 250°C, thermal cracks begin to appear in the FR-SCC specimens. The cracks rapidly expand during loading and thus increase the peak strain. For specimens exposed to 500°C, the peak strain of FR-SCC-S0, FR-SCC-S5, and FR-SCC-S10 increased by 84%, 92% and 85% respectively. At temperatures higher than 500°C, several cracks are formed and later expanded in compression test.



(a) Effect of temperature level on peak strain



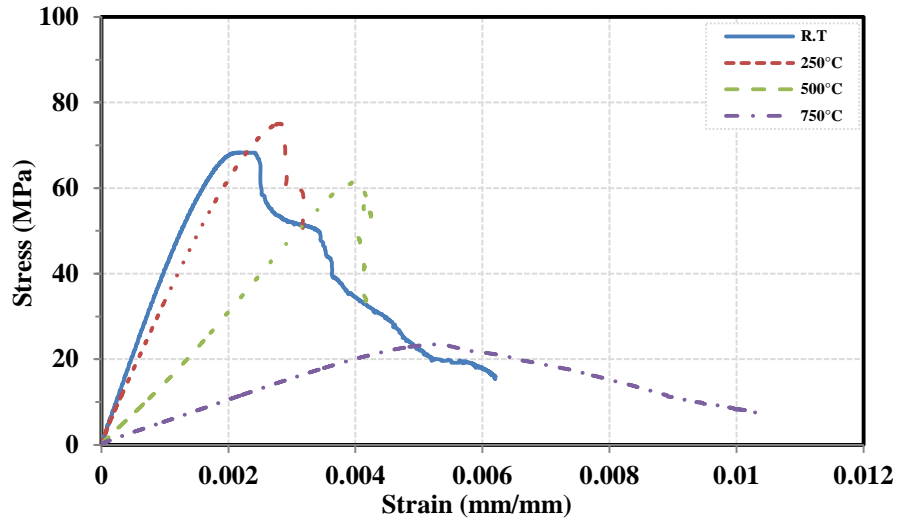
(b) Effect of steel fiber content on peak strain

Figure 5.3 Effect of temperature on the peak strain of FR-SCC. (R.T = room temperature)

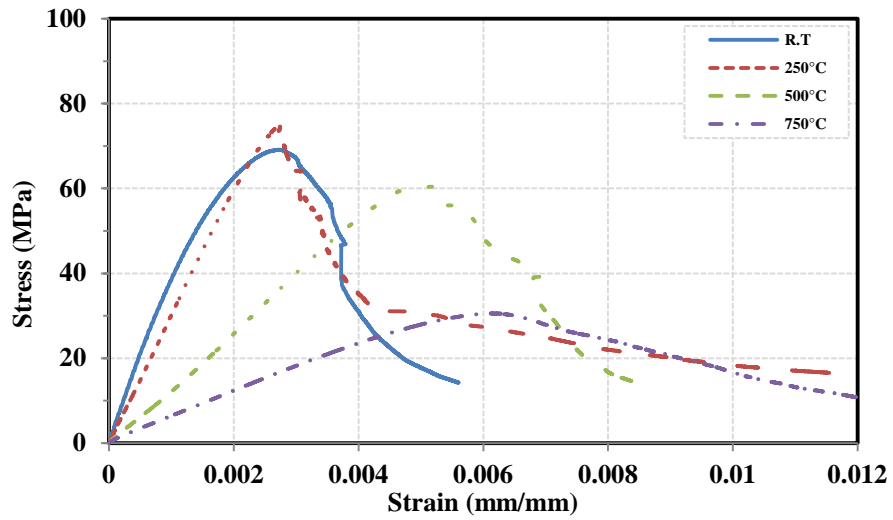
In general, the addition of SF to the FR-SCC mixtures led to a change in the trend of peak strain from linear to exponential shape when the temperature is less than the critical temperature (500°C). The concrete deterioration caused an decrease in crack intensity, leading to relative reductions in peak strain and thus changing the behavior of peak strain to linear after exposure to 750°C.

5.2.4 Compressive stress-strain curve

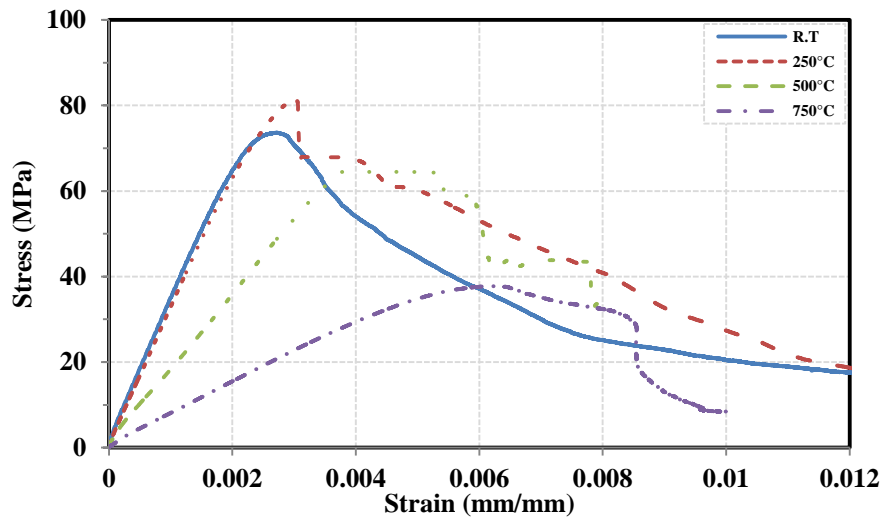
Figure 5.4 shows the stress-strain curves ($f_{c,T}, \epsilon_{c,T}$) for FR-SCC specimens obtained from the compression tests before and after exposure to elevated temperatures. Each stress-strain curve is the average of the three specimen results. In general, FR-SCC behaves elastically at the beginning of loading. Therefore, the relationship between stress and corresponding strain is almost linear until the peak stress (i.e. Compressive strength). The post-peak behavior (descending path) of the stress-strain curve depends on the temperature level and the presence of steel fiber. After exposure to 250°C, the stress-strain trended slightly upward as a result of increase in the peak stress for all FR-SCC specimens.



(a) Stress-strain curves for **FR-SCC-S0** exposure to different temperatures



b) Stress-strain curves for **FR-SCC-S5** exposure to different temperatures



(c) Stress-strain curves for **FR-SCC-S10** exposure to different temperatures

Figure 5.4 Stress-strain curves of FR-SCC with various steel fiber content exposure to different temperatures.

In general, it can be concluded that SF improves the peak stress, enhances the post-peak performance, and extends the descending curve, thus contribute considerably to the increase the ductility of the stress-strain curve. Therefore, the FR-SCC specimens reinforced with SF showed additional ductile behavior after exposure to higher temperatures as shown in Figure 5.5. Provision of SF and PP fibers together contributed to improvements in the ductility and durability for SCC specimens after exposure to elevated temperatures. It is observed that the SFs increased the slope of the ascending curve and helped to extend the descending part of the stress-strain curve of FR-SCC specimens as shown in Figure 5.5. Figure 5.6 shows the crashed FR-SCC specimens after compression tests, for heated and unheated mixtures. A larger damage is visible for samples heated up to 750°C.

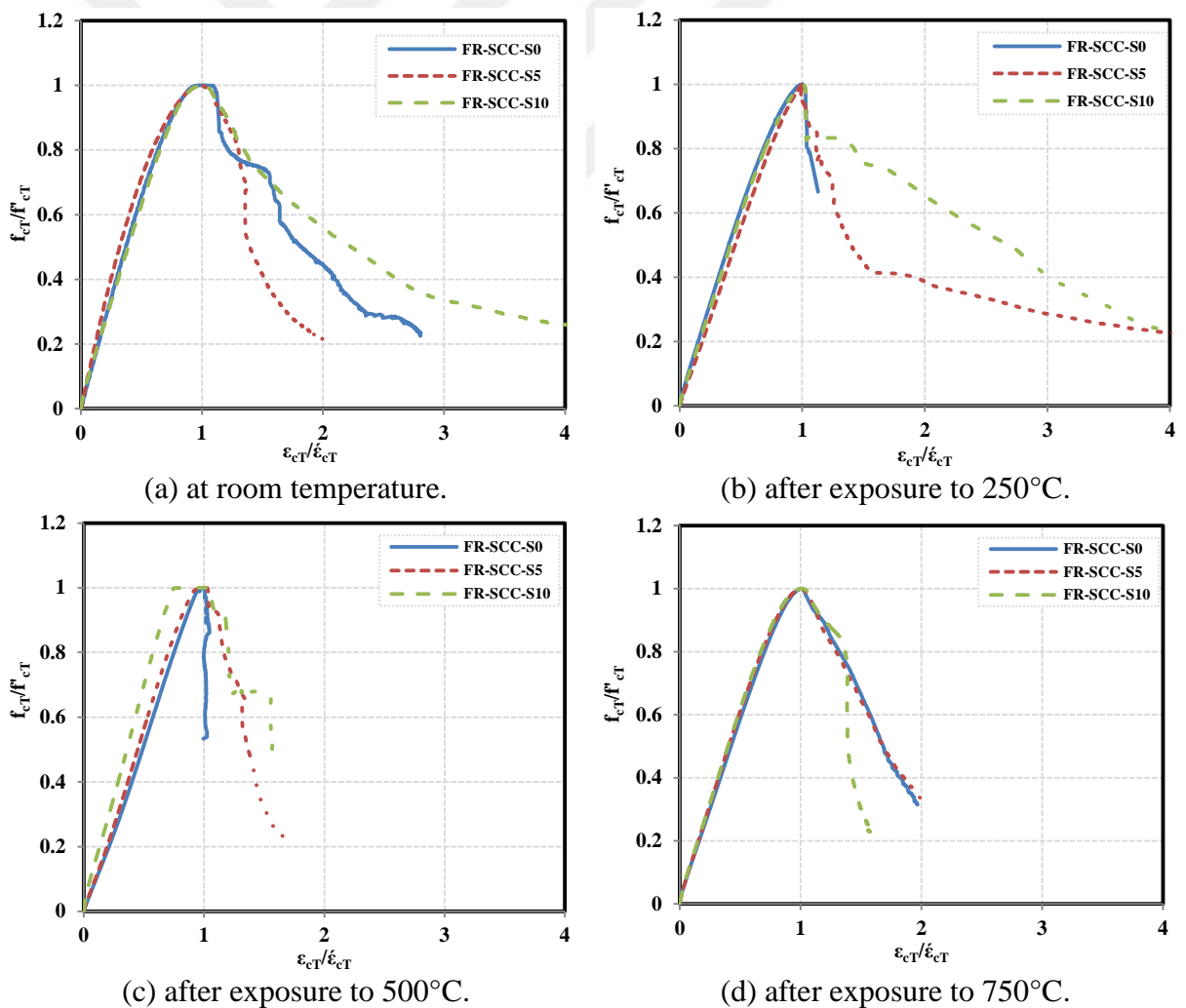


Figure 5.5 Normalized stress-strain curves for FR-SCC specimens before and after exposure to elevated temperatures.

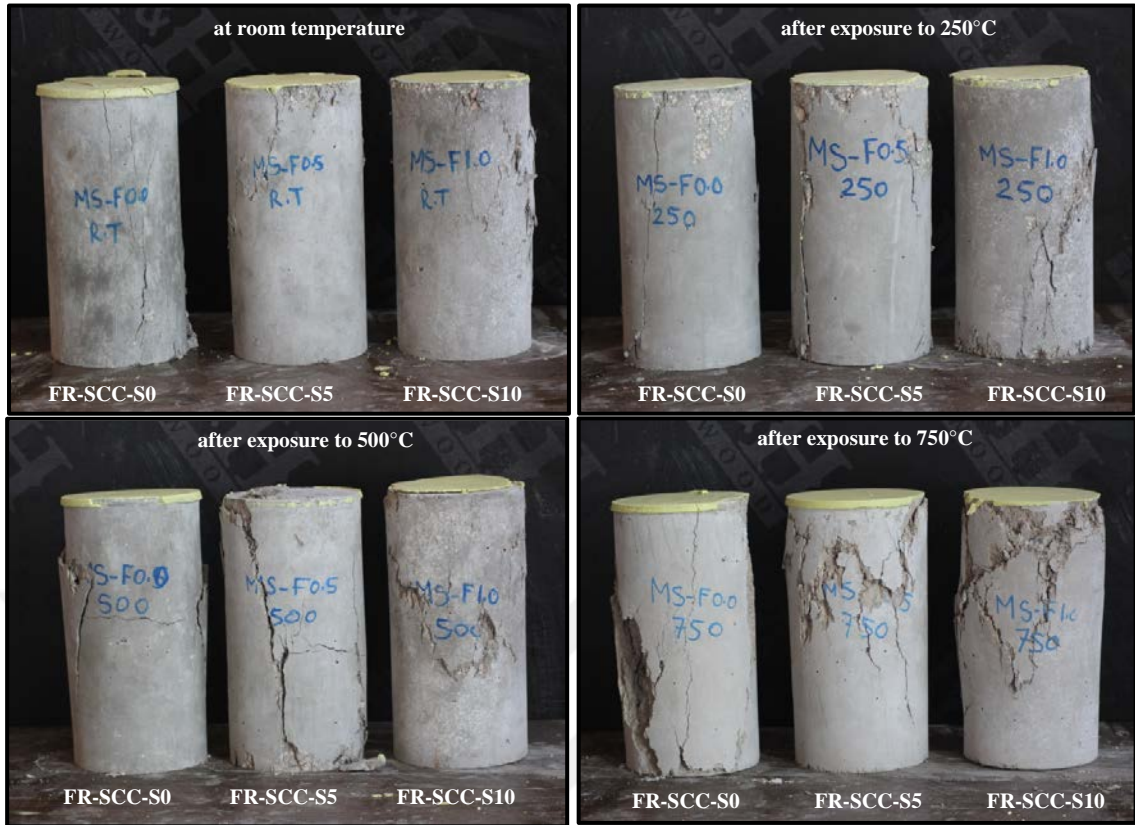


Figure 5.6 Compressive failure modes for cylinders of FR-SCC with various steel fiber content after different temperatures

5.3 Development of the stress-strain relationship

5.3.1 Basic model equation

In the present study, the stress-strain relationship (Eq.1) proposed by Popovics (1973) for normal strength concrete at room temperature is used for modification:

$$\frac{f_c'}{f_c} = \frac{x \cdot r}{r - 1 + x^r} \quad (1)$$

$$\text{Where, } r = \frac{E_c}{E_c - E_p} \quad \text{and} \quad E_p = \frac{f_c'}{\epsilon_c}$$

5.3.2 Proposed model

Proposed model takes SF and temperature effects into account and presents a general formula to simulate the stress-strain relationship for fiber-reinforced self-

compacting concrete (FR-SCC) after exposure to elevated temperatures as shown below:

$$\frac{f_{c,T}}{f'_{c,T}} = \frac{n \left(\frac{\varepsilon_{c,T}}{\varepsilon'_{c,T}} \right)}{n-1 + \left(\frac{\varepsilon_{c,T}}{\varepsilon'_{c,T}} \right)^n} \quad (2)$$

where

$$n = n_1 = 18.22r - 8.83 \quad \text{if } \varepsilon_{c,T} \leq \varepsilon'_{c,T} \quad (3-a)$$

$$r = E_{p,T} / E_{c,T} \quad (3-b)$$

$$n = n_2 = 3.26 + T \times V_f \times r + 2.77 \times \text{Cos}(\alpha - \beta) \quad \text{if } \varepsilon_{c,T} \geq \varepsilon'_{c,T} \quad (4-a)$$

$$\alpha = 7.86 \times T \times V_f \times r \quad (4-b)$$

$$\beta = \text{Cos} \left(25046.42 \times T \times V_f \times r \right) \quad (4-c)$$

In Equations (3-a) and (4-a); n_1 and n_2 represent the independent parameters that control the shape of ascending and descending parts of the curves, respectively. The ascending parameter (n_1) is related to the $\left(\frac{E_{p,T}}{E_{c,T}}\right)$ ratio. As previously mentioned in section 5.2.4, it can be concluded that the steel fiber content (V_f) and temperature (T) significantly affects the shape of the descending parameter (n_2) of the stress-strain curve where $f_{c,T}, f'_{c,T}$ and $\varepsilon_{c,T}, \varepsilon'_{c,T}$ are stresses and the corresponding strains on the stress-strain curve of FR-SCC after exposure to elevated temperature (T). $E_{c,T}$ and $E_{p,T}$ are the elastic modulus at 40% of peak stress $\left(\frac{0.4f'_{c,T}}{\varepsilon_{c,T}}\right)$ and secant modulus at maximum stress $\left(\frac{f'_{c,T}}{\varepsilon_{c,T}}\right)$, respectively. The proposed equations

are valid for SF content between 0 and 1% and temperature levels between room temperature and 750°C. The stress-strain curve for each SCC specimen can be easily obtained by taking the corresponding compressive strength and elastic modulus values for any selected strain value.

5.3.3 Verification of proposed model

In order to check the generalization capability of the proposed model, experimental stress-strain curves were compared to proposed ones for all types of FR-SCC after different temperatures, as shown in Figure 5.7. A good agreement is observed between experimental and numerical stress-strain curves obtained by the proposed equations.

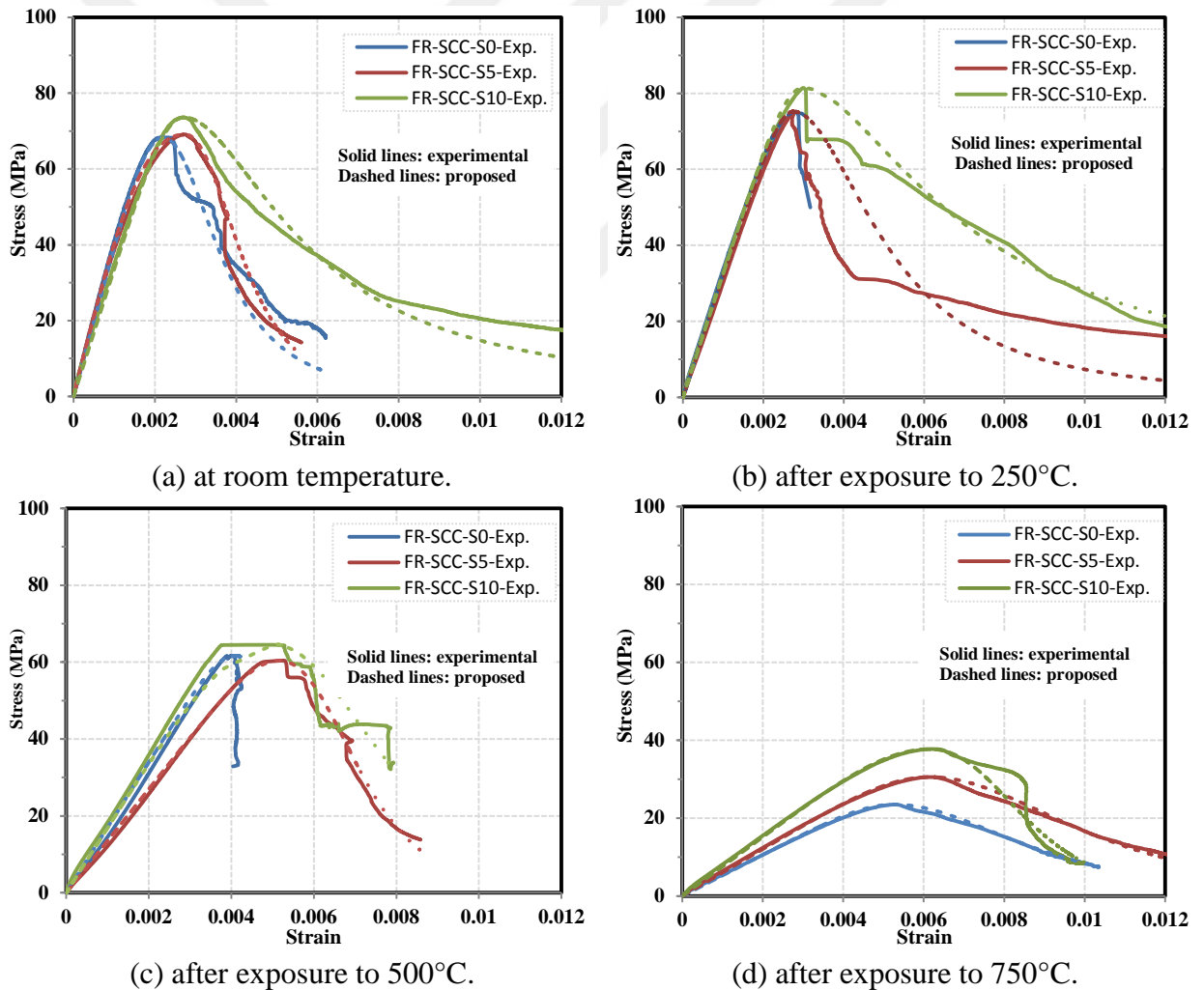


Figure 5.7 Comparison of proposed with experimental stress-strain curves for FR-SCC cylinders before and after exposure to elevated temperature.

CHAPTER 6

SIZE EFFECT ON RESIDUAL STRENGTH OF FR-SCC AFTER EXPOSURE TO ELEVATED TEMPERATURES

6.1 General

Fire is one of the most severe risks to a building or structure. A research related with the temperature effect on different concrete specimens gives an indication regarding the influence extent for each specimen type under the same conditions. Therefore, the mechanical performance of concrete structural members with different shaped and sized cross-section can be predicted when exposed to elevated temperatures during a possible fire. No study, as of yet, has investigated the size effect on the mechanical properties (compressive and tensile strengths) of different FR-SCC specimens after exposure to elevated temperatures.

In this chapter, an experimental program was implemented to examine the size effect (size and shape of the specimen) on compressive and tensile strengths of FR-SCC after exposure to elevated temperatures for the first time in literature. To this end, 432 cubic and cylindrical specimens of different sizes were prepared. Additionally, numerical models were developed to obtain the size effect on the residual compressive and tensile strengths for common specimens of FR-SCC before and after exposure to elevated temperatures.

6.2 Compressive strength

In general, the increment in temperature level resulted in lower compressive strength for FR-SCC specimens. However, a slight increase in compressive strength was recorded for FR-SCC specimens after exposure to 250°C. This can be attributed to the re-hydration of concrete paste induced to combine water migration in the pores (Fares et al., 2010, Dias et al., 1990). Thereafter, rise in temperature resulted in higher thermal expansion differences and, water evaporation increased pore pressure, leading to a significant reduction in compressive strength (Zhang and Bicanic, 2002).

The compressive strength dropped abruptly after exposure to temperatures higher than 500 °C. No explosive spalling was observed at each temperature for any SCC specimens, which is attributable to the presence of polypropylene fibers (PP).

Provision of steel fibers (SF) improved the residual strength of FR-SCC specimens after exposure to elevated temperatures.

6.2.1 Medium strength self-compacting concrete (FR-MSCC)

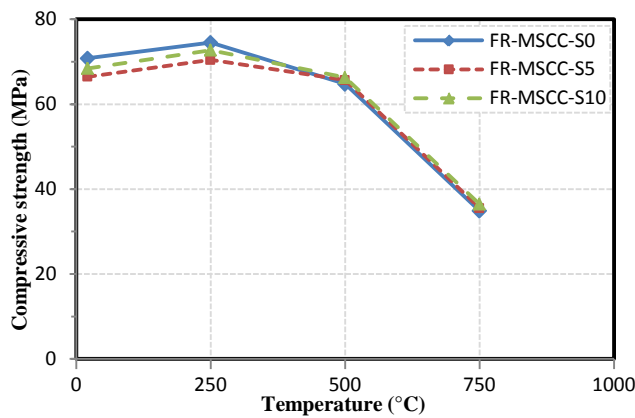
Figure 6.1 and Table 6.1 show the compressive strength of fiber-reinforced medium strength self-compacting concrete (FR-MSCC), with and without steel fiber for cubic and cylindrical specimens before and after subjected to elevated temperatures. For the specimen of the same shape, the temperature effect increased as specimen size decreased.

After exposure to 750°C, the residual strength of the large cylinder (S-150) decreased by 52%, whereas the small cube maintained 52% of its strength at room temperature. After exposure to temperatures higher than 250°C, strength of small cylinder (S-100) suffered a reduction greater than the other specimens, whereas large cube (C-150) was least affected at elevated temperature.

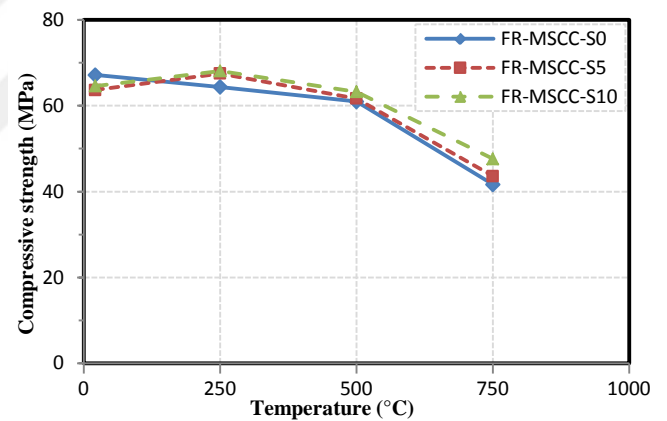
The cylindrical specimens were more responsive to steel fibers as compared to cubic specimens. However, the residual compressive strength of cubic specimens was higher than that of the cylindrical specimens. This can be attributed to the fact that the temperature transfer from the surface to the center of a cylindrical specimen was easier as compared to cubic specimens. Therefore, the distribution of temperature is more symmetrical and homogeneous in cylindrical specimens. For this reason, sensitivity of the cylindrical specimens when subjected to elevated temperatures is higher.

Table 6.1 Compressive strength of FR-MSCC specimens after exposure to different temperatures

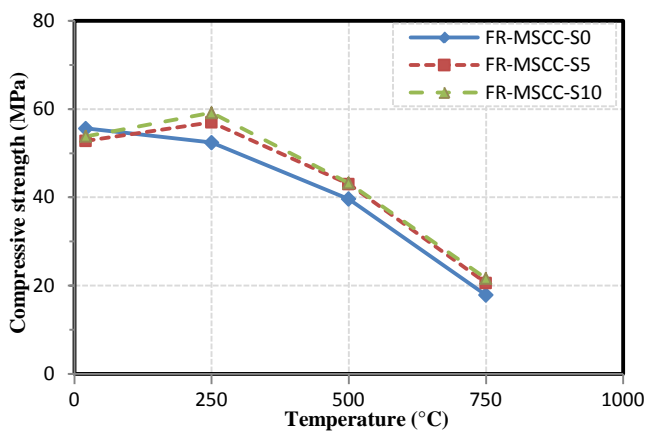
Mixture	Specimen	Compressive strength at room temperature (MPa)	Residual strength (%) after exposure to elevated temperature		
			250°C	500°C	750°C
FR-MSCC-S0	C-100	70.8	105	91	49
	C-150	67.2	96	91	62
	S-100	55.6	94	71	32
	S-150	52.9	101	92	40
FR-MSCC-S5	C-100	66.5	106	99	53
	C-150	63.7	106	97	69
	S-100	52.8	108	81	39
	S-150	51.1	107	99	50
FR-MSCC-S10	C-100	68.4	106	97	53
	C-150	64.6	105	98	74
	S-100	53.8	110	80	40
	S-150	50.8	108	97	53



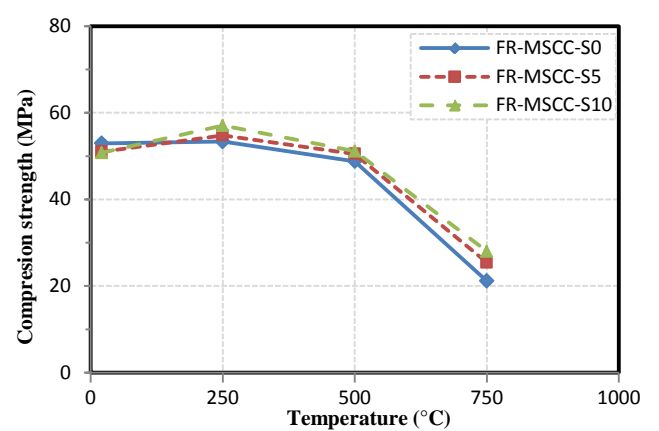
a) Cube 100 mm



b) Cube 150 mm



c) Cylinder 100 × 200 mm



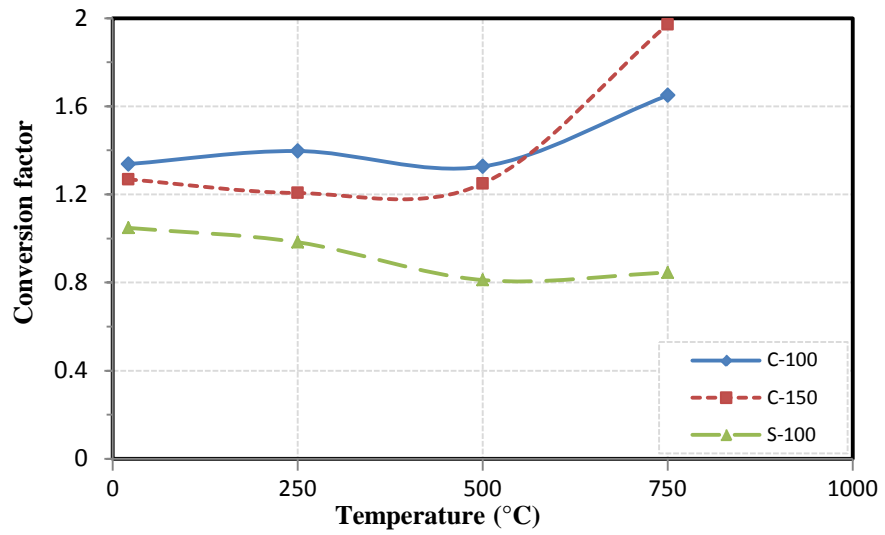
d) Cylinder 150 × 300 mm

Figure 6.1 Compressive strength of FR-MSCC specimens before and after exposure to elevated temperatures

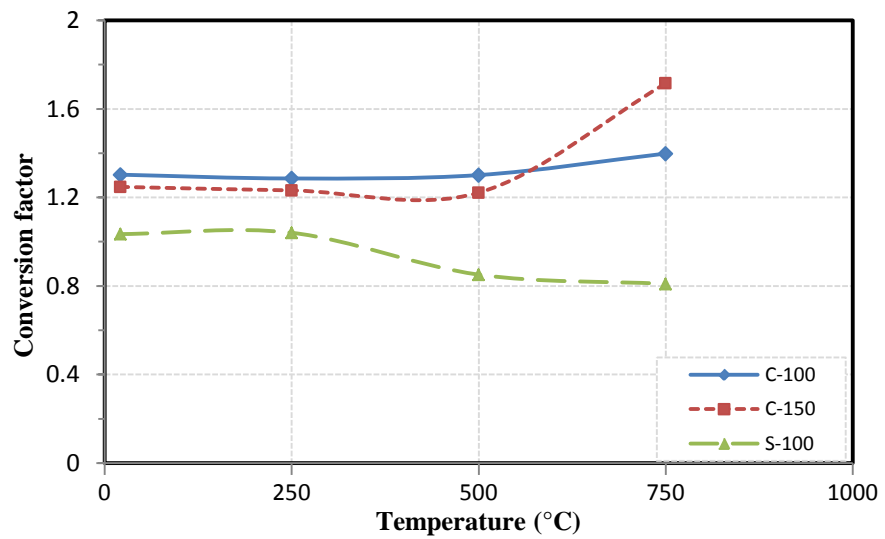
6.2.1.1 Conversion factor

Conversion factor was calculated based on the test results. It represents the compressive strength ratio between the different specimens (C-100, C-150 and S-100) and the standard specimen (S-150) as shown in Figure 6.2. Although the small cube (C-100) kept a fixed ratio, the difference in the conversion factor for the other specimens increased as the temperature rose. After exposure to 750°C, the conversion factor for the small cylinder decreased by 22%, whereas it was nearly 42% higher for the large cube at room temperature. The addition of steel fiber to FR-MSCC mixtures contributed to a reduction in the variation of conversion factor for the concrete specimen particularly for the small cube (C-100).

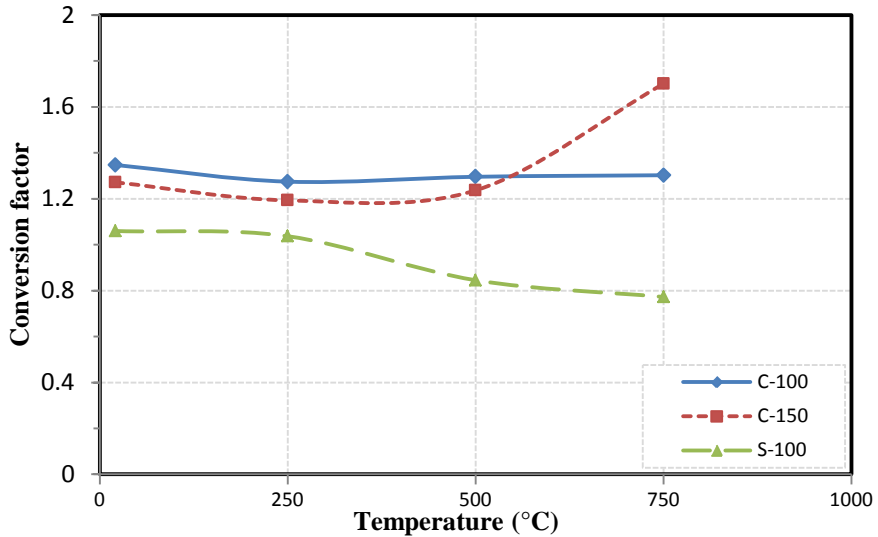




a) FR-MSCC-S0 specimens



b) FR-MSCC-S5 specimens



c) FR-MSCC-S10 specimens

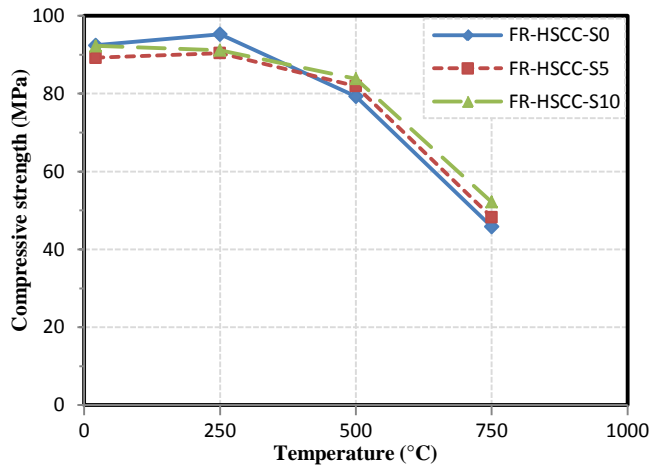
Figure 6.2 Conversion factor for FR-MSCC specimens before and after exposure to elevated temperatures

6.2.2 High strength self-compacting concrete (FR-HSCC)

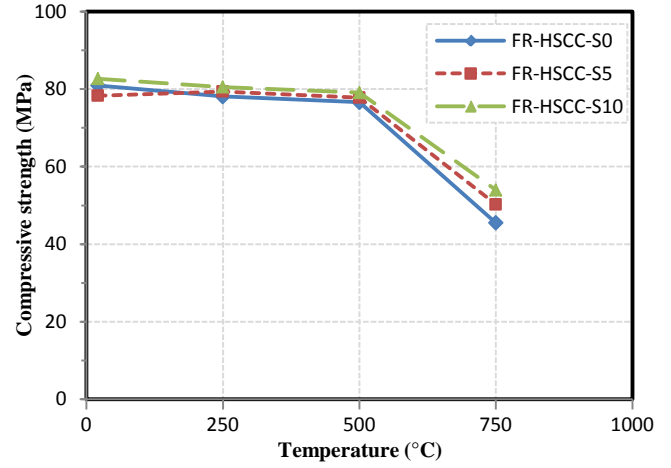
The compressive strength of fiber-reinforced high strength self-compacting concrete (FR-HSCC) for the specimens before and after exposure to elevated temperatures is shown in Figure 6.3 and Table 6.2. After FR-HSCC specimens without steel fibers were exposed to 750°C, large cube had a significant residual strength while the large cylinder suffered a higher loss in compressive strength. Considering the improvement in residual strength with respect to the amount of steel fiber, it was observed that the small cylinder yielded best performance, while the small cube affected after subjected to 750°C. In general, the addition of 1% steel fiber to SCC mixtures improved the residual strength of cylindrical specimens as much as 3 times as compared to cubic specimens as shown in Table 6.2.

Table 6.2 Compressive strength of FR-HSCC specimens after exposure to different temperatures

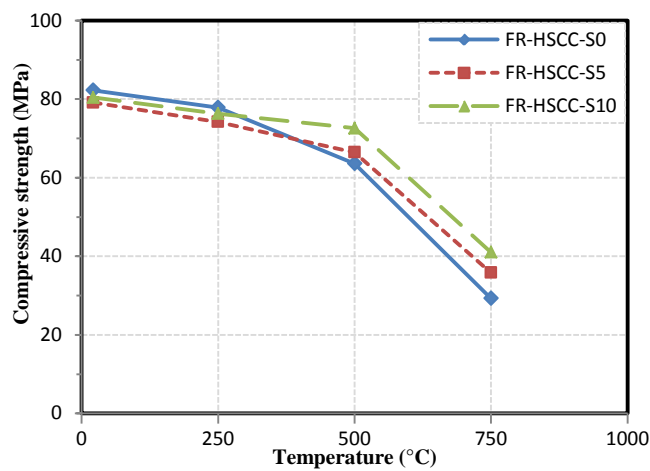
Mixture	Specimen	Compressive strength at room temperature (MPa)	Residual strength (%) after exposure to elevated temperature		
			250°C	500°C	750°C
FR-HSCC-S0	C-100	92.4	103	86	50
	C-150	81.0	97	95	56
	S-100	82.2	95	77	36
	S-150	83.4	93	85	35
FR-HSCC-S5	C-100	89.2	101	92	54
	C-150	78.3	101	99	64
	S-100	79.1	94	84	45
	S-150	79.5	92	90	49
FR-HSCC-S10	C-100	92.2	99	91	57
	C-150	82.7	97	96	65
	S-100	80.4	95	90	51
	S-150	79.8	94	90	50



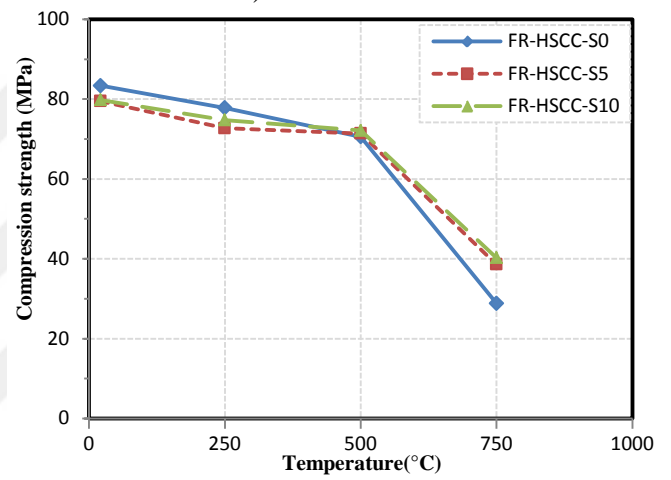
a) Cube 100 mm



b) Cube 150 mm



c) Cylinder 100 × 200 mm

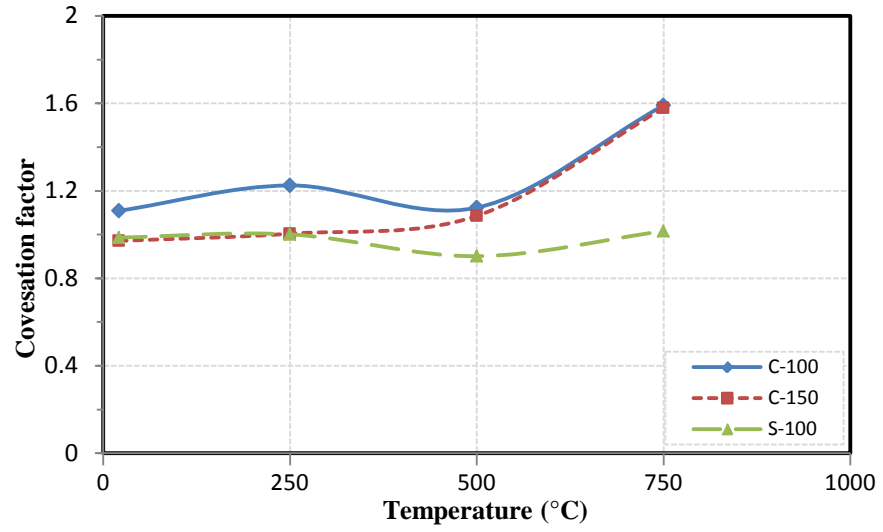


d) Cylinder 150 × 300 mm

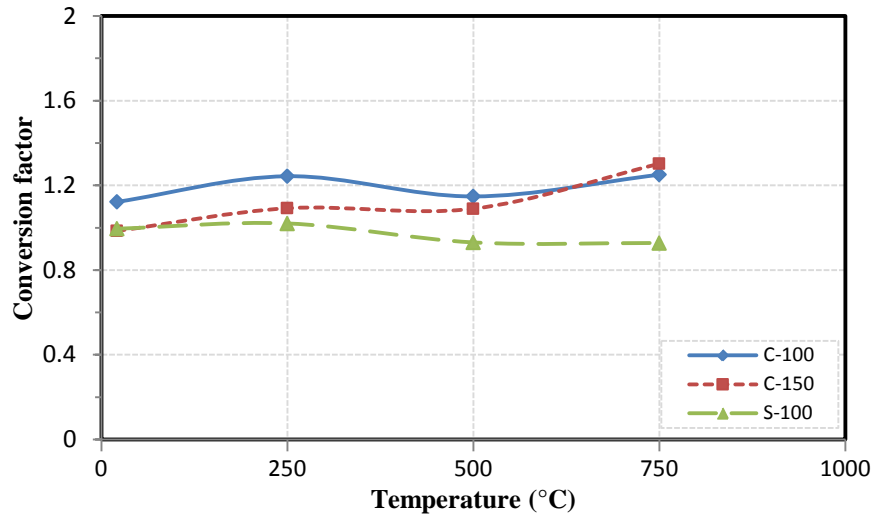
Figure 6.3 Compressive strength of FR-HSCC specimens before and after exposure to elevated temperatures

6.2.2.1 Conversion factor

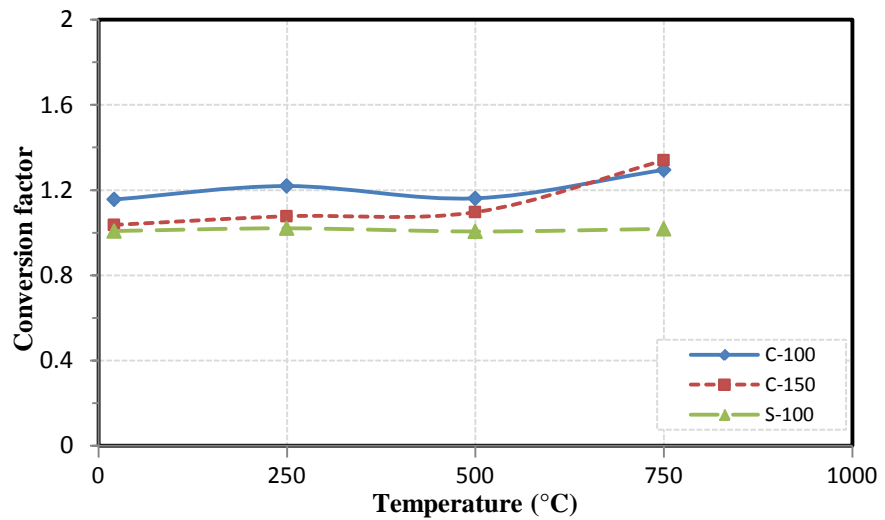
Figure 6.4 shows the conversion factor for FR-HSCC specimens with and without steel fibers, before and after subjected to elevated temperatures. The conversion factor for the small cylinder maintained almost constant after exposure to elevated temperatures. The addition of 1% steel fiber reduced the variance of conversion factor for cubic specimens nearly 20% after exposure to 750°C. In general, variation of conversion factor decreased as the concrete grade increased for the same specimen after exposure to elevated temperatures. Also, presence of steel fibers in FR-HSCC mixtures contributed to a reduction in temperature effect on the variation of a conversion factor.



a) FR-HSCC-S0 specimens



b) FR-HSCC-S5 specimens



c) FR-HSCC-S10 specimens

Figure 6.4 Conversion factor for FR-HSCC specimens before and after exposure to elevated temperatures



FR-HSCC-S0 FR-HSCC-S5 FR-HSCC-S10

Figure 6.5 Shape of failure for different FR-SCC specimens under compression test, after exposure to temperature 750°C.

6.3 Tensile strength

Tensile strength of FR-SCC with and without steel, fiber before and after elevated temperatures is shown in Figure 6.6, Table 6.3 and Table 6.4 for the small and large cylinders. It was observed that small cylinder (S-100) affected more than the large one (S-150) when subjected to elevated temperatures. Reduction in strength of small cylinder was much faster than the strength loss of the large cylinder after exposure to elevated temperatures, as shown in Table 6.3 and Table 6.4. It was observed that the determination of tensile strength of FR-SCC large cylinder (standard specimen) is more reliable, particularly when the risk of high temperatures is a concern.

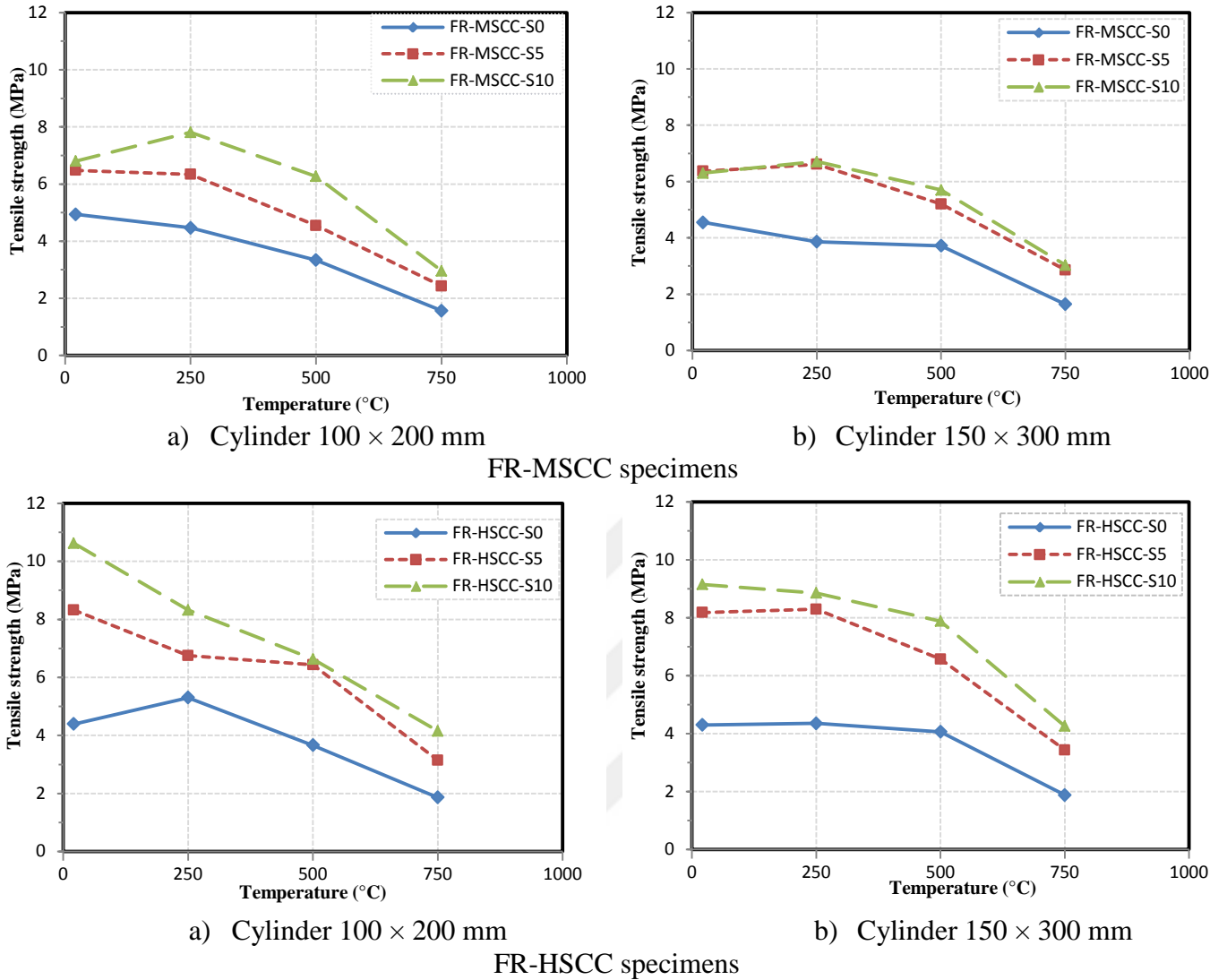


Figure 6.6 Tensile strength of FR-SCC specimens before and after exposure to elevated temperatures

Table 6.3 Tensile strength of FR-MSCC specimens after exposure to different temperatures

Mixture	Specimen	Tensile strength at room temperature (MPa)	Residual strength (%) after exposure to elevated temperature		
			250°C	500°C	750°C
FR-MSCC-S0	S-100	4.9	91	68	32
	S-150	4.6	85	82	36
FR-MSCC-S5	S-100	6.5	98	70	38
	S-150	6.4	104	82	45
FR-MSCC-S10	S-100	6.8	115	92	44
	S-150	6.3	107	91	48

Table 6.4 Tensile strength of FR-HSCC specimens after exposure to different temperatures

Mixture	Specimen	Tensile strength at room temperature (MPa)	Residual strength (%) after exposure to elevated temperature		
			250°C	500°C	750°C
FR-HSCC-S0	S-100	4.4	121	84	43
	S-150	4.3	101	95	44
FR-HSCC-S5	S-100	8.3	81	77	38
	S-150	8.2	102	80	42
FR-HSCC-S10	S-100	10.6	78	63	39
	S-150	9.2	97	86	47

6.4 Theoretical analysis

6.4.1 Specimen size effect

6.4.1.1 The size effect law

The size effect law (SEL) is derived in this study by taking Bazant's theory (1984) and fracture mechanics rules into account. Kim and Eo (1990) added a size independent strength term, $\sigma_o(=\alpha.f_{ct})$ to SEL and proposed a new formulation, called as modified size effect law (MSEL, Eq.1). The strength of concrete members can be predicted by the formulation even there are initial cracks and similar or dissimilar cracks in the members. A similar approach is also introduced by Bazant (1993), and Bazant and Xiang (1997) with a different method.

$$\sigma_N(d) = \frac{\beta \cdot f_{ct}}{\sqrt{1 + d/\lambda_o d_a}} + \alpha \cdot f_{ct} \quad (1)$$

where $\sigma_N(d)$ represents the nominal strength, f_{ct} refers to the direct tensile strength, d is the characteristic dimension, d_a corresponds to the maximum aggregate size and α, β, λ_o are the empirical constants. Although the size effect of tensile failure and failure mechanism have been studied extensively, the behavior of compressive failure has not been sufficiently examined in comparison with the mechanism of tensile failure. Since concrete is a construction material mostly used to withstand compressive forces, it is useful to extend the tensile size effect to size effect in the compressive failure mechanism. New and comprehensive equations are proposed by symbolic regression method. In these equations, the direct tensile strength term, f_{ct} used in size effect law is substituted by the compressive strength of standard cylinder

f_{cs} , and λ_o is an approximate constant with values between 2.0 and 3.0 according to researchers (Bazant,1984, Kim et al., 2001). This constant is selected 2.0 in the present regression analysis. The term l_o is used in the proposed equations and is equal to [$l_o = \lambda_o \times d_a = 2.0 \times d_a = 2.0 \times 11.0 = 22.0mm$], where d_a is the maximum aggregate size used in SCC production, and equal to 11.0mm for the present study.

6.4.1.2 Size effect on compressive strength

6.4.1.2.a Cubic specimens

A new formulation (Eq. 2) is proposed to calculate the compressive strength of the cubic specimens in terms of standard strength for FR-SCC both with and without steel fiber, before and after exposure to elevated temperatures, by taking size effect into consideration. The correlation coefficient (R^2) of the equation is 0.90.

$$f_{cu} = \frac{0.76f_K}{\sqrt{1 + \frac{d}{l_o}}} + 0.81f_K \quad (2)$$

$$\text{where } f_K = f_{cs} + \frac{R.I}{26.9} + \frac{T}{86.7}$$

f_{cu} is the compressive strength (in MPa) of general cubic specimen, with or without steel fiber (SF) after subjected to different temperatures (T). As well, d is the cube dimension in cm, $l_o = 2.0 \times d_a$ and d_a is the maximum aggregate size. f_{cs} is the compressive strength of the standard specimen (S-150) in MPa for FR-MSCC or FR-HSCC mixtures. ($R.I$) is the fiber reinforcing index $= V_f \times l_f / d_f$, where V_f is the volume fraction of SF, l_f / d_f is the aspect ratio, (l_f and d_f are the length and diameter of steel fiber, respectively) and T is the temperature in ($^{\circ}C$). Figure 6.7 compares the experimental and theoretical results of the compressive strength for FR-SCC cubes. Figure 6.8 shows the main effects of variables in Eq. 2 on the compressive strength for cubic specimens of FR-SCC mixtures. As expected, size effect on the compressive strength of cubic specimens decreases with the increase in concrete grade, along with the addition of SF, particularly when exposed to high temperatures. For temperature levels higher than $500^{\circ}C$, size effect on the residual strength of cubes was higher for larger cubes.

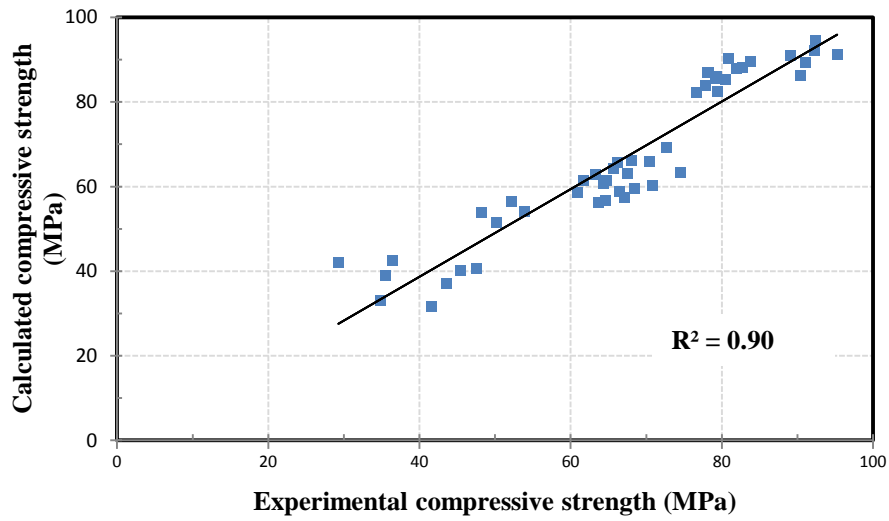
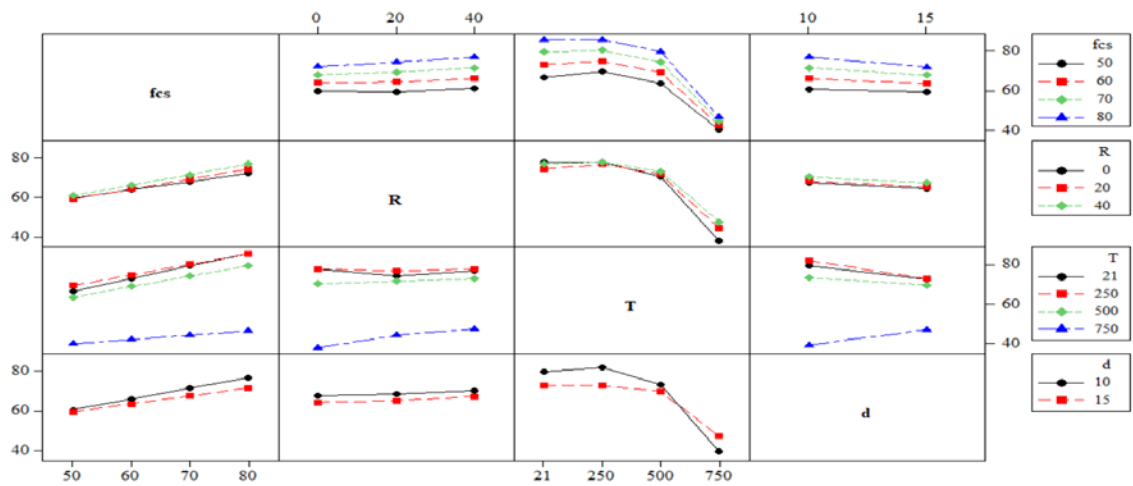
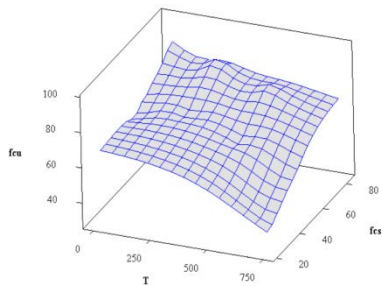


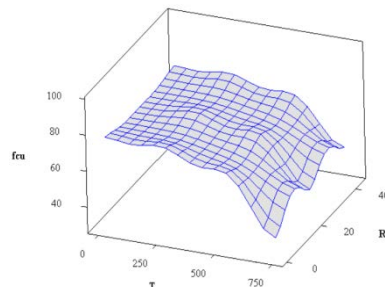
Figure 6.7 Comparison between experimental and calculated compressive strength of FR-SCC cubes



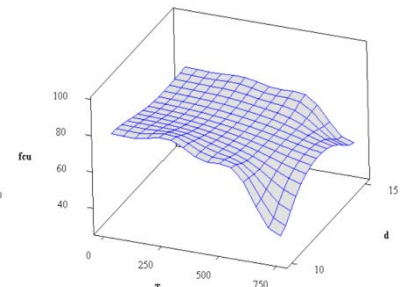
a) Main effects on the compressive strength of cubic specimens



b) Effect of standard strength on the compressive strength of cubes



c) Effect the addition of fiber on the compressive strength of cubes



d) Effect of specimen dimension on the compressive strength of cubes

Figure 6.8 Size effect on compressive strength for FR-SCC cubes before and after exposure to elevated temperatures

6.4.1.2.b Cylindrical specimens

The proposed formulation to predict the compressive strength for different size of cylindrical specimens in terms of standard strength of FR-SCC is given in Eq. 3. The correlation coefficient (R^2) in Eq. 3 was 0.97.

$$f_{cy} = \frac{f_L}{\sqrt{1+d/l_o}} + 0.58f_L \quad (3)$$

$$\text{where } f_L = f_{cs} + \frac{R.I}{97.4} - \frac{T}{245.3}$$

f_{cy} is the compressive strength with the size of general cylinder, and f_{cs} the compressive strength of standard cylinder (in MPa). The term "general" represents the cylindrical specimens with arbitrary chosen dimensions. A good agreement between the experimental results and the results obtained from the proposed equations, as shown in Figure 6.9.

Figure 6.10 shows the interaction between the factors in Eq. 3, and their effects on the compressive strength of different cylindrical specimens of FR-SCC after different temperatures. This general compressive strength (f_{cy}) was a function of the standard strength (f_{cs}), fiber content, and temperature (T). The size effect on compressive strength of cylinders decreases with the concrete grade increase and/or after steel fiber addition.

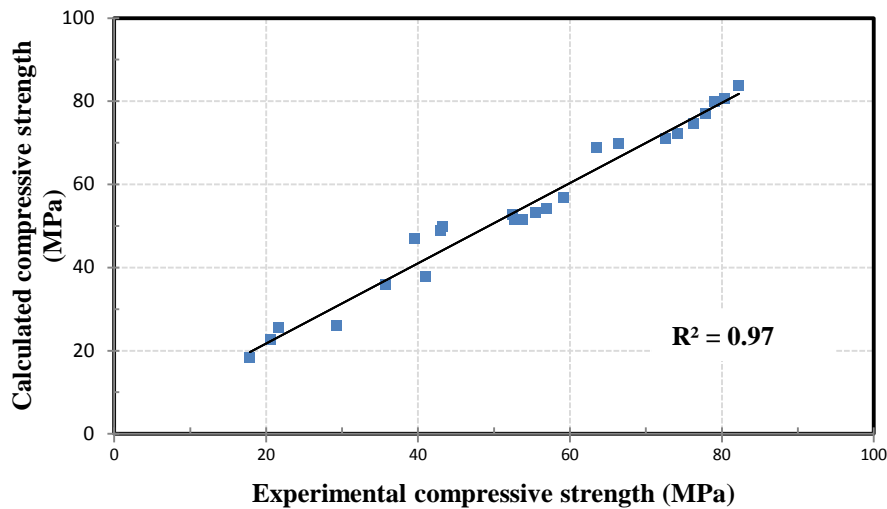
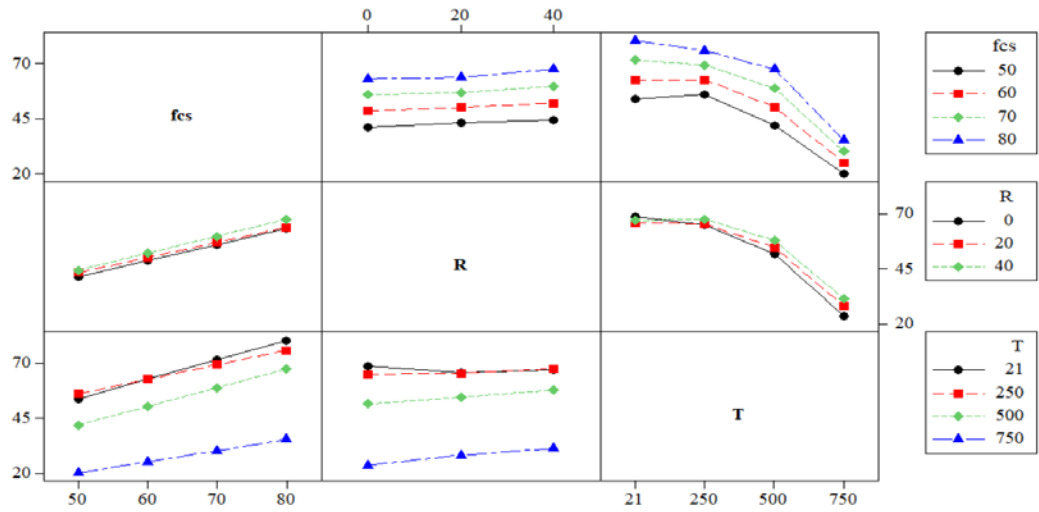
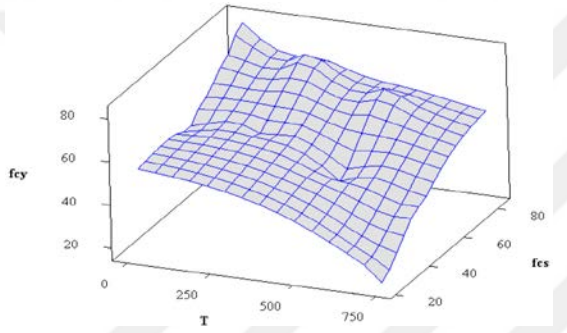


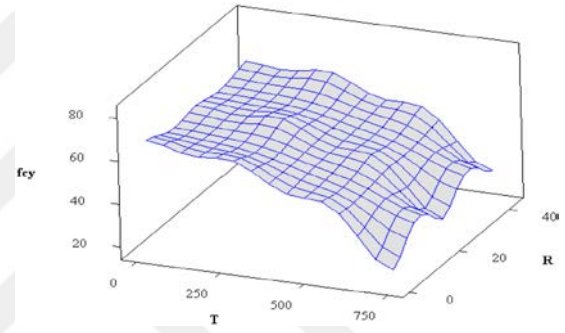
Figure 6.9 Comparison between experimental and calculated compressive strength of FR-SCC cylinders



a) Main effects on the compressive strength of cylindrical specimens



b) Effect of standard strength on the compressive strength of cylinders



c) Effect the addition of fiber on the compressive strength of cylinders

Figure 6.10 Size effect on compressive strength for FR-SCC cylinders before and after exposure to elevated temperatures.

6.4.1.3 Size effect on tensile strength

The proposed formulation obtained as a result of the regression analyses for the tensile strength results is given in Eq. 4. The tensile strength for different cylindrical specimens of FR-SCC mixtures after different temperatures can be obtained, in terms of the tensile strength of the standard cylinder practically with the proposed equation (Eq.4). The correlation coefficient R^2 was found to be 0.924.

$$f_t = \frac{87.5 \times f_M}{\sqrt{1 + d/l_o}} - 36.2 \times f_M \quad (4)$$

$$\text{Where } f_M = f_{ts} + \frac{R.I}{118.7} - \frac{T}{1673}$$

f_t is the tensile strength with the size of a general cylinder with or without steel fiber before and after exposure to elevated temperatures, and f_{ts} is the tensile strength of standard cylinder in MPa. There was a clear convergence between the experimental and theoretical results of tensile strength as shown in Figure 6.11.

Figure 6.12 shows the main effects affecting on the general tensile strength of FR-SCC mixtures. From Eq. 4; the tensile strength for general size of the cylindrical specimens (f_t) was a function of standard tensile strength (f_{ts}) of FR-SCC (in MPa), steel fiber content, and temperature. In general, size effect on tensile strength increased with the temperature increasing, while decreases with the steel fibers addition and increase the concrete grade.

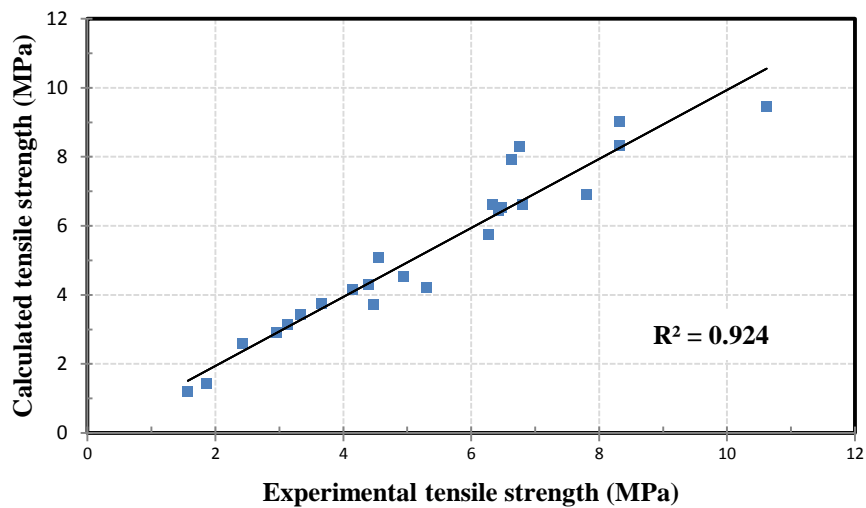
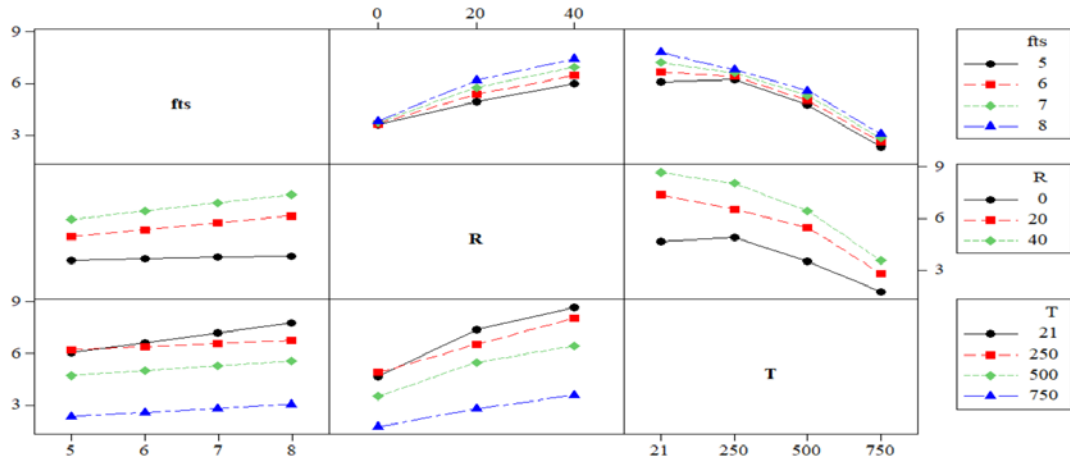
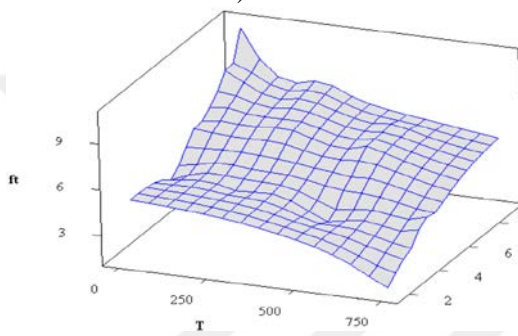


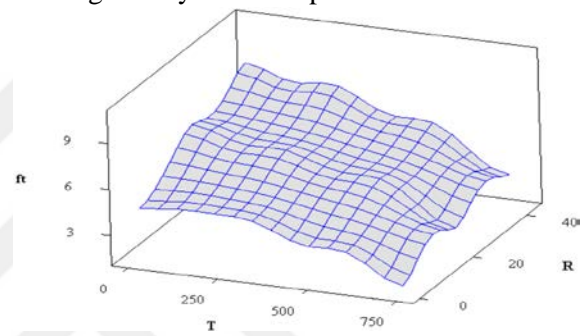
Figure 6.11 Comparison between experimental and calculated tensile strength of FR-SCC cylinders.



a) Main effects on the tensile strength of cylindrical specimens



b) Effect of standard strength on the tensile strength of cylinders



c) Effect the addition of fiber on the tensile strength of cylinders

Figure 6.12 Size effect on tensile strength for FR-SCC cylinders before and after exposure to elevated temperatures.

6.4.2 Specimen shape effect

Figures. 6.13 and 6.14 show the plots of compressive strength of the cylinders compared to the cubes, to represent the specimen shape effect. In these graphs, the dashed and solid lines indicate the lines of best-fit obtained from linear regression analyses and the line of equality ($Y=X$) respectively. The equations shown in Figures 6.13 and 6.14 are obtained as a result of the linear regression analysis. Comparing the compressive strength results of S-100 and C-100 specimens (see Figures. 6.13.a and 6.13.c), it can be seen that all trends show that the strength of C-100 specimens is higher than that of small cylinder (S-100) specimens for all concrete grades. Therefore, the difference between the strengths was approximately constant for all temperatures. However, the difference between the compressive strength of large cube (C-150) and small cylinder (S-100) decreased when the concrete grade increased, while it increased with higher temperatures, as shown in Figures. 6.13.b

and 6.13.d.

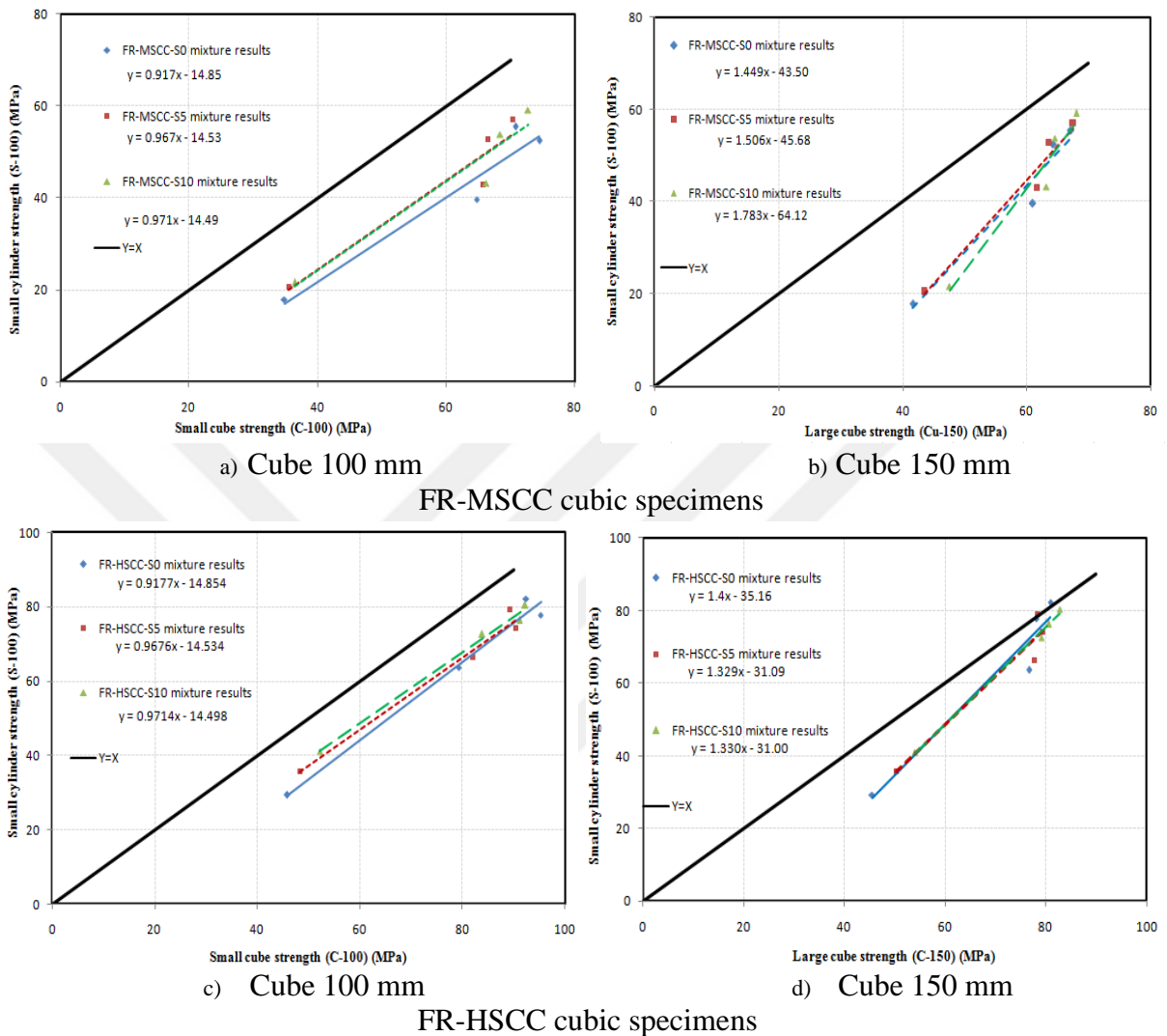
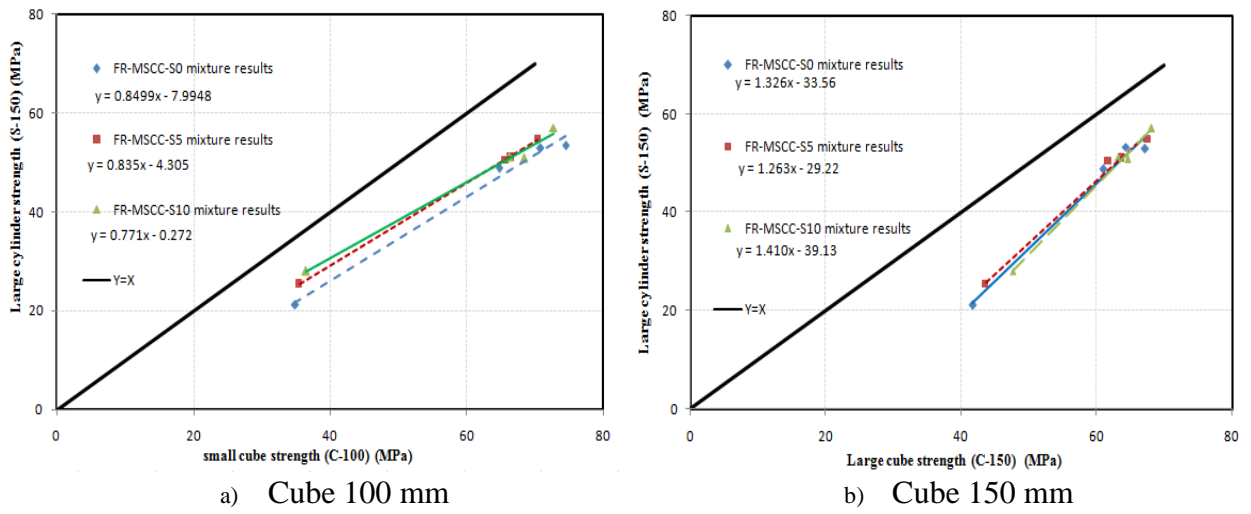
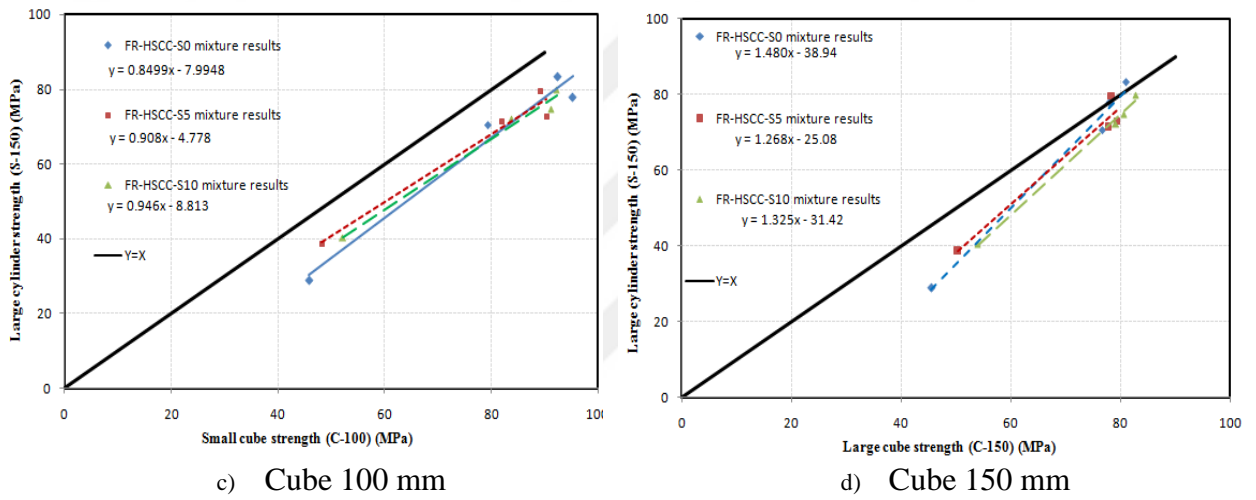


Figure 6.13 Relationship between compressive strengths of the 100×200 mm cylinder and cubic specimens before and after exposure to elevated temperatures.

It can be concluded from Figures. 6.14 (b and d) that the difference in compressive strength for the large cube (C-150) and large cylinder (S-150) increased with the temperature increase or decrease the concrete grade for all SCC mixtures. Figures 6.14.a and 6.14.c show that the compressive strength of the small cylinder (C-100) is higher than that of the large cylinder (S-150). The variance between these two specimens decreased when concrete grade increased or with steel fiber additions.



FR-MSCC cubic specimens



FR-HSCC cubic specimens

Figure 6.14 Relationship between compressive strengths of the 150 × 300 mm cylinder and cubic specimens before and after exposure to elevated temperatures.

CHAPTER 7

MECHANICAL BEHAVIOR OF FR-SCC CORBELS AFTER EXPOSURE TO ELEVATED TEMPERATURES

7.1 General

Corbels are structural members that transfer the vertical and horizontal loads to principle members such as beams and columns. Reinforced Concrete corbels (RC-corbels) are frequently utilized in industrial structures, which are oftentimes exposed to high temperatures or fire. Typically, when reinforced concrete structural members are exposed to elevated temperatures, the concrete deteriorates and therefore the mechanical properties of concrete significantly degrade that leads to failure. As a result of exposure of the reinforcing steel to fire directly, the load-carrying capacity of structural members may be destroyed, which in turn may lead to catastrophic destruction of the structure.

Many researchers (Fattuhi, 1987,1988, 1994, 1994, Fattuhi and Hughes, 1989, 1989, Campione et al., 2005, Campione et al., 2007, Campione, 2009, Foster et al., 1996, Abdel Hafez et al., 2012, Abdul-Wahab, 1989) used steel fiber (SF) in RC-corbels to obtain a significant increase in the load-carrying capacity, improve the mechanical behavior of RC-corbels and transforming failure mode from abrupt or catastrophic to a gradual or ductile failure mode.

The parameters influence on the structural response of RC-corbels include the type and direction of applied load, strength of concrete used, shear span-to-depth ratio, type and amount of reinforcement, and possibly corbel geometry. Based on the combination of the above mentioned parameters, the mechanical behavior of RC-corbels may be affected and their failure modes changed from the worst case brittle failure (diagonal splitting or shear) to a more ductile failure (such as flexure) (Fattuhi, 1988).

Bentur and Mindess (2007) found that the addition of SFs to high-strength concrete

improves the load-carrying capacity of flexural members, thereby extending toughness and also the deflection capacity in post-cracking zone.

Kim et al. (2014) observed that the steel fiber enhances the mechanical behavior of RC member through the improvement in bond stress between reinforced steel and concrete.

Ahmed et al. (2016) proved that the steel fibers tend to control cracking by reducing crack width and spacing at different loads on the structural members at high temperatures. In general, steel fibers provide a necessary safe guarantee for rescue work and structure repair after fire suppression.

Several studies have already predicted the various influential factors on the mechanical behavior of fiber-reinforced concrete corbels (Fattuhi, 1987,1988, 1994, 1994, Fattuhi and Hughes, 1989, 1989, Campione et al., 2005, Campione et al., 2007, Campione, 2009, Abdel Hafez et al., 2012, Abdul-Wahab, 1989).

None of the respective previous studies have investigated the mechanical behavior of fiber-reinforced concrete corbels after exposure to elevated temperatures. For this reason, the present study is a novel attempt using experimental work to investigate the behavior of FR-SCC corbels after subjected to temperatures up to 750°C. This work accounts for the effects of some parameters on the behavior of RC-corbels, and also reveals the ability of SFs to improve ductility and enhance mechanical behavior of RC-corbels after elevated temperatures. The results are inserted in terms of load-deflection curves, crack patterns and failure modes.

7.2 Load-carrying capacity

In general, as the temperature increases, there is a tendency of the load-carrying capacity of RC-corbels to reduce. However, a slight increase in maximum load was recorded for corbels after exposure to 250°C. This can be attributed to re-hydration of the concrete paste caused by migration of water in pores (Fares et al., 2010, Dias et al. 1990). It is also related with the fact that when the concrete is exposed to temperatures not higher than 300°C, the cement hydration of concrete is fully completed. Beyond 250°C, a rise in temperature causes thermal cracks between cement paste and aggregates due to difference in thermal expansion that leads to

obvious reduction in the strength of the concrete (Zheng et al., 2012) and as a result, load carrying capacity of corbels reduces. After exposure to temperatures higher than 500°C, it was noted that the maximum load drops abruptly as temperature increases.

Another reason for the reduction in load carrying capacity of the RC-corbels may be due to damage of the bond-slip behavior between reinforcement (steel fibers and steel bars) and concrete thereby resulting in a significant reduction in tensile strength after exposed to elevated temperatures.

The load-carrying capacity of the RC-corbels is summarized in Table 7.1. The tabulated results showed improvement on mechanical behavior of RC-corbels incorporating fibers for all temperature levels. For instance, the addition of 1% SF increases the residual maximum loads for FR-MSCC and FR-HSCC corbels (have the same parameter) by 41% and 24%, respectively after exposed to 750°C.

No explosive spalling was observed at each temperature treatment for all SCC specimens as this can be controlled using the polypropylene fibers (PP). While, the addition of steel fibers (SF) improved the residual maximum loads of the RC-corbels after exposure to elevated temperatures.

Table 7.1 Mechanical characteristics of test specimens after exposure to elevated temperatures.

Mixture Type	SF %	Temperature (°C)	Mechanical properties of concrete used		RC-corbels characteristics			Max. Load for Corbel (kN)	Failure mode
			Compressive strength (MPa)	Tensile strength (MPa)	Corbel Name	Shear span (mm)	Reinforcing steel (mm)		
Medium Strength Self-Compacting Concrete (FR-MSCC)	0	21	52.9	4.6	CR-1	90	10	202	S
					CR-2	120		109	D.S
		250	53.3	3.9	CR-3	90	10	208	D.S
					CR-4	120		130	S
		500	48.8	3.7	CR-5	90	10	175	S
					CR-6	120		80	D.S
		750	21.1	1.6	CR-7	90	10	82	S
					CR-8	120		51	D.S
	0.5	21	51.1	6.4	CR-9	90	10	217	S
					CR-10	120		140	S
		250	54.8	6.6	CR-11	90	10	243	S
					CR-12	120		201	S
		500	50.5	5.2	CR-13	90	10	193	S
					CR-14	120		117	S
		750	25.4	2.9	CR-15	90	10	119	S
					CR-16	120		88	S
	1.0	21	50.8	6.3	CR-17	90	10	231	S
					CR-18	120		156	F
		250	57.1	6.7	CR-19	90	10	247	S
					CR-20	120		212	S
		500	51.1	5.7	CR-21	90	10	207	S
					CR-22	120		136	S
		750	27.9	3.0	CR-23	90	10	132	S
					CR-24	120		99	D.S
High Strength Self-Compacting Concrete (FR-HSCC)	0.0	21	83.3	4.3	CR-25	90	10	235	S
					CR-26		14	265	S
		250	77.8	4.4	CR-27	90	10	227	D.S
					CR-28		14	268	S
		500	70.6	4.0	CR-29	90	10	195	S
					CR-30		14	210	D.S
		750	28.8	1.9	CR-31	90	10	107	S
					CR-32		14	113	D.S
	0.5	21	79.5	8.2	CR-33	90	10	272	F
					CR-34		14	286	S
		250	72.7	8.3	CR-35	90	10	280	S
					CR-36		14	370	S
		500	71.4	6.6	CR-37	90	10	235	S
					CR-38		14	251	S
		750	38.6	3.4	CR-39	90	10	150	S
					CR-40		14	134	S
	1.0	21	79.8	9.2	CR-41	90	10	327	F+S
					CR-42		14	335	S
		250	74.8	8.9	CR-43	90	10	317	F+S
					CR-44		14	382	S
		500	72.2	7.9	CR-45	90	10	267	F
					CR-46		14	294	S
		750	40.3	4.3	CR-47	90	10	171	D.S
					CR-48		14	183	S

7.3 Load-deflection behavior

The load-carrying capacity of RC-corbels after exposure to elevated temperatures decreases gradually as a result of the deterioration in mechanical properties of concrete caused by reduction in internal forces of the RC-corbels. Eventually, result in the catastrophic destruction of the structure.

As the temperatures rise, deflection of the corbel is increased quickly when cracks appear, thereby, decrease the slope of the ascending portion of the load-deflection curves, and the maximum load also decreased and shifted towards the downright with rising temperature exposure. The RC-corbels initially behave elastic behavior, meaning that the load-deflection curve being approximately straight line until the first-cracking load for each temperature level. The post-peak behavior (descending path) of the load-deflection curve depends on the presence of SF and temperature.

Steel fiber (SF) improves the maximum loads, enhances the post-peak performance, and extends the deflection value corresponding to the failure load. The fibers transmit the heat more uniformly cause a decrease in the cracks that are induced due to thermal gradients in the concrete. And therefore, steel fibers provide uniform stress redistribution during heating and cooling process. Incorporating steel and polypropylene fibers have significantly contributed to the enhancement of the ductility and durability of the RC-corbels after exposure to elevated temperatures.

Steel fiber significantly improved the maximum load (P_{max}) for the RC-corbels after different temperatures. On the other hand, the stiffness of the RC-corbels have been influenced by the mechanical properties of fiber-reinforced SCC. Generally, the shape of the load-deflection curve depends on the Concrete Compressive Strength (CCS), Shear Span-to-depth Ratio (SSR), and the Steel-Reinforcement Ratio (SRR), as well as the steel fiber ratio and temperature.

7.3.1 Concrete Compressive Strength (CCS)

The load-carrying capacity of the RC-corbels increases as the grade of concrete increases, but the loss in the maximum loads was increased with the rise in the concrete grade after subjected to the same temperature as shown in Table 7.2.

After exposure to 250°C, the concrete specimens will completely dry, therefore the

increase in the degree of concrete increases the brittleness of the corbels, particularly for corbels which not contain steel fibers. After this temperature, the effect of concrete grade is decreasing, therefore the contribution of steel fibers to increase in both residual maximum load and ductility of the corbel significantly. The load-deflection curves of corbels according to concrete compressive strengths are shown in Figure 7.1.

Table 7.2 Results of flexural tests for corbels with different values of concrete compressive strength (CCS)^ψ.

Corbel Name	CCS	SF%	Temperature (°C)	P _{cr} * (kN)	P _{max} * (kN)	P _F * (kN)	Δ _{max} * (mm)	Δ _u * (mm)	Δ _F * (mm)	Stiffness* (kN/mm)	Ductility index* [♣]	Failure mode [†]	
CR-1	MS	0	21	56	202	70	1.178	1.191	1.236	172	1.01	S	
CR-25	HS			56	235	74	2.174	2.203	2.308	108	1.02	S	
CR-3	MS		250	87	208	144	0.77	1.018	2.372	270	1.32	D.S	
CR-27	HS			99	227	103	1.046	1.062	1.104	217	1.02	D.S	
CR-5	MS		500	500	114	175	140	1.686	2.078	2.206	104	1.23	S
CR-29	HS				105	195	121	1.14	1.478	2.294	171	1.3	S
CR-7	MS		750	750	64	82	30	1.31	1.498	2.108	63	1.14	S
CR-31	HS				96	107	67	1.506	1.693	1.958	71	1.12	S
CR-9	MS	0.5	21	36	217	74	1.73	1.879	3.272	125	1.09	S	
CR-33	HS			69	272	187	1.318	3.117	4.638	206	2.37	F	
CR-11	MS		250	250	111	243	130	1.136	2.012	3.872	214	1.77	S
CR-35	HS				99	280	280	2.798	2.798	2.798	100	1.0	S
CR-13	MS		500	500	113	193	120	1.546	1.712	1.828	125	1.11	S
CR-37	HS				171	235	77	1.274	1.66	3.472	185	1.3	S
CR-15	MS		750	750	80	119	76	1.874	2.107	3.182	64	1.12	S
CR-39	HS				107	150	90	1.776	2.317	3.632	85	1.31	S
CR-17	MS	1.0	21	58	231	52	1.59	1.852	3.93	145	1.17	S	
CR-41	HS			85	327	127	2.204	3.112	4.366	148	1.41	F+S	
CR-19	MS		250	250	106	247	191	1.324	2.185	3.42	187	1.65	S
CR-43	HS				132	317	180	1.774	1.89	2.044	179	1.07	F+S
CR-21	MS		500	500	139	207	46	2.264	3.091	4.672	91	1.37	S
CR-45	HS				123	267	180	1.872	3.082	4.864	143	1.65	F
CR-23	MS		750	750	77	132	82	1.88	2.106	3.484	70	1.12	S
CR-47	HS				140	171	127	1.36	2.145	3.292	126	1.58	D.S

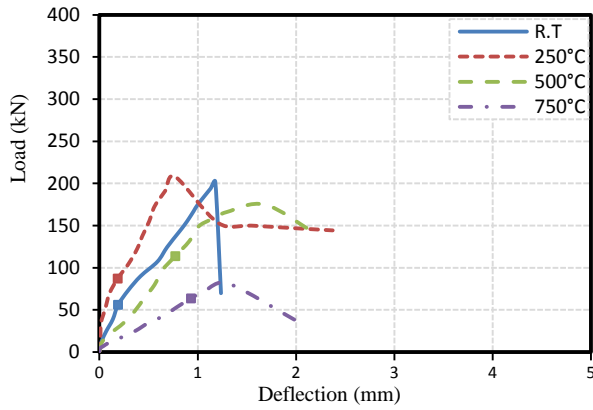
^ψ All the RC-corbels have same shear span ratio (a/d=0.6), and with the same steel reinforcement ratio (ρ=0.0082)

* P_{cr}, P_{max}, P_F represent the first-cracking load, maximum load, failure load and the corresponding deflections are Δ_{max}, Δ_F respectively, and Δ_u is the deflection at 0.85P_{max} after peak load.

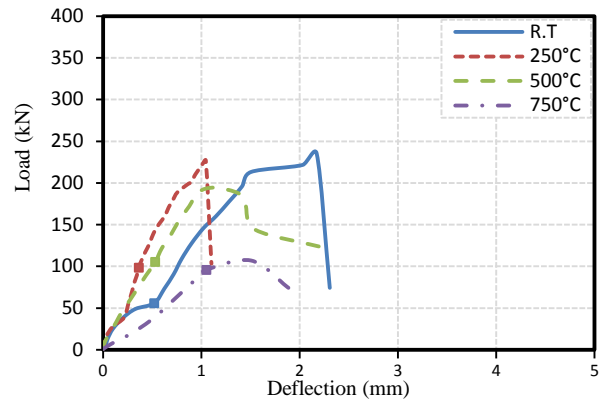
♦ Stiffness of the corbel=P_{max}/Δ_{max} have been adopted by Ahmed et al. [23].

♣ Ductility index = Δ_u/Δ_{max} has been certified by Campione et al. [30].

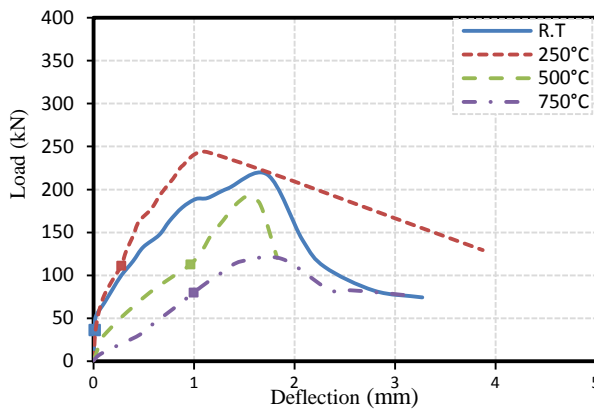
† F: Flexural failure, S: Shear failure, D.S: Diagonal splitting failure.



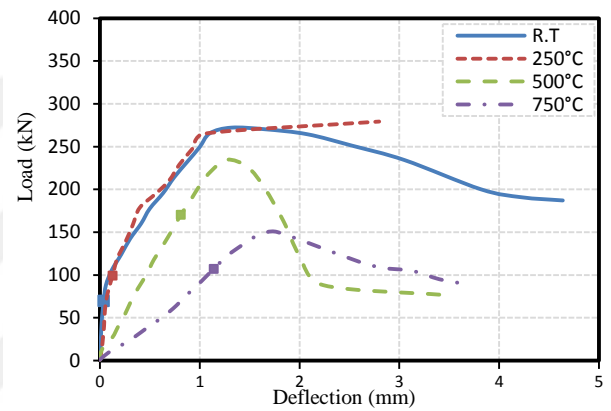
(a) SF= 0%, CCS= 50MPa



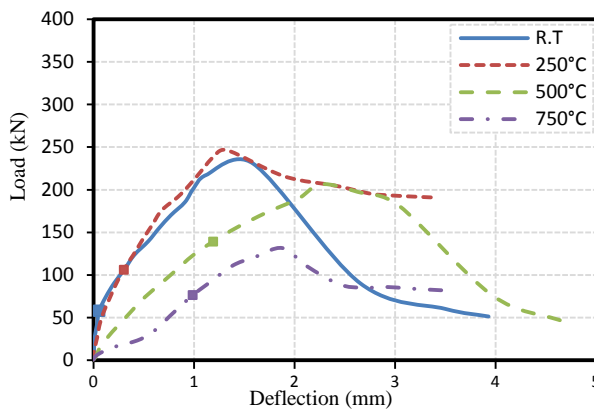
(b) SF= 0%, CCS= 80MPa



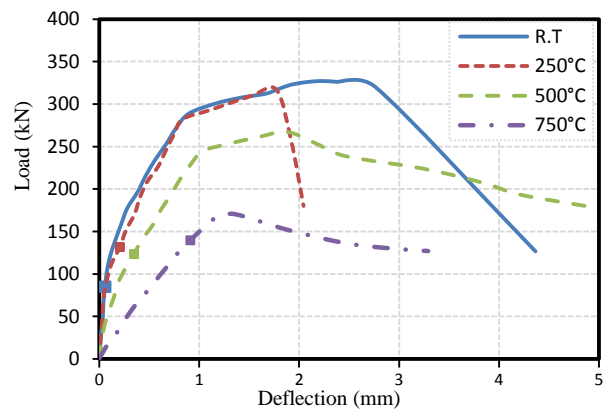
(c) SF= 0.5%, CCS= 50MPa



(d) SF= 0.5%, CCS= 80MPa



(e) SF= 1.0%, CCS= 50MPa



(f) SF= 1.0%, CCS= 80MPa

❖ The point on the curve represents the first cracking load.

Figure 7.1 Load-deflection curves for corbels with the different values of concrete compressive strength (CCS).

7.3.2 Shear Span-to-depth Ratio (SSR)

Two shear span-to-depth ratios (a/h) were taken into account to investigate the effect of shear span ratio (SSR) on the load capacities of RC-corbels. These ratios were 0.6 and 0.8 for FR-MSCC corbels. As expected, the load-carrying capacity of RC-corbels decreases when the shear span-to-depth ratio (SSR) is increased for all the corbels. However, When load capacities of the corbels with shear span values of 90 mm and 120 mm are compared, high difference is observed between the results for the corbels without steel fiber. The reason of this difference is due to early and sudden failure of the corbels, CR-2 and CR-6 corbels, caused by the diagonal splitting of the concrete as stated in Table 6.

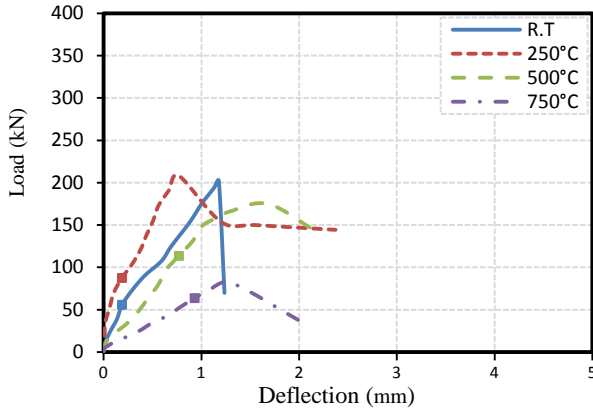
When the shear span of the corbel is increased, bending stresses become more important than shear stresses. However, the concrete is very weak in tension, and there are no any steel fiber or horizontal stirrups in compression zones of the corbel. Therefore, these corbels fail earlier and suddenly because of the splitting of the concrete and lower capacities than expected are observed for the corresponding corbels.

When SSR is increased, RC-corbels achieved higher deflection before failure. Thus, the increase improves the ductility of the RC-corbels after elevated temperatures, particularly when used the steel fiber as a secondary reinforcement as shown in Figure 7.2. It should be also noted that the residual maximum load (P_{max}) and stiffness of corbels decreases as SSR is increased at the same temperature level as listed in Table 7.3.

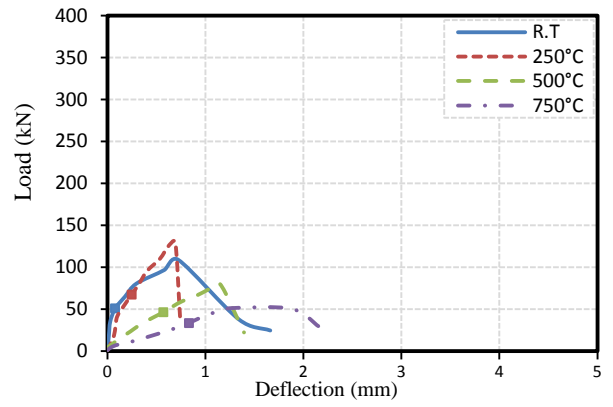
Table 7.3 Results of flexural tests for corbels with different values of shear span-to-depth ratio (SSR)^ψ.

Corbel Name	SSR	SF%	Temperature (°C)	P _{cr} [*] (kN)	P _{max} [*] (kN)	P _F [*] (kN)	Δ _{max} [*] (mm)	Δ _u [*] (mm)	Δ _F [*] (mm)	Stiffness [♦] (kN/mm)	Ductility index [♣]	Failure mode [†]	
CR-1	0.6	0	21	56	202	70	1.178	1.191	1.236	172	1.01	S	
CR-2	0.8			50	109	25	0.724	0.865	1.662	151	1.19	D.S	
CR-3	0.6		250	87	208	144	0.77	1.018	2.372	270	1.32	D.S	
CR-4	0.8			67	130	41	0.692	0.703	0.742	188	1.02	S	
CR-5	0.6		500	500	114	175	140	1.686	2.078	2.206	104	1.23	S
CR-6	0.8				46	80	22	1.15	1.2	1.394	70	1.04	D.S
CR-7	0.6		750	750	64	82	30	1.31	1.498	2.108	63	1.14	S
CR-8	0.8				33	51	28	1.266	1.969	2.17	40	1.56	D.S
CR-9	0.6	0.5	21	36	217	74	1.73	1.879	3.272	125	1.09	S	
CR-10	0.8			55	140	36	1.24	1.447	4.626	113	1.17	S	
CR-11	0.6		250	250	111	243	130	1.136	2.012	3.872	214	1.77	S
CR-12	0.8				91	201	176	1.628	3.436	3.436	124	2.11	S
CR-13	0.6		500	500	113	193	120	1.546	1.712	1.828	125	1.11	S
CR-14	0.8				54	117	82	0.956	1.185	1.364	122	1.24	S
CR-15	0.6		750	750	80	119	76	1.874	2.107	3.182	64	1.12	S
CR-16	0.8				68	88	38	1.956	2.198	4.166	45	1.12	S
CR-17	0.6	1	21	58	231	52	1.59	1.852	3.93	145	1.17	S	
CR-18	0.8			30	156	128	1.258	2.105	7.122	124	1.67	F	
CR-19	0.6		250	250	106	247	191	1.324	2.185	3.42	187	1.65	S
CR-20	0.8				78	212	45	2.134	2.37	4.566	99	1.11	S
CR-21	0.6		500	500	139	207	46	2.264	3.091	4.672	91	1.37	S
CR-22	0.8				106	136	63	1.07	1.286	3.446	127	1.2	S
CR-23	0.6		750	750	77	132	82	1.88	2.106	3.484	70	1.12	S
CR-24	0.8				35	99	66	2.038	2.146	3.704	49	1.05	D.S

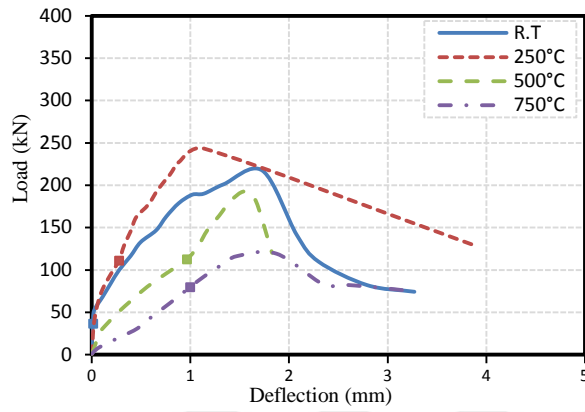
^ψ All the RC-corbels produced by FR-MSCC mixtures, and have the same steel reinforcement ratio ($\rho=0.0082$)
^{*} P_{cr}, P_{max}, P_F represent the first-cracking load, maximum load, failure load and the corresponding deflections are Δ_{max}, Δ_F respectively, and Δ_u is the deflection at 0.85P_{max} after peak load.
[♦] Stiffness of the corbel = P_{max}/Δ_{max} have been adopted by Ahmed et al. [23].
[♣] Ductility index = Δ_u/Δ_{max} has been certified by Campione et al. [30].
[†] F: Flexural failure, S: Shear failure, D.S: Diagonal splitting failure.



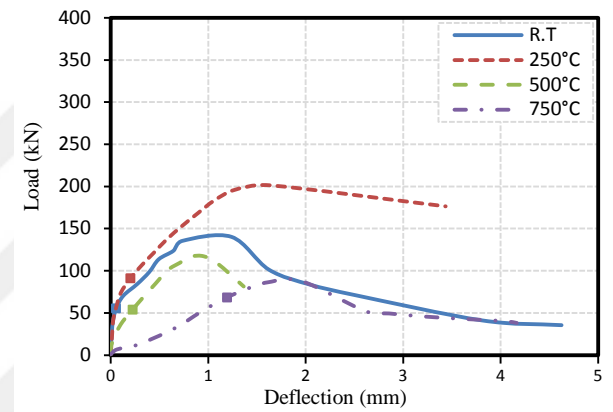
(a) SF= 0%, SSR= 0.6



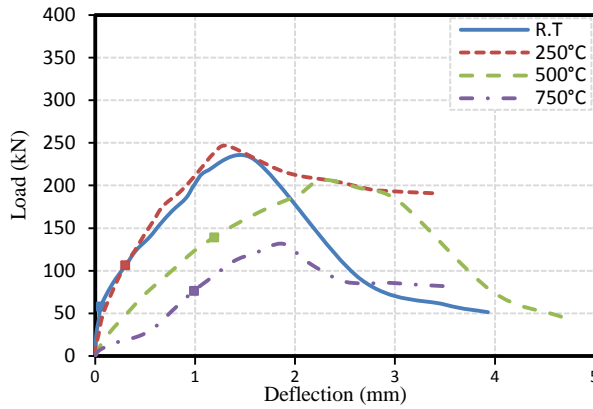
(b) SF= 0%, SSR= 0.8



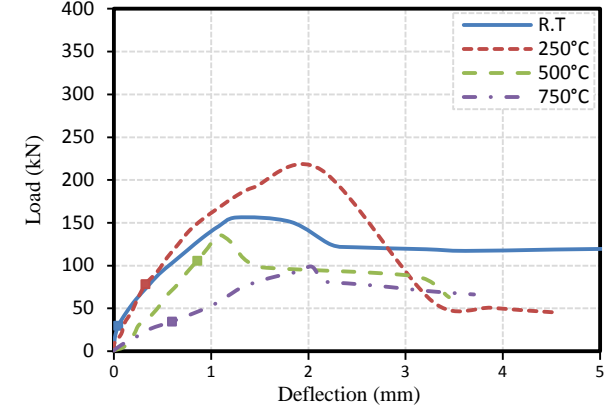
(c) SF= 0.5%, SSR= 0.6



(d) SF= 0.5%, SSR= 0.8



(e) SF= 1.0%, SSR= 0.6



(f) SF= 1.0%, SSR= 0.8

❖ The point on the curve represents the first cracking load.

Figure 7.2 Load-deflection curves for corbels with the different values of shear span-to-depth ratio (SSR).

7.3.3 Steel-Reinforcement Ratio (SRR)

A gradual increase in the steel reinforcement ratio (SRR) causes a noticeable increase in the load-carrying capacity, which also influences the stiffness of RC-corbels after exposed to elevated temperatures as shown in Table 7.4.

Generally, the RC-corbels which only reinforced with steel bars fail because of concrete crushing after reaching the maximum loads (P_{max}) at different temperatures.

On the other hand, up to 250°C, the addition of steel fiber improves the behavior of RC-corbels that were reinforced by the low SRR ($\rho=0.82\%$) and thus yielding the reinforcing steel before crush the concrete. On the contrary, when the RC-corbel reinforced with higher SRR ($\rho=1.6\%$, reinforced with 2Ø14) in addition to steel fiber does not exhibit yielding failure (flexure failure), but rather results in brittle failure induced by the crushing of the compressed regions. Furthermore, the thermal cracks due to exposure to high temperature rapidly promote concrete crushing before reinforcing steel yielding. This situation weakens the ability of steel fiber to provide more elastic-plastic behavior for RC-corbels, regardless of SRR as illustrated in Figure 7.3.

Table 7.4 Results of flexural tests for corbels with different values of steel reinforcement ratio (SRR)^ψ.

Corbel Name	SRR (ρ)	SF %	Temperature level (°C)	P _{cr} [*] (kN)	P _{max} [*] (kN)	P _F [*] (kN)	Δ _{max} [*] (mm)	Δ _u [*] (mm)	Δ _F [*] (mm)	Stiffness [♦] (kN/mm)	Ductility index [♣]	Failure mode [†]	
CR-25	0.0082	0	21	56	235	74	2.174	2.203	2.308	108	1.02	S	
CR-26	0.016			68	265	98	1.752	1.911	2.416	151	1.09	S	
CR-27	0.0082		250	99	227	103	1.046	1.062	1.104	217	1.02	D.S	
CR-28	0.016			71	268	38	1.408	1.421	1.49	190	1.01	S	
CR-29	0.0082		500	500	105	195	121	1.14	1.478	2.294	171	1.3	S
CR-30	0.016				138	210	12	1.088	2.2	3.31	193	2.02	D.S
CR-31	0.0082		750	750	96	107	67	1.506	1.693	1.958	71	1.12	S
CR-32	0.016				95	113	62	1.764	1.895	2.464	64	1.07	D.S
CR-33	0.0082	0.5	21	69	272	187	1.318	3.117	4.638	206	2.37	F	
CR-34	0.016			69	286	135	0.68	1.321	3.896	421	1.94	S	
CR-35	0.0082		250	99	280	280	2.798	2.798	2.798	100	1.0	S	
CR-36	0.016			97	370	370	3.202	3.202	3.202	116	1.0	S	
CR-37	0.0082		500	500	171	235	77	1.274	1.66	3.472	185	1.3	S
CR-38	0.016				122	251	27	1.488	1.775	4.618	169	1.19	S
CR-39	0.0082		750	750	107	150	90	1.776	2.317	3.632	85	1.31	S
CR-40	0.016				86	134	93	1.504	1.845	3.31	89	1.23	S
CR-41	0.0082	1	21	85	327	127	2.204	3.112	4.366	148	1.41	F+S	
CR-42	0.016			95	335	115	2.418	3.068	6.642	139	1.27	S	
CR-43	0.0082		250	132	317	180	1.774	1.89	2.044	179	1.07	F+S	
CR-44	0.016			132	382	73	1.576	2.393	4.914	242	1.52	S	
CR-45	0.0082		500	500	123	267	180	1.872	3.082	4.864	143	1.65	F
CR-46	0.016				161	294	117	1.664	2.029	4.658	177	1.22	S
CR-47	0.0082		750	750	140	171	127	1.36	2.145	3.292	126	1.58	D.S
CR-48	0.016				109	183	145	1.838	2.813	3.362	100	1.53	S

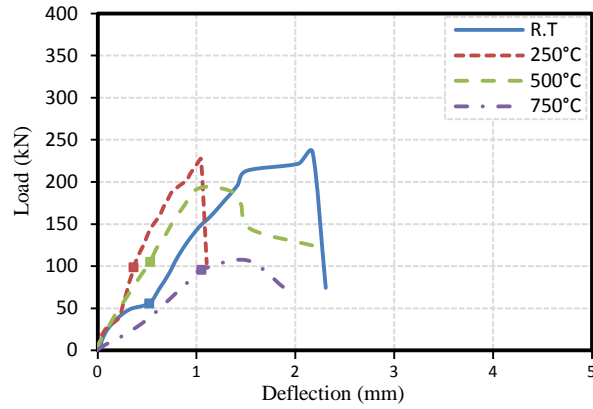
^ψ All the RC-corbels produced by FR-HSCC mixtures, and with the same shear span ratio (a/d=0.6)

* P_{cr}, P_{max}, P_F represent the first-cracking load, maximum load, failure load and the corresponding deflections are Δ_{max}, Δ_F respectively, and Δ_u is the deflection at 0.85P_{max} after peak load.

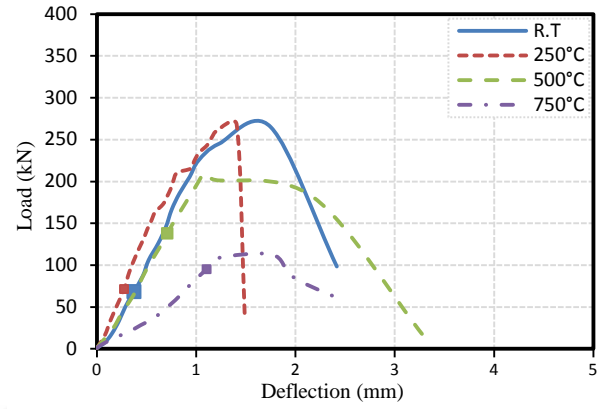
♦ Stiffness of the corbel=P_{max}/Δ_{max} have been adopted by Ahmed et al. [23].

♣ Ductility index = Δ_u/Δ_{max} has been certified by Campione et al. [30].

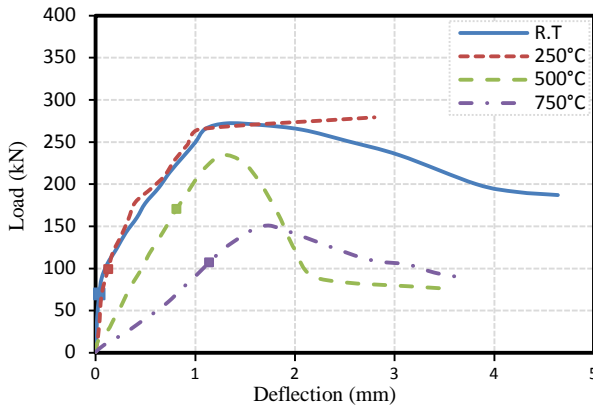
† F: Flexural failure, S: Shear failure, D.S: Diagonal splitting failure.



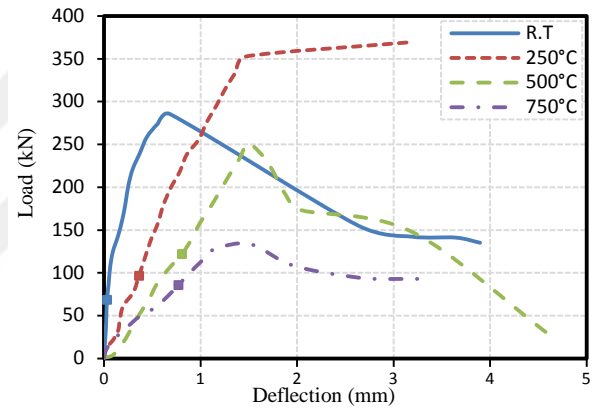
(a) SF= 0%, $\rho= 0.0082$



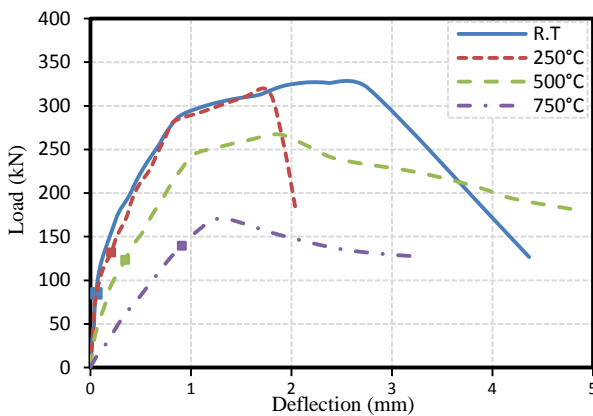
(b) SF= 0%, $\rho=0.016$



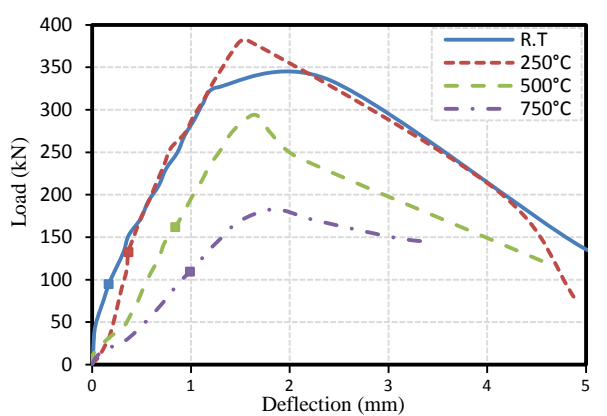
(c) SF= 0.5%, $\rho= 0.0082$



(d) SF= 0.5%, $\rho= 0.016$



(e) SF= 1.0%, $\rho= 0.0082$



(f) SF= 1.0%, $\rho= 0.016$

❖ The point on the curve represents the first cracking load.

Figure 7.3 Load-deflection curves for corbels with the different values of the steel reinforcement ratio (SRR).

7.4 Cracks pattern and failure modes

Three principal modes of failure appeared to occur in the RC-corbels (Kriz and Raths, 1965); the first one is a flexure failure (F) which occurred at or close to the column-corbel junction after extensive yielding of the steel reinforcement bars before concrete crushing. The second mode of failure is the diagonal splitting (D.S) of the concrete caused due to concrete splitting into several parts and thereby induced damage in tensile strength of concrete. The third mode is shear failure (S) of the concrete, which featured as an inclined crack on the corbel. The inclined shear cracks are oriented towards the supports.

After the RC-corbels have been exposed to elevated temperatures, cracks form inside the concrete mixture due to the incompatibility of thermal stresses between cement binder and aggregate. The cracks are likely to have developed rapidly during loading test resulting in degradation of load-carrying capacity. The use of steel fiber effectively contributed in reducing the differences in thermal stresses for FR-SCC mixtures, and thus improved the post-crack behavior during the heating process in the RC-corbels.

Furthermore, the steel fiber also tended to delay the formation of cracks, reduce the crack width and spacing in FR-SCC specimens before and after exposure to elevated temperatures. Also, the addition of fibers result in a bridging action across the cracks. On the other hand, after exposure to 750°C, the oxidization of steel fiber result in reducing its mechanical efficiency (Ding et al. 2012). Therefore, the load-carrying capacity is decreasing due to deterioration of the concrete and the decline in steel fiber efficiency. Therefore, the dominant failure mode of all RC-corbels types which exposed to 750°C is shear failure.

7.4.1 Concrete Compressive Strength (CCS)

The shape and depth of the cracks in the RC-corbels depend on the compressive strength of concrete used (CCS) and the temperatures. After exposure to temperatures not higher than 250°C, the brittleness of RC-corbels increases as the concrete grade (CCS) increases. Beyond this temperature, gradual increase in the CCS extends the deflection and improves the ductility for RC-corbels as listed in Table 7.2.

In general, after exposure to 750°C the first crack to form is a shear crack which propagates from the supports of corbel to the corbel-column junction. The deterioration in concrete cause significant reduction in cracks intensity, thus shear crack developed much more rapidly under loading and all RC-corbels fail in shear failure as depicted in Figure 7.4.

7.4.2 Shear Span-to-depth ratio (SSR)

As the shear span ratio (SSR) increases, stiffness of the RC-corbels decreases that leads to increase in ductility of corbel when exposure to the same temperatures as shown in Table 7.3 and Figure 7.5.

7.4.3 Steel-Reinforcement Ratio (SRR)

The failure mode for RC-corbels reinforced with steel fiber additionally to steel reinforcement depend on the SRR and the temperature levels. When exposed to the temperatures not higher than 250°C, although the higher SRR ($\rho=1.6\%$, reinforced with 2Ø14) increases the maximum load of the RC-corbels, but the steel fiber is unable to change the failure mode to more ductile. At the same temperature, the addition of SF to the RC-corbels reinforced with a lower SRR ($\rho=0.82\%$, reinforced with 2Ø10) create multi-axial stresses that lead to yielding of steel bars which results in flexure failure (F) as listed in Table 7.4 For the RC-corbel that reinforced 1% SF and exposed to 750°C, the width and extension of the thermal cracks develop much more rapidly under loading test. Additionally, the bond between the reinforcement and the concrete becomes damaged, and thus the crack extension continues under loading until shear failure occurs, regardless of the SRR as shown in Figure 7.6.

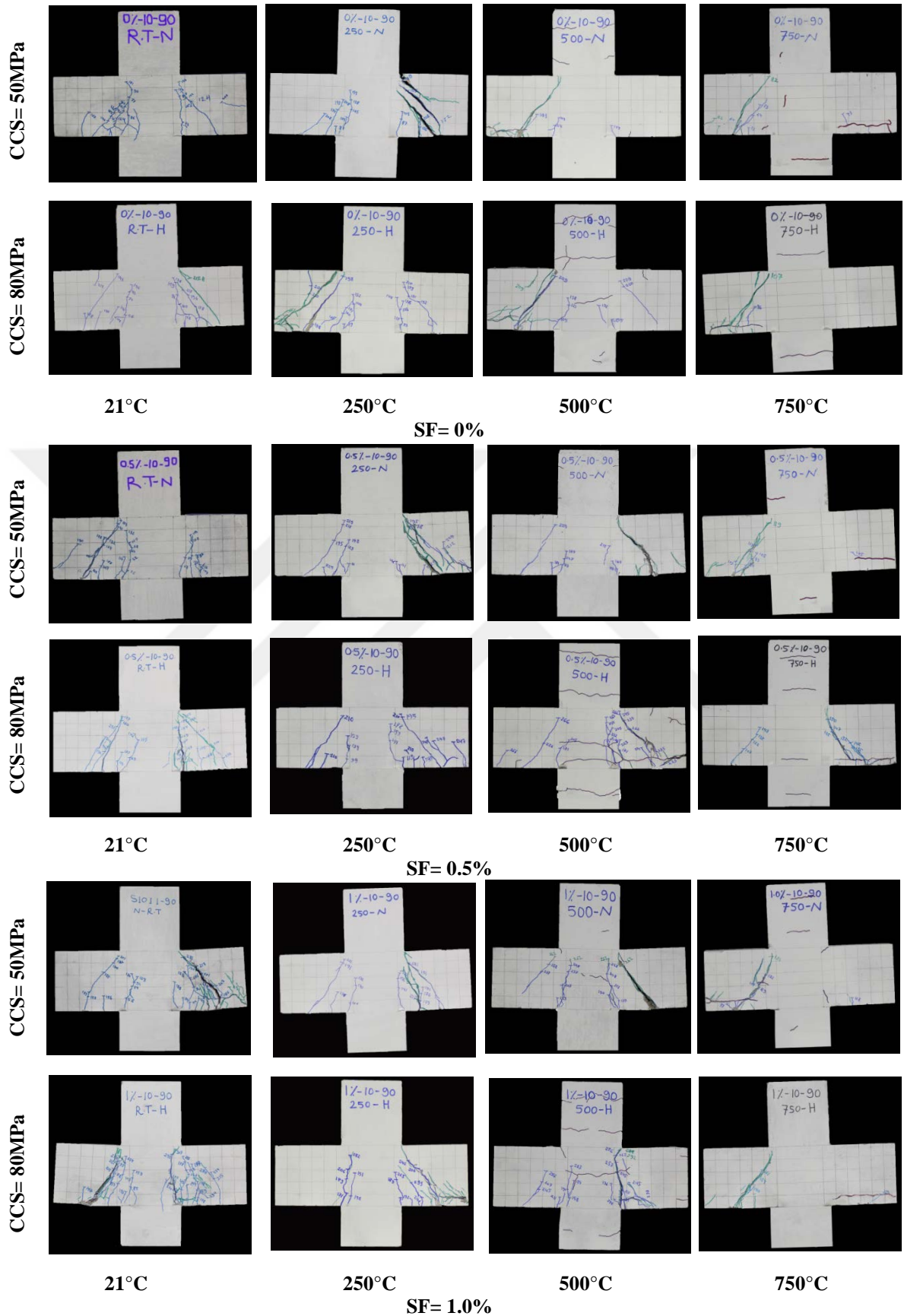


Figure 7.4 Failure modes for RC-corbels with the different values of concrete compressive strength (CCS)

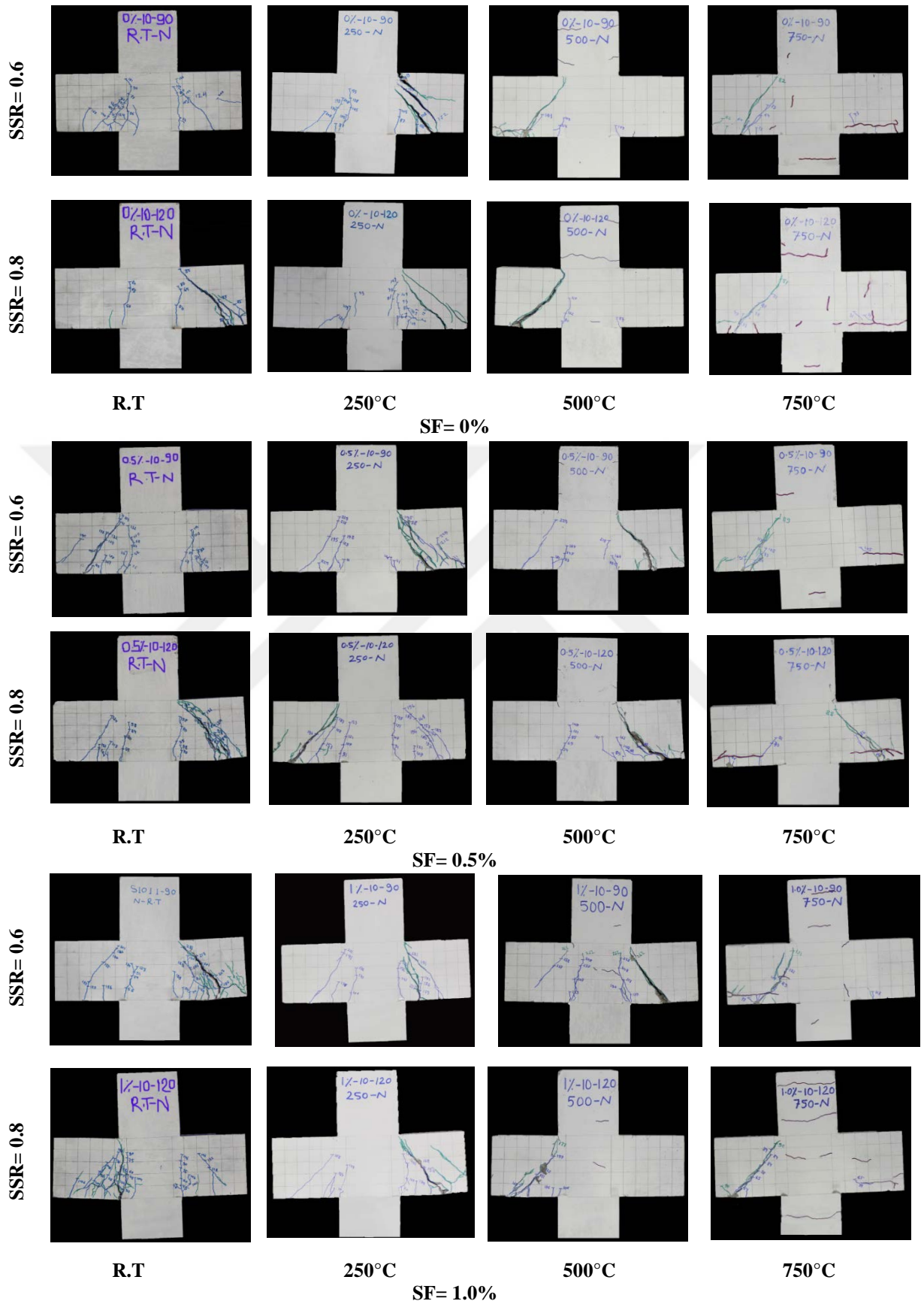


Figure 7.5 Failure modes for RC-corbels with the different values of shear span ratio (SSR).

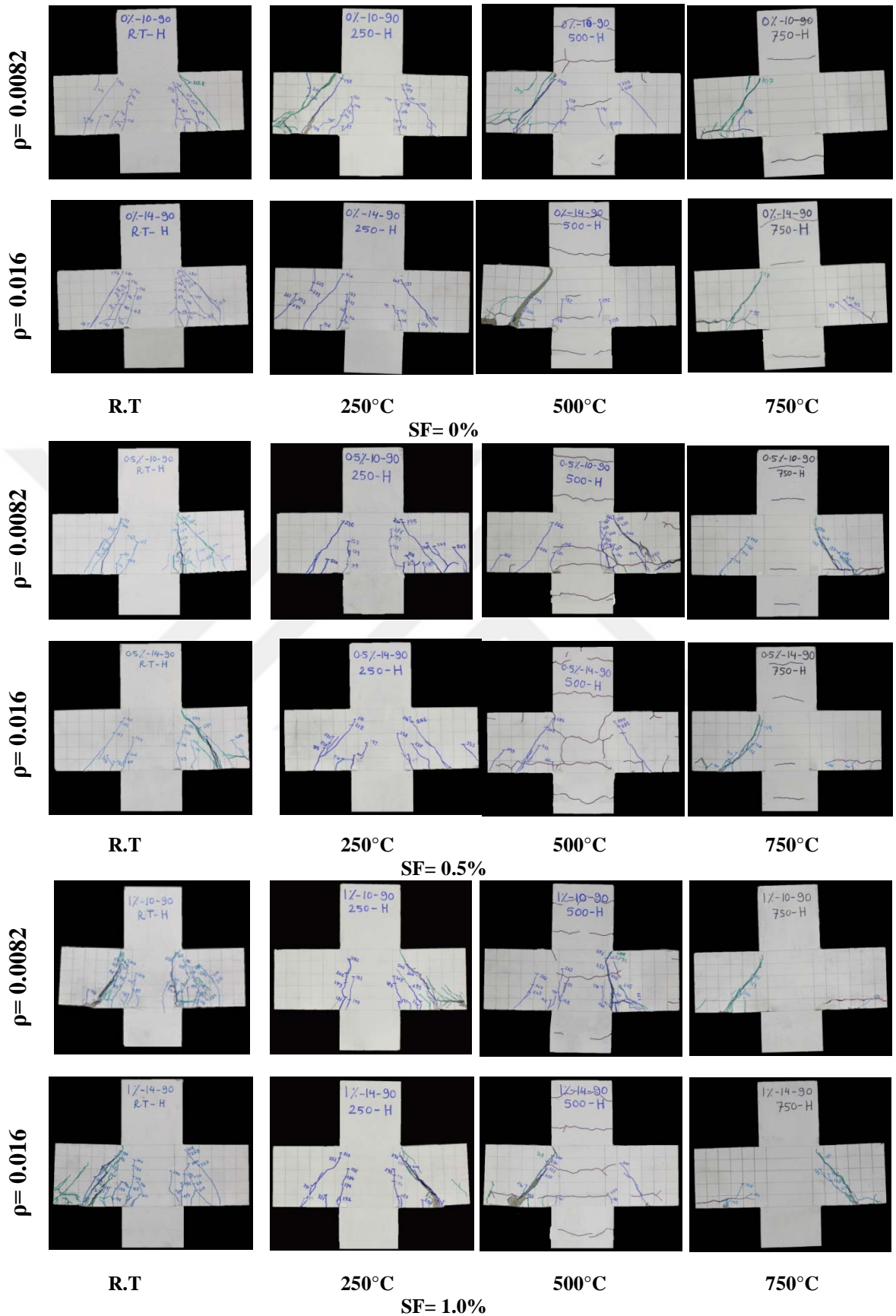


Figure 7.6 Failure modes for RC-corbels with the different values of the steel reinforcement ratio (SRR).

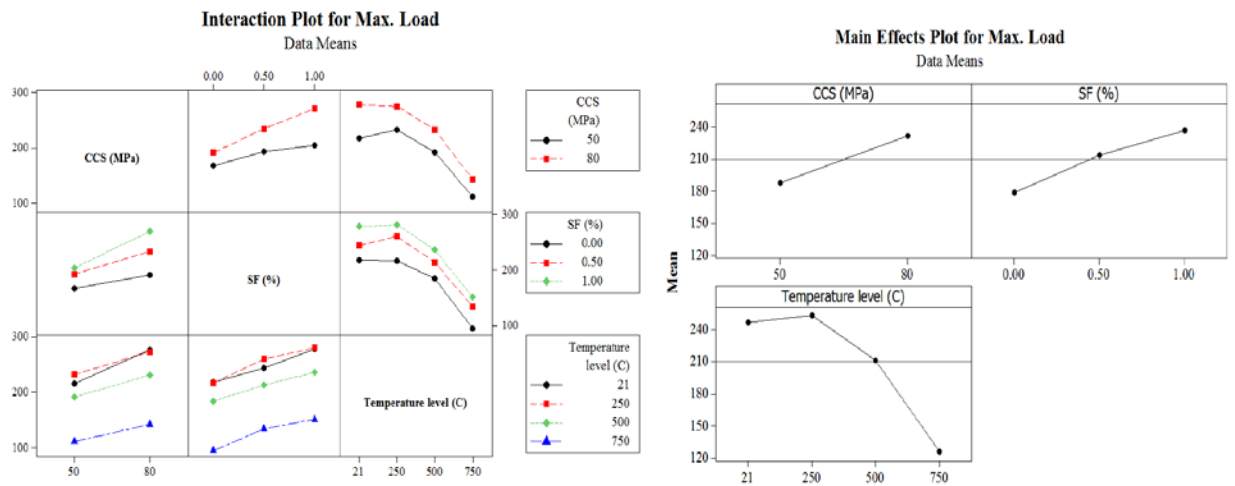
7.5 Parametric study

A parametric study was conducted to investigate the interaction between main effects (steel fiber (SF) and temperature) with the influencing parameters (concrete compressive strength (CCS), shear span ratio (SSR), and steel reinforcement ratio (SRR)) on the maximum load (mean values) for the RC-corbels before and after exposure to elevated temperatures.

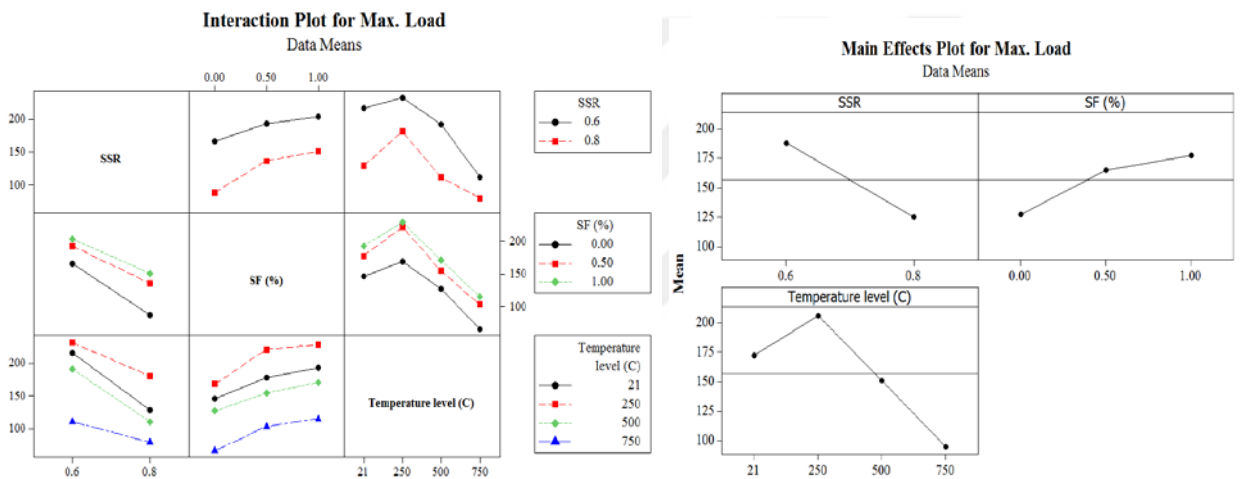
The maximum load capacity of all corbels considered in the study increases as amount of 35% averagely when the shear span ratio (SSR) declines from 0.8 to 0.6. The maximum load rises by the amount of 25% averagely when the compressive strength (CCS) is increased from 50 to 80MPa, and doubling the steel reinforcement ratio (SRR) resulted in a 10% addition to the maximum loads as shown in Figure 7.7.

When observing the effect of elevated temperatures on maximum load values for corbel's parameters, it is worthy to note that the SSR factor is the least affected, while the CCS parameter is the most sensitive parameter. When examining the improvement in the maximum loads (mean value) with respect to the amount of steel fiber (SF).

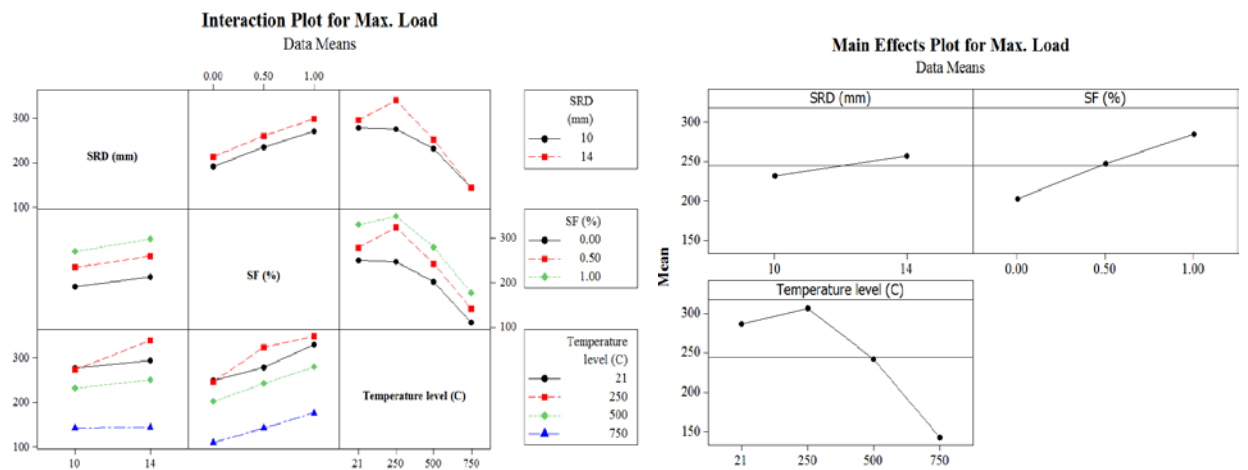
It is observed that the SSR parameter is the most responsive, while the CCS parameter is the least affected. Finally, it is concluded that the shear span ratio (SSR) variation is the most dominant parameter about improvement in the mechanical behavior of RC-corbels before and after exposure to elevated temperatures.



a) CCS parameter



b) SSR parameter



(c) SRR parameter

Figure 7.7 Interaction effect between the main effects and the corbel's parameters on the maximum loads (mean values).

CHAPTER 8

CONCLUSIONS AND RECOMMENDATIONS

8.1 General

The influence of steel fibers on the mechanical behavior of SCC before and after exposure to elevated temperature up to 750°C has been investigated in the present study. Two mixes (medium (C50) and high strength concrete (C80) were prepared from SCC, each mixture contains a constant percentage of polypropylene fiber (0.1%) and three different volume fractions of steel fibers (0, 0.5%, and 1.0%).

This thesis was a novel attempt to using an experimental work in order to investigate the behavior of fiber-reinforced SCC corbels after exposure to elevated temperatures. In the current work, the effect of the steel fibers has been studied on the ductility and enhancement of the mechanical behavior of RC-corbels before and after exposure to elevated temperatures.

8.2 Conclusions

In this thesis, an experimental study is presented on the mechanical properties of SCC and also the mechanical behavior of RC-corbels before and after exposure to elevated temperatures. The effect of SFs on the mechanical properties of SCC including, compressive strength, tensile strength, elastic modulus, and strain at peak stress were studied in details. Additionally, the characteristics of stress-strain curves for the SCC used under compression loading were practically analyzed, also the database of these curves was used to propose a theoretical formula for predicting the behavior of stress-strain for heat-exposed FR-SCC specimens, for the first time in literature.

In the present study, the size effect of different specimens on residual compressive and tensile strengths for the concrete mixtures used after exposure to different temperatures were investigated.

The main aim of this thesis was to understand the mechanical behavior of FR-SCC corbels before and after exposure to elevated temperatures in terms of load-deflection responses and failure patterns. Moreover, the effects of SFs and specific parameters on the residual load capacities of RC-corbels were investigated. The following important conclusions can be drawn as a result of this study:

1- Considering the fresh SCC test results, it can be concluded that the addition of fibers decreases workability of SCC. Also the abilities of flow and passing of the concrete decreased with the increase of the steel fiber content.

2- No explosive spalling is observed in the SCC specimens during the heating and cooling processes, which can be controlled using the PP fibers.

3- Presence of SFs in concrete, effectively contributed in reducing the differences in thermal stresses between cement paste and aggregates. The fibers are transmitting the heat more uniformly which cause a decrease in the cracks that are induced due to thermal gradient in the concrete mixtures. Thus steel fibers provide a uniform stress distribution during heating and cooling processes. Moreover, the steel fibers tend to delay the formation of cracks, and also improve the post-cracks behavior within the concrete specimens under loading test.

4- It can be concluded that the combined use of steel and polypropylene fibers significantly improves the behavior and enhances the characteristics of the SCC subjected to elevated temperatures, which justify the use of hybrid fibers in SCC as a fire-resistance materials.

5- Based on the practical results of the present study, it can be observed that the mechanical properties of SCCs were slightly affected when exposed to temperature not exceeding 500°C, which are decreasing rapidly after this degree. This degree can therefore be considered as a critical temperature degree.

6- Compressive strength of FR-SCC specimens increases gradually when they are heated up to 250°C, then the strength starts to decline continuously with further increase in temperature. However, the steel fiber can be mitigate the degradation of the compressive strength, thus enhance the residual strength of SCC subjected to elevated temperatures.

7- The addition of SFs to concrete, acts to bridging the opening of the cracks. Thus reduce width and extension the cracks in SCC specimens under tension load testing, which results in improving the splitting tensile strength of SCC specimens before and after exposure to elevated temperatures. On the other hand, the deterioration of concrete and damage the bond between the SFs and concrete at temperature higher than 500°C, thereby resulting in a significant reduction in tensile strength more than the gradual loss in compressive strength.

8- When the SCC specimens reinforced with steel fiber has retained a relatively high residual elastic modulus. Since it can be relied on the modulus of elasticity in the assessment and repair of heat-damaged concrete structures. Therefore, SCC structures which contain steel fibers may show a good performance when exposed to high temperatures.

9- Peak strain of FR-SCCs increases with temperature increase. Peak strain for SCC including SF increases exponentially with temperature increase up to the critical temperature (500°C). After the critical temperature, however, presence of SF in SCC does not affect the linear development of strain with temperature increasing.

10- For the stress-strain curves, slope of the ascending part drops as the temperature rises. The slope and non-linearity of the descending curves depend on the presence of steel fiber and temperature. Therefore, the SCC mixtures with SF exhibit a more ductile behavior as compared to counterparts without SF.

11- In general, the rise in temperature level leads to higher peak strain and lower peak stress. Therefore, the peak point on the stress-strain curve shifted towards the downright resulting in a flatter stress-strain curve.

12- Since the findings of the proposed constitutive model are highly consistent with the experimental results, the proposed stress-strain formula be reliable and applicable to simulate the compressive behavior of SCC with or without SF, for heated and unheated concrete.

13- Cubic specimens can retain considerably higher compressive strength as compared to cylindrical specimens after exposure to high temperatures. Also, the temperature effect on 150 mm cube was the least as compared to other specimens (cylinders and

cubes).

14-Size effect on the conversion factor difference is lower for greater concrete grades. Addition of steel fiber to SCC mixtures, on the other hand, causes a reduction in temperature effect on the variation of a conversion factor.

15-Performance of cubic specimens with steel fibers was the most efficient case. However, the residual compressive strength of cubic specimens is higher than that of the cylindrical specimens. Therefore, the preference of the cubic shaped structural element can be more reliable when the risk of high temperature is concerned.

16-Reduction in tensile strength of small cylinders (100*200 mm) is quicker as compared to that of large cylinder (150*300 mm) when exposed to elevated temperatures. Therefore, tensile strength results of the standard size cylinder are more reliable than cylinder specimens with other sizes.

17- High prediction accuracy of proposed models confirms that the size effect equations can be used safely to predict the strength values for different specimens of FR-SCC subjected to high temperatures. Since the generalization capability of proposed formulations is high it enables the designers to use the formulations for all types of SCC (medium or high strength, with or without steel fiber).

18-The presence of SF in corbel mixtures has a slight influence on the magnitude of the first-cracking load. However, it significantly improves the maximum load for the RC-corbels before and after exposure to elevated temperatures.

19-As expected, when the concrete grade is increased, the load carrying capacity of corbels also increases. However, the effectiveness of the steel fiber on the corbels characteristics is more noticeable when the concrete grade decreases for RC-corbels exposed to elevated temperatures.

20-Although an increase in shear span-to-depth ratio leads to a reduction in the maximum load capacity of RC-corbels, it improves the ductility of the RC-corbels exposed to elevated temperatures.

21-Even for high temperature (750°C), the addition of SF prevents the sudden failure and improve the characteristics (ductility and residual maximum load) of the corbels.

22-When exposed to temperatures higher than 500°C, the RC-corbels tend to fail in shear failure caused by concrete deterioration, and the efficiency of steel fiber decreases due to oxidation.

23-According to the present parametric study, the shear span ratio is the most effective parameter needed to improve the load-carrying capacity of fiber-reinforced corbels before and after subjected to elevated temperatures.

24- Since steel fiber certainly provides ductility and prevents sudden and diagonal splitting failure in corbels this leads to the achievement of rescue work without risk of collapse of the structure during a possible fire. Furthermore, repair and rehabilitation works can be achieved easily after fire suppression.

8.3 Recommendations for future studies

1- Use of hybrid fibers (i.e., SF and PP fibers) in concrete mixtures, particularly in the industrial structures exposed to high risk of fire explosion.

2- Based on the proposed equations, the mechanical properties of high-performance concrete can be predicted particularly when exposed to elevated temperatures. Therefore, these formulations can be developed to include all types of concrete.

3- The proposed stress-strain model can be typically used in computer applications such as finite element modeling, when analyzing the mechanical behavior of concrete structural members at elevated temperatures.

4- The database obtained from the practical results of the mechanical behavior of the RC-corbels after exposure to elevated temperatures, it can be used in theoretical study or related engineering programs to simulate and compare the behavior of these members at elevated temperatures.

REFERENCES

Abdel Hafez, A.M., Ahmed, M.M., Diab, H., Drar, A.A. (2012). Shear Behavior of High Strength Fiber Reinforced Concrete Corbels. *Journal of Engineering Sciences-Assiut University*. **40(4)**, 969-987.

Abdul-Wahab, H.M.S. (1989). Strength of Reinforced Concrete Corbels with Fibers. *ACI Structural Journal*. **86(1)**, 60-66.

Ahmed, R.H., Abdel-Hameed G.D., Farahat, A.M. (2016). Behavior of hybrid high-strength fiber reinforced concrete slab-column connections under the effect of high temperature. *Housing and Building National Research Center*. **12**, 54-62.

Al Qadi, A.N.S., Al-Zaidyeen, S.M. (2014). Effect of fibre content and specimen shape on residual strength of polypropylene fibre self-compacting concrete exposed to elevated temperatures. *Journal of King Saud University-Engineering Sciences*. **26**, 33-39.

Aslani, F. (2013). Effect of specimen size and shape on compressive and tensile strengths of self-compacting concrete with or without fibers. *Magazine of Concrete Research*. **65(15)**, 914-929.

Aslani, F., Samali, B. (2015). Constitutive relationships for self compacting concrete at elevated temperatures. *Materials and Structures*. **48**, 337-356.

Aslani, F., Nejadi, S. (2013). Self-compacting concrete incorporating steel and polypropylene fibers: Compressive and tensile strengths, moduli of elasticity and rupture, compressive stress-strain curve, and energy dissipated under compression. *Composites: Part B*. **53**, 121-133.

B.S-EN 12390-3. (2002). Testing hardened concrete. In: Part 3: Compressive Strength of Test Specimens. BSI, London, UK.

Bakhtiyari, S., Allahverdi, A., Rais-Ghasemi, M., Zarrabi, B.A., Parhizkar, T. (2011) Self-compacting concrete containing different powders at elevated temperatures—Mechanical properties and changes in the phase composition of the paste. *Thermochimica Acta*. **514(1)**, 74-81.

Bazant, Z.P. (1984). Size effect in blunt fracture, Concrete, Rock, and Metal. *Journal of Engineering Mechanics (ASCE)*. **110(4)**, 518–535.

Bazant, Z.P. (1993). Size effect in tensile and compressive quasi-brittle failures. *JCI International Workshop on Size Effect in Concrete Structures*. 141–160.

Bazant, Z.P., Xiang, Y. (1997). Size effect in compression fracture: splitting crack band propagation. *Journal of Engineering Mechanics (ASCE)*. **123(2)**, 162–172.

Bentur, A., Mindess, S. (2007). Fiber Reinforced Cementitious Composites. *Taylor & Francis-second edition*. New York-USA.

Campione, G. (2009). Flexural response of FRC corbels. *Cement & Concrete Composites*. **31**, 204-210.

Campione, G., Mendola, L.L., Mangiavillano M.L. (2007). Steel Fiber Reinforced Concrete Corbels: Experimental Behavior and Shear Strength Prediction. *ACI Structural Journal*. **104(5)**, 570-579.

Campione, G., Mendola, L.L., Papia, M. (2005). Flexural behaviour of concrete corbels containing steel fibers or wrapped with FRP sheets. *Material and Structures*. **38**, 617-625.

Chan, Y.N., Luo, X., Sun, W. (2000). Compressive strength and pore structure of high-performance concrete after exposure to high temperature up to 800°C. *Cement*

and Concrete Research. **30(2)**, 247-251.

Chang, Y.F., Chen, Y.H., Sheu, M.S., Yao, G.C. (2006). Residual stress-strain relationship for concrete after exposure to high temperatures. *Cement and Concrete Research*. **36**, 1999-2005.

Chen, B., Liu, J. (2004). Residual strength of hybrid-fiber-reinforced high-strength concrete after exposure to high temperatures. *Cement and Concrete Research*. **34(6)**, 1065-1069.

Chen, G.M., He, Y.H., Yang, H., Chen, J.F., Guo, Y.C. (2014). Compressive behavior of steel fiber reinforced recycled aggregate concrete after exposure to elevated temperatures. *Construction and Building Materials*. **71(1)**, 1-15.

Dias, W.P.S., Khoury, G.A., Sullivan, P.J.E. (1990). Mechanical properties of hardened cement paste exposed to temperatures up to 700 C (1292 F). *Materials Journal*. **87(2)**, 160-166.

Ding, Y., Azevedo, C., Aguiar, J.B., Jalali, S. (2012). Study on residual behaviour and flexural toughness of fibre cocktail reinforced self compacting high performance concrete after exposure to high temperature. *Construction and Building Materials*. **26(1)**, 21-31.

Ding, Y.N., Wang, Y.H., Zhang, Y.L. (2010). Investigation on Toughness of Fiber Cocktail Reinforced Self Consolidating Concrete after High Temperature. *Materials Science Forum*. **650**, 67-77.

Dong, X., Ding, Y., Wang, T. (2008). Spalling and Mechanical Properties of Fiber Reinforced High-performance Concrete Subjected to Fire. *Journal of Wuhan University of Technology-Material*. **5**, 743-749.

EFNARC, The European Guidelines for Self-Compacting Concrete. Specification, Production and Use. London, UK, Association House, 2005.

Fares, H., Remond, S., Noumowe, A., Cousture, A. (2010). High temperature behaviour of self-consolidating concrete: microstructure and physicochemical properties. *Cement and Concrete Research*. **40(3)**, 488-496.

Fattuhi, N.I. (1987). SFRC Corbel Tests. *ACI Structural Journal*. **84(2)**, 119-123.

Fattuhi, N.I. (1988). Strength of SFRC Corbels subjected to vertical load. *Journal of Structural Engineering (ASCE)*. **116(3)**, 701-718.

Fattuhi, N.I. (1994). Reinforced Corbels Made with Plain and Fibrous Concretes. *ACI Structural Journal*. **91(5)**, 530-536.

Fattuhi, N.I. (1994). Strength of FRC Corbels in flexure. *Journal of Structural Engineering (ASCE)*. **120(2)**, 360-377.

Fattuhi, N.I., Hughes, B. (1989). Ductility of Reinforced Concrete Corbels Containing either Steel Fibers or Stirrups. *ACI Structural Journal*. **86(6)**, 644-651.

Fattuhi, N.I., Hughes, B. (1989). Reinforced Steel Fiber Concrete Corbels with Various Shear Span-to-Depth Ratios. *ACI Materials Journal*. **86(6)**, 590-596.

Foster, S.J., Powell, R.E., Selim H.S. (1996). Performance of High-Strength Concrete Corbels. *ACI Structural Journal*. **93(5)**, 1-8.

Jansson, R., Bostrom L. (2013). Factors influencing fire spalling of self compacting concrete. *Material and Structures*. **46**, 1683-1694.

Kalifa, P., Chene, G., Galle, C. (2001). High-temperature behaviour of HPC with polypropylene fibres from spalling to microstructure. *Cement and Concrete Research*. **31(10)**, 1487-1499.

Kalifa, P., Menneteau, F-D., Quenard, D. (2000). Spalling and pore pressure in HPC at high temperatures. *Cement and concrete research*. **30(12)**:pp. 1915-1927, 2000.

Khaliq, W., Kodur, V. (2011). Thermal and mechanical properties of fiber reinforced high performance self-consolidating concrete at elevated temperatures. *Cement and Concrete Research*. **41(11)**, 1112-1122.

Kim, D.J., Kang, S.H., Ahn, T. (2014). Mechanical characterization of high-performance steel-fiber reinforced cement composites with self-healing effect. *Materials*. **7**, 508–526.

Kim, J.K., Eo, S.H. (1990). Size effect in concrete specimens with dissimilar initial cracks. *Magazine of Concrete Research*. **42(153)**, 233–238.

Kim, J.K., Yi, S.T., Kim, J.H.J. (2001). Effect of specimen sizes on flexural compressive strength of concrete. *Fracture Mechanics of Concrete Structures*. **90**, 697–704.

Kim, Y-S., Lee, T-G., Kim, G-Y. (2013). An experimental study on the residual mechanical properties of fiber reinforced concrete with high temperature and load. *Materials and Structures*. **46**, 607-620.

Kriz, L.B., Raths, C.H. (1965). Connections in Precast Concrete Structures- Strength of Corbels. *PCI Journal*. **10(1)**, 16–61.

Lau, A., Anson, M. (2006). Effect of high temperatures on high performance steel fibre reinforced concrete. *Cement and Concrete Research*. **36(9)**, 1698-1707.

Li, H., Liu, G. (2016). Tensile Properties of Hybrid Fiber-Reinforced Reactive Powder Concrete After Exposure to Elevated Temperatures. *International Journal of Concrete Structures and Materials*. **10(1)**, 29-37.

Nikbin, I.M., Dehestani, M., Beygi, M.H.A., Rezvani, M. (2014). Effects of cube size and placement direction on compressive strength of self-consolidating concrete. *Construction and Building Materials*. **59**, 144–150.

Noumowé, A. (2005). Mechanical properties and microstructure of high strength concrete containing polypropylene fibres exposed to temperatures up to 200 C. *Cement and Concrete Research*. **35(11)**, 2192-2198.

Noumowé, A., Carré, H., Daoud, A., Toutanji, H. (2006). High-strength self-compacting concrete exposed to fire test. *Journal of materials in civil engineering*. **18(6)**, 754-758.

Okamura, H., Ouchi, M. (2003). Self-compacting concrete. *Journal of advanced concrete technology*. **1(1)**, 5-15.

Pathak, N., and Siddique, R. (2012). Properties of self-compacting-concrete containing fly ash subjected to elevated temperatures. *Construction and Building Materials*. **30**, 274-280.

Pathak, N., Siddique, R. (2012). Effect of elevated temperatures on properties of self-compacting-concrete containing fly ash and spent foundry sand. *Construction and Building Materials*. **34**, 512-521.

Peng, G-F., Yang, W-W., Zhao, J., Liu, Y-F., Bian, S-H., Zhao, L-H. (2006). Explosive spalling and residual mechanical properties of fiber-toughened high-performance concrete subjected to high temperatures. *Cement and Concrete Research*. **36**. 723-727.

Persson, B. (2004). Fire resistance of self-compacting concrete SCC. *Materials and Structures*. **37(9)**, 575-584.

Pliya, P., Beaucour, A-L., Noumowé, A. (2011). Contribution of cocktail of polypropylene and steel fibres in improving the behaviour of high strength concrete subjected to high temperature. *Construction and Building Materials*. **25(4)**, 1926-1934.

Poon, C.S., Shui, Z.H., Lam, L. (2004). Compressive behavior of fiber reinforced

high-performance concrete subjected to elevated temperatures. *Cement and Concrete Research*. **34**, 2215-2222.

Popovics, S. (1973). A numerical approach to the complete stress-strain curve of concrete. *Cement and Concrete Research*. **3(5)**, 583-599.

Sahmaran, M., Yurtseven, A., Yaman I.O. (2005). Workability of hybrid fiber reinforced self-compacting concrete. *Building and Environment*. **40(12)**, 1672-1677.

Shaikh, F.U.A., Hosan, A. (2016). Mechanical properties of steel fibre reinforced geopolymer concretes at elevated temperatures. *Construction and Building Materials*. **114**, 15-28.

Sideris, K. K., Manita, P. (2013). Residual mechanical characteristics and spalling resistance of fiber reinforced self-compacting concretes exposed to elevated temperatures. *Construction and Building Materials*. **41**, 296-302.

Sideris, K.K. (2007). Mechanical characteristics of self-consolidating concretes exposed to elevated temperatures. *Journal of Materials in Civil Engineering*. **19(8)**, 648-654.

Standard Test Method for Compressive Strength of Cylindrical Concrete Specimens. *C39/C39M ASTM international*, USA, 2005.

Standard Test Method for Splitting Tensile Strength of Cylindrical Concrete Specimens. *C496/C 496M ASTM international*, USA, 2005.

Sukontasukkul, P., Pomchiengpin, W., Songpiriyakij, S. (2010). Post-crack (or post-peak) flexural response and toughness of fiber reinforced concrete after exposure to high temperature. *Construction and Building Materials*. **24(1)**, 1967-1974.

Tai, Y-S., Pan, H-H., Kung, Y-N. (2011). Mechanical properties of steel fiber reinforced reactive powder concrete following exposure to high temperature reaching

800 °C. *Nuclear Engineering and Design*. **241**, 2416-2424.

Yi, S-T., Yang, E-I., Choi, J-C. (2006). Effects of specimen sizes, specimen shapes and placement directions on compressive strength of concrete. *Nuclear Engineering and Design*. **236**, 115–127.

Zhang, B., Bicanic, N. (2002). Residual fracture toughness of normal and high-strength gravel concrete after heating to 600°C. *ACI-Materials Journal*. **99(3)**, 217–226.

Zheng, W., Li, H., Wang, Y. (2012). Compressive behaviour of hybrid fiber-reinforced reactive powder concrete after high temperature. *Materials and Design*. **41**, 403-409.

Zheng, W., Li, H., Wang, Y. (2012). Compressive stress-strain relationship of steel fiber-reinforced reactive powder concrete after exposure to elevated temperatures. *Construction and Building Materials*, **35**, 931-940.

Zheng, W., Luo, B., Wang, Y. (2013). Compressive and tensile properties of reactive powder concrete with steel fibers at elevated temperatures. *Construction and Building Materials*, **41**, 844-851.

Zheng, W., Luo, B., Wang, Y. (2015). Stress-strain relationship of steel-fibre reinforced reactive powder concrete at elevated temperatures. *Materials and Structures*. **48**, 2299-2314.

CURRICULUM VITAE

PERSONAL INFORMATION

Name and Surname : Khamees Nayyef ABDULHALEEM
Nationality : Iraqi
Birth place and date : Kirkuk-Iraq / 01-07-1977
Marital status : Married
Phone number : +964 770 170 9640/ +90 539 844 4920
E-mail : khamees.civ.str@gmail.com / khamees_civ_st@yahoo.com

EDUCATION

Degree	Graduate School	Year
Masters	University of Mosul	2004
Bachelors	University of Mosul	2001
High School	Al-Zab Secondary School	1997

WORK EXPERIENCE

Year	Place	Enrollment
2005-present	Kirkuk University	Assistant lecturer

PUBLICATIONS

A. International Journals

- 1- **ABDULHALEEM**, K. N., GÜLŞAN, M. E., ÇEVİK, A. Mechanical behavior of steel fiber-reinforced self-compacting concrete corbels after exposure to elevated temperatures. *Structural Concrete Journal*, Vol. 19, No. 2, pp. 1-14, DOI: 10.1002/suco.201700034.
- 2- GÜLŞAN, M. E., **ABDULHALEEM**, K. N., KURTOĞLU., A, ÇEVİK, A. E. Size effect on strength of fiber-reinforced self-compacting concrete (SCC) after exposure to high temperatures. *Computers and Concrete Journal*, Vol. 21, No. 6, pp. 681-695, DOI: 10.12989/cac.2018.21.6.681.
- 3- GÜLŞAN, M. E., Al JAWAHERY, M. S., ALSHAWAF, A. H., HUSSEIN, T. A., **ABDULHALEEM**, K. N., ÇEVİK, A. Rehabilitation of Normal and Self-Compacted Steel Fiber Reinforced Concrete Corbels via Basalt Fiber. *Advances in concrete construction journal*, (accepted).
- 4- GÜLŞAN, M. E., **ABDULHALEEM**, K. N., ÇEVİK, A., Alpegmbrli, H., KURTOĞLU., A. E. Residual mechanical properties of hybrid-fiber reinforced self-compacting concrete at elevated temperatures. *Gradevinar journal*, (under review).
- 5- GÜLŞAN, M. E., **ABDULHALEEM**, K. N., SONEBI, M., KURTOĞLU., A. E., Alpegmbrli, H., ÇEVİK, A. Constitutive stress-strain relationships of steel fiber-reinforced self-compacting concrete after exposure to elevated temperatures. *KSCE journal*, (under review).

B. International/National Congress, Conference and Symposium

- 1- Alshawaf, A. H., GÜLŞAN, M. E., **ABDULHALEEM**, K. N. (2017). Rehabilitation of high strength reinforced concrete corbels using basalt fiber fabric. *The international journal of energy & engineering sciences*. Gaziantep University, Vol. 2, No. 3, pp. 47-57.